AWARD NUMBER: W81XWH-11-1-0329

TITLE: Genomewide Search of Oncogenic Pathways Cooperating With ETS Fusions in Prostate Cancer

PRINCIPAL INVESTIGATOR: Zhe Li, PhD

CONTRACTING ORGANIZATION:
Brigham and Women's Hospital
Boston, MA 02115

REPORT DATE: September 2014

TYPE OF REPORT: Final

PREPARED FOR: U.S. Army Medical Research and Materiel Command
Fort Detrick, Maryland 21702-5012

REPORT DOCUMENTATION PAGE

Form Approved
OMB No. 0704-0188

1. REPORT DATE	2. REPORT TYPE	3. DATES COVERED
September 2014	Final report	1 July 2011 – 30 June 2014

4. TITLE AND SUBTITLE

Genomewide Search of Oncogenic Pathways Cooperating with ETS Fusions in Prostate Cancer

5a. CONTRACT NUMBER
W81XWH-11-1-0329

5b. GRANT NUMBER

5c. PROGRAM ELEMENT NUMBER

6. AUTHOR(S)
Linn, Douglas; Zhang, Xin; Li, Zhe

E-Mail: zli4@rics.bwh.harvard.edu

5d. PROJECT NUMBER

5e. TASK NUMBER

5f. WORK UNIT NUMBER

7. PERFORMING ORGANIZATION NAME(S) AND ADDRESS(ES)

Brigham and Women's Hospital
Boston, MA 02115

8. PERFORMING ORGANIZATION REPORT NUMBER

9. SPONSORING / MONITORING AGENCY NAME(S) AND ADDRESS(ES)

U.S. Army Medical Research and Materiel Command
Fort Detrick, Maryland 21702-5012

10. SPONSOR/MONITOR'S ACRONYM(S)

11. SPONSOR/MONITOR'S REPORT NUMBER(S)

12. DISTRIBUTION / AVAILABILITY STATEMENT

Approved for Public Release; Distribution Unlimited

13. SUPPLEMENTARY NOTES

14. ABSTRACT

Gene fusions involving ETS family transcription factors (TFs) (mainly ERG and ETV1) have been identified in ~50% of prostate cancer cases. To address their roles in prostate cancer, we generated multiple Tmprss2-ETS knockin mouse models. The goal of this project is to identify oncogenic pathways cooperating with ETS fusions using these knockin models. During the three-year grant period, we found that: 1) Tmprss2-ETS fusions cooperate with Pten-loss, but not with Nkx3.1-loss, to promote development of localized prostate cancer. 2) Genes deleted in the interstitial region between Tmprss2 and Erg cooperate with Pten-loss, or Pten-loss plus ectopic Tmprss2-Erg expression (at the early stage), leading to development of invasive prostate cancer with features of epithelial-mesenchymal transition. We identified several interstitial genes, including ETS2, HMGN1 and BACE2, as candidate tumor suppressors and confirmed that loss of one copy of Ets2 was sufficient for prostate cancer progression under a Pten-null background. 3) Another ETS family TF, ETV6, which is deleted in some prostate cancer cases (including TMPRSS2-ERG fusion positive case), is also a tumor suppressor in prostate cancer and it may contribute to prostate tumorigenesis via the PRC2 complex (thus similar to ERG). Overall, our work has unveiled several oncogenic pathways (due to loss of tumor suppressors) in prostate cancer under the context of TMPRSS2-ETS gene fusions.

15. SUBJECT TERMS

Prostate cancer, ETS gene fusion, TMPRSS2, ERG, ETV1, PTEN, NKX3.1, ETV6, ETS2, tumor suppressor, interstitial deletion, cooperating oncogenic pathway

16. SECURITY CLASSIFICATION OF:			17. LIMITATION OF ABSTRACT	18. NUMBER OF PAGES	19a. NAME OF RESPONSIBLE PERSON
a. REPORT	b. ABSTRACT	c. THIS PAGE			USAMRMC
Unclassified	Unclassified	Unclassified	Unclassified	47	19b. TELEPHONE NUMBER *(include area code)*

Table of Contents

Page

INTRODUCTION:

During prostate tumorigenesis, multiple oncogenic pathways cooperate to drive disease progression. Identification of these cooperating pathways is the key for defining novel therapeutic targets and for combined therapeutic interventions for treating advanced prostate cancer. Gene fusions involving the ETS family transcription factors (TFs), particularly ERG and ETV1, have been identified in at least 40-50% of human prostate cancer cases [1, 2]. Coding regions of these *ETS* genes are often rearranged to control regions of several androgen-responsive genes, particularly the *TMPRSS2* gene, leading to aberrant expression of *ETS* genes. In animal models, aberrant *ERG* or *ETV1* expression in mouse prostates under the control of the *Probasin* (*Pb*) promoter [3-6] leads to either a minor phenotype [*i.e.*, Prostatic intraepithelial neoplasia (PIN) lesions] or almost no observable abnormalities. However, ectopic *ERG* expression can cooperate with *Pten* loss to drive prostate cancer development [7, 8]. Consistent with this, in a tissue reconstitution model, lentiviral overexpression of *ERG* in prostate cells collaborates with activation of the PI3K pathway or the androgen receptor (AR) pathway to induce distinct prostate carcinomas. These observations suggest that although aberrant expression of ETS factors alone in prostates is insufficient for prostate cancer, it sensitizes prostate epithelial cells for cooperation with additional oncogenic mutations to drive full-blown prostate cancer. The main hypothesis of this study is that aberrant ERG or ETV1 expression in prostate cells may cooperate with multiple alternative oncogenic pathways to drive prostate tumorigenesis. Since *TMPRSS2-ERG* fusions (particularly those with the interstitial deletion) are highly prevalent in advanced, castration-resistant (CR) prostate tumors [9, 10], understanding cooperative interactions between *ETS* fusions and other oncogenic pathways would be the key to develop novel combined therapies for treating this deadly disease. Since mouse models with aberrant *ETS* expression alone do not develop prostate cancer but serve as a sensitized system, the main purpose of this research is to identify additional oncogenic pathways that may cooperate with *ETS* gene fusions, leading to prostate cancer. This will be achieved by genetic approaches (e.g., genetic screens; crosses with existing mouse models) under the background of various *Tmprss2-ETS* knockin models we have generated. Novel tumor suppressors may be identified from this study that may cooperate with *ETS* fusions (upon their loss) to drive prostate cancer development, and pathways affected by their loss will be determined.

KEYWORDS:

Prostate cancer, ETS gene fusion, TMPRSS2, ERG, ETV1, PTEN, NKX3.1, ETV6, ETS2, tumor suppressor, interstitial deletion, cooperating oncogenic pathway

OVERALL PROJECT SUMMARY:

The major goal of this research project is to identify oncogenic pathways that cooperate with *TMPRSS2-ETS* gene fusions, leading to prostate cancer formation. During the three-year grant period, we further characterized several *Tmprss2-ETS* knockin mouse models we generated [*Tmprss2-ERG* knockin (*T-ERG*), *Tmprss2-ETV1* knockin (*T-ETV1*), *Tmprss2-loxP-3Mb-loxP-Erg* knockin (*3Mb* refers to the 3Mb interstitial region between *Tmprss2* and *Erg* loci; before excision *T-3Mb-Erg*, after excision *T-Δ-Erg*)] and have identified several oncogenic pathways (e.g., due to loss of tumor suppressors such as ETS2 and ETV6) in prostate cancer under the context of *TMPRSS2-ETS* gene fusions. Below is a detailed summary of our research activity addressing Tasks 1-5 in the SOW:

Tasks 1-2:

These two tasks were proposed to further characterize various *Tmprss2-ETS* knockin mouse models we generated as the starting materials for searching for and testing oncogenic cooperation, and to establish and optimize the prostate cancer reconstitution model.

Further characterization of the *Tmprss2-ETS* knockin mouse models

The majority portion of this work was published in *Genes & Development* in 2013 (*Baena et al., Genes Dev. 27:683-98*) and is provided in the *Appendix*. The major conclusion from this study is that both *Tmprss2-ERG* and *Tmprss2-ETV1* gene fusions can cooperate with loss of a single copy of *Pten*, leading to localized cancer (PIN lesions), but only ETV1 appeared to support development of invasive adenocarcinoma under the background of full *Pten* loss. Furthermore, these two types of ETS fusions appear to cooperate with *Pten*-loss in different ways: ERG negatively regulates the androgen receptor (AR) transcriptional program and thus it may cooperate with *Pten*-loss, which also downregulates the AR program, in leading to an immature phenotype and increased proliferation. In contrast, ETV1 appears to enhance AR signaling and reprogram the metabolism of prostate cells, and it may cooperate with *Pten*-loss by further enhancing metabolic reprogramming, in particular, by favoring steroid biosynthesis, a pathway critical for invasive adenocarcinoma cells. Thus, our initial work has provided mechanistic insights into how different *ETS* gene fusions cooperate with other oncogenic pathway in leading to development of prostate cancer.

Establish and optimize the prostate cancer reconstitution model based on *Pten* knockdown in *Tmprss2-ETS* knockin prostate epithelial cells

We have established the renal capsule reconstitution assay and performed reconstitution experiments by transplanting wild type (WT), or *T-ETV1*, or *T-ERG* prostate cells (lineage-negative cells enriched by MACS beads) infected with shRNA lentivirus for *Pten* to recipient mice. Compared to WT, we saw certain degree of cooperation between *T-ETV1* and *Pten* knockdown, but only very slight cooperation (if any) between *T-ERG* and *Pten* knockdown (Figure 1). This could be due to the fact that ETV1 is robustly expressed from the *T-ETV1* knockin allele whereas ERG is only weakly expressed from the endogenous *Tmprss2* promoter from the *T-ERG* knockin allele, as described in more details in the attached paper (*Baena et al., Genes Dev. 27:683-98*). This could also be due to insufficient lentiviral infection of prostate cells and/or insufficient *Pten* knockdown. To determine these possibilities, we used an alternative reconstitution approach. In this approach, we first generated prostate cells carrying homozygous *Pten* conditional knockout alleles (i.e., $Pten^{L/L}$ prostate cells) with or without the *T-ERG* knockin allele; we then infected these prostate cells with Cre-expressing adenovirus (Adeno-Cre) *in vitro* to disrupt *Pten* and transplanted the resulting *Pten*-null (with or without *T-ERG*) prostate cells to recipient male mice. In addition to this alternative strategy, we have also further optimized the reconstitution assays: (1) we determined the lowest number of UGSM stromal cells required to support prostate cell reconstitution (~2.5 x 10^5 cells); (2) we found that using dissociated prostate sphere cells (rather than fresh primary prostate cells) was much more efficient for reconstitution assay; (3) we also found that we had more success when using the subcutaneous implantation (with Matrigel), rather than using renal capsule (where the cells were suspended in collagen). Based on the Adeno-Cre approach, we found that *Pten*-null only prostate cells formed outgrowths that exhibited infrequent regions with features of low-grade PIN (LG-PIN) lesions, whereas *Pten*-null prostate cells with *T-ERG* formed outgrowths resembling high-grade PIN (HG-PIN) lesions (Figure 8). Thus, the weak-to-no cooperation of *Pten* knockdown with *T-ERG* knockin in our reconstitution assay when using lentiviral shRNA for *Pten* was most likely due to insufficient *Pten* knockdown and/or insufficient lentiviral infection of primary prostate cells.

Tasks 3-5:

These tasks were proposed to perform a small-scale RNAi-based genetic screen with pooled shRNAs for candidate tumor suppressors, validate shRNA hits from the screen, and then validate the affected candidate oncogenic pathways for their potential cooperation with the *Tmprss2-ERG* fusion. As described in our previous annual progress report, since the expected oncogenic cooperation of *T-ERG* with *Pten* knockdown by shRNA was supposed to serve as the positive control for our *in vivo* shRNA screen, yet the cooperation phenotype was too weak to score (as positive) (Figure 1), we were concerned that our originally proposed genetic screen based on shRNA library (even a small customized shRNA library) might not work, as we could not reliably score our

"positive control" in this assay. In addition, recent progress in the field suggested that the prostate reconstitution assay might not be the most ideal system for searching for ETS-cooperating pathways, as this assay is heavily biased toward basal cells (i.e., prostate luminal cells cannot engraft well in this assay), and although both luminal and basal cells could serve as cells of origin of prostate cancer, luminal cells could initiate prostate cancer much more effectively than basal cells, and that the barrier for basal cells to serve as the cellular origin was the need for them to differentiate into luminal cells first [11]. Thus, it appears that prostate luminal cells may serve as the main cellular origin for prostate cancer. We therefore more favor a strategy to search for ETS-cooperating mutations in prostate luminal cells. As stated in the previous annual reports, we favor an alternative approach for the genetic screen by using the potentially more sensitive insertional mutagenesis approach based on the *Sleeping Beauty* (*SB*) transposon-based somatic mutagenesis system. However, this approach would require more time and most likely additional funding. To fulfill our originally proposed goal of identifying additional oncogenic pathways that may cooperate with *ETS* fusions within the funded time window, we used a backup approach. In our original proposal, we proposed to construct a small customized shRNA library containing shRNA hairpins targeting known or predicted tumor suppressors that have been described in literature (e.g., *NKX3.1*, *TEL/ETV6*) or genes that are frequently deleted in human prostate cancer samples (e.g., microdeletion of the interstitial region between *TMPRSS2* and *ERG* on human chromosome 21, which harbors a potential tumor suppressor *ETS2*). Some of these candidate tumor suppressor genes have knockout or conditional knockout mouse alleles available. Among them, we focused on those that have evidence for potential cooperation with *ETS* fusions, including *NKX3.1*, *TEL/ETV6*, interstitial deletion between *TMPRSS2* and *ERG* (e.g., *ETS2*). We determined whether their loss could contribute to prostate tumorigenesis and what candidate oncogenic pathways resulted from their loss would be involved, by both prostate reconstitution assay and mouse genetics. We summarize our research efforts and key findings for candidate/oncogenic pathway validation below, which are related to Tasks 4-5 (validation experiments) in the SOW:

Candidate #1: *NKX3.1*

Test whether *Tmprss2-ETS* fusions cooperate with *Nkx3.1*-loss

In addition to *ETS* gene fusions and aberrant genetic alterations that activate the PI3K pathway (e.g., *PTEN*-loss), another frequent mutational event in prostate cancer is loss of regions within chromosome 8p21, to which the homeobox gene *NKX3.1* maps [12, 13]. Strong evidence supports the notion that loss of *NKX3.1* is an early event in prostate carcinogenesis, as it occurs in up to 85% of PIN lesions and early invasive cancers [14]. *Nkx3.1* is one of the earliest known genes expressed in the developing prostate and subsequent studies have validated its importance in prostate epithelial cell differentiation [14]. Previously expression profiling has defined three subtypes of prostate cancer and among these, the subtype-2 prostate cancer cases, which often exhibit a more aggressive phenotype, have been found to harbor deletions at 8p21 (*NKX3.1*) and 21q22 (resulting in *TMPRSS2-ERG* fusion) [13]; thus, loss of *NKX3.1* has been predicted to synergize with *TMPRSS2-ERG* fusion to promote prostate tumorigenesis, but this has not been validated experimentally. Furthermore, it has also been reported that ERG could lead to epigenetic silencing of *NKX3.1* in prostate cancer cells through induction of the histone methyltransferase EZH2 [15].

While mouse models of *Nkx3.1*-loss do not exhibit signs of prostate cancer [16, 17], they are hyperplastic in their prostates and display cooperativity with *Pten*-loss for prostate cancer development [18], thus offering a sensitized background to test whether *Tmprss2-ETS* fusions exhibit a similar synergy. To that end, we crossed our *T-ERG* knockin mouse line [19] with a previously characterized *Nkx3.1*-null line [16] and analyzed prostate histopathology in aged cohorts. We observed a slight increase in *T-ERG* expression after *Nkx3.1*-loss, consistent with a recent report detailing negative regulation of the *TMPRSS2* locus by NKX3.1 [20] (Figure 2). However, this subtle increase in *T-ERG* fusion expression coupled with *Nkx3.1*-loss did not promote prostate tumorigenesis (Figures 3-4). A similar phenotype was observed for our *T-ETV1* model [19] under the complete *Nkx3.1*-loss background (Figure 5). Collectively these results suggest that although there is a genetic interaction between *Nkx3.1*-loss and *Tmprss2-ERG* gene fusion (to increase the *Tmprss2* promoter activity, Figure 2), this

interaction does not enhance prostate cancer development (Figures 3-5). Our study further highlights the selectivity *TMPRSS2-ETS* fusions have with cooperating mutations.

Candidate #2: Interstitial deletion between *TMPRSS2* and *ERG* (candidate tumor suppressor, *ETS2*)

Test potential contribution of genes deleted in the interstitial region between *Tmprss2* and *Erg* to prostate cancer with *Tmprss2-Erg* gene fusion

The majority of prostate cancer cases with gene rearrangements carry the *TMPRSS2-ERG* fusion [1]. Both *ERG* and *TMPRSS2* are located ~3Mb apart on human chromosome 21. The predominant mechanism to generate the *TMPRSS2-ERG* fusion is the intrachromosomal deletion between these two genes [21-26]. The 3Mb interstitial deletion may lead to haploinsufficiency of one or more genes within this region. In fact, previous studies have suggested that several genes in this region may have tumor/metastasis suppression roles. For example, knockout of one of the genes within this region, *HMGN1*, leads to increased N-cadherin expression [27], which is associated with high-grade prostate cancer [28], and altered G2/M checkpoint [29]. In addition, an ETS family transcription factor gene located in this region, *ETS2*, appears to serve as a tumor suppressor when expressed at an elevated level, as it represses Apc^{min}-mediated tumors in mouse models of Down Syndrome, but not in normal mice (i.e., three copies of *Ets2* in Down Syndrome mouse models versus two copies of *Ets2* in normal mice) [30]; Both point mutation (e.g., R437C) and focal deletions of *ETS2* have been found in prostate cancer, and overexpression of wild-type ETS2 (but not R437C-mutant ETS2) resulted in decreased migration, invasion and proliferation in VCaP cells [31]. Moreover, an interferon-inducible GTPase, MxA, encoded by *MX1*, another gene located in this interstitial region, was shown to express in the human prostate carcinoma cell line PC-3, but not in its highly metastatic derivative PC-3M [32]; this protein suppresses metastasis by inhibiting tumor cell motility and invasion. Combining these together, it seems that reduced expression of one or more genes within this interstitial region may promote prostate tumor progression and metastasis. To date, clinical data regarding potential involvement of the interstitial deletion in prostate tumorigenesis remains contradictory. In a study involving primary prostate cancers and hormone naïve lymph node metastasis, *TMPRSS2-ERG* rearranged tumors through interstitial deletion (the so-called Edel subtype) were found to significantly associate with higher tumor stage and the presence of metastatic disease involving pelvic lymph nodes [25]. In another study, patients with prostate tumors with a duplication of *TMPRSS2-ERG* in combination with deletion of 5'-*ERG* (the 2+Edel subtype) exhibited poor cause specific survival [33]. Furthermore, it has been reported that in androgen-independent metastatic lethal prostate cancers, all metastatic sites harboring the *TMPRSS2-ERG* fusion were associated with the Edel subtype [34]. These studies strongly suggest that the Edel subtype of *TMPRSS2-ERG* fusion is a distinct and aggressive molecular subtype of prostate cancer.

<u>*Tmprss2-Erg* fusion allele with interstitial deletion more strongly cooperates with *Pten*-loss</u>

In our two *Tmprss2-Erg* knockin models, one was generated by knocking in the N-terminus-truncated *ERG* cDNA directly to the mouse *Tmprss2* locus (thus <u>without</u> the interstitial deletion, i.e., the *T-ERG* model), the other was generated by Cre-mediated excision of the interstitial region and subsequent rearrangement of the *Erg* coding region to the *Tmprss2* promoter (i.e., *T-3Mb-Erg* model before excision, *T-Δ-Erg* after excision of the interstitial region). In the presence of biallelic *Pten* inactivation mediated by *Pb-Cre*, however, nearly all *Pb-Cre;T-3Mb-Erg;*$Pten^{L/L}$ male mice developed large poorly differentiated prostate tumors in dorsolateral and ventral lobes by 12 months of age [19]. To determine whether this advanced prostate cancer phenotype is caused by *Tmprss2-Erg* fusion expression or interstitial deletion, or both, we similarly generated *Pb-Cre;T-ERG;*$Pten^{L/L}$ males and characterized their prostate phenotype at 12 months of age. Intriguingly, none of the *Pb-Cre;T-ERG;*$Pten^{L/L}$ males developed poorly differentiated prostate adenocarcinoma at this age (Figure 6A) [compared to almost 100% penetrance for *Pb-Cre;T-3Mb-Erg;*$Pten^{L/L}$ males to develop such advanced prostate cancers (Figure 6B)]. The prostate lesions developed in these males were very similar to those high-grade PIN (HG-PIN) lesions often observed in *Pb-Cre;*$Pten^{L/L}$ control males at this age, although quite surprisingly, HG-PIN lesions developed in many *Pb-Cre;T-ERG;*$Pten^{L/L}$ mice lacked robust stromal proliferation, a common phenotype in the *Pb-Cre;*$Pten^{L/L}$ model [35] (Figure 6A). Furthermore, control *Pb-Cre;*$Pten^{L/L}$ males and *Pb-*

Cre;T-ERG;Pten$^{L/L}$ males only displayed signs of local invasion, which was confirmed through immunohistochemistry (IHC) staining of smooth muscle actin (SMA) (Figure 6A). In stark contrast, *Pb-Cre;T-3Mb-Erg;Pten*$^{L/L}$ males generated invasive prostate tumors that lacked expression of SMA and basal marker p63 (Figure 6A). Such large poorly differentiated prostate adenocarcinomas developed in *Pb-Cre;T-3Mb-Erg;Pten*$^{L/L}$ mice were positive for the prostate luminal epithelial marker Keratin 8 (K8), but are negative for the basal epithelial markers Keratin 5 (K5) (Figure 6C); these males also possessed typical HG-PIN lesions composed of K8^{+} luminal cells surrounded by K5^{+} basal cells that are often observed in the control *Pb-Cre;Pten*$^{L/L}$ males (Figure 6C), as well as localized invasive cancers with microducts mainly composed of K8^{+} prostate luminal cells [with almost no K5^{+} basal cells (Figure 6C), and almost no SMA and p63 expression]. Poorly differentiated adenocarcinomas were never observed in control *Pb-Cre;Pten*$^{L/L}$ control males or *Pb-Cre;T-ERG;Pten*$^{L/L}$ males whereas presence of invasive microducts consistent with moderately differentiated adenocarcinoma were infrequently detected.

Erg overexpression is required for early PIN formation but not advanced tumor progression

The more advanced prostate cancer phenotype observed in *Pb-Cre;T-3Mb-Erg;Pten*$^{L/L}$ mice could be due to cooperation of *Pten*-loss with haploinsufficiency of interstitial genes (since one copy of all these interstitial genes is deleted when Cre-mediated recombination converts the *T-3Mb-Erg* allele to *T-Δ-Erg* allele), or with both interstitial deletion and Erg overexpression. To determine these possibilities, we first examined Erg expression levels in these animal models. Interestingly, in the *Pb-Cre;T-ERG;Pten*$^{L/L}$ model, despite the fact that these mice had largely indistinguishable histology from that of the control *Pb-Cre;Pten*$^{L/L}$ mice, they exhibited strong Erg overexpression in epithelial cells of all prostate lobes (Figure 7A). Conversely, poorly differentiated adenocarcinomas from *Pb-Cre;T-3Mb-Erg;Pten*$^{L/L}$ mice almost completely lacked Erg expression in their prostate tumor cells (Figure 7A). This loss of Erg staining in the more advanced lesions was not attributed to a lack of androgen receptor (AR) expression, which is believed to be positively correlated with *TMPRSS2-ERG* expression in human patient data [21, 25], as even these poorly differentiated tumors are AR positive (Figure 7A). Interestingly, a striking negative correlation of Erg immunostaining was observed with severity of lesions in *Pb-Cre;T-3Mb-Erg;Pten*$^{L/L}$ mice (Figure 7B). Approximately half of epithelial cells within HG-PIN lesions expressed ERG, yet this frequency was lower in invasive microducts (Figure 7C), which lacked basal keratin expression (Figure 7C) and are generally considered to be moderately differentiated adenocarcinomas [35]. Nearly all *Pb-Cre;T-3Mb-Erg;Pten*$^{L/L}$ prostates had these invasive prostate cancer lesions, yet they were only rarely detected in control *Pb-Cre;Pten*$^{L/L}$ or *Pb-Cre;T-ERG;Pten*$^{L/L}$ prostates. Of note, HG-PIN lesions in *Pb-Cre;T-3Mb-Erg;Pten*$^{L/L}$ mice tended to exhibit mosaic Erg overexpression, whereas moderately differentiated adenocarcinoma foci in these mice were homogenously Erg positive or negative (Figure 7B). This suggested that these early prostate cancer lesions were clonally derived, yet only Erg negative lesions might advance to become poorly differentiated adenocarcinoma.

Our data, as well as those from other investigators, demonstrate that Erg overexpression may provide an advantage only during PIN development in the context of *Pten*-loss [7, 8, 19], yet it may not be further required during progression from PIN to prostate adenocarcinoma. To further validate the early requirement of Erg expression during prostate tumorigenesis, we performed a prostate regeneration assay [36]. For this approach *Pb-Cre*-negative prostate cells carrying these conditional alleles were grown as prostate spheres, dissociated, then infected with adenovirus encoding *CMV-Cre* (*Ad-CMV-Cre*). Both *T-ERG;Pten*$^{L/L}$ and *T-3Mb-Erg;Pten*$^{L/L}$ prostate epithelial cells used for this assay formed outgrowths resembling HG-PIN lesions, which were larger and more expansive than outgrowths control from *Pten*$^{L/L}$ cell, which exhibited infrequent regions consistent with LG-PIN (Figure 8). All cells from these outgrowths highly expressed phosphorylated Akt (pAkt), thus confirming Pten-loss due to Cre-mediated excision after adenovirus infection (data not shown). This data thus further confirmed that Erg overexpression is critical for early transformation events. This is in line with human prostate cancer data, where *TMPRSS2-ERG* acquisition has been suggested as an early event in tumorigenesis [37, 38].

Adenocarcinomas and HG-PINs developed in *Pb-Cre;T-3Mb-Erg;Pten*$^{L/L}$ mice exhibited Cre-mediated interstitial deletion

Since prostate lesions developed in *Pb-Cre;T-3Mb-Erg;Pten*$^{L/L}$ mice exhibited progressive loss of Erg overexpression (Figure 7B-C), we wanted to rule out a possibility in which loss of Erg expression was due to reduced efficiency in generating *Tmprss2-Erg* gene fusion from Cre-mediated interstitial deletion. To determine this, we performed laser capture microdissection to isolate epithelial cells from well-defined regions of either HG-PIN (Erg positive) or poorly differentiated adenocarcinoma (Erg negative). We then extracted genomic DNA from these isolated tissues as well as from the whole prostates (i.e., containing both Erg positive and negative lesions) and by genomic DNA PCR analysis (Figure 9A), we verified that in both types of tissues, the *Tmprss2-Erg* gene fusion was generated effectively via Cre-mediated interstitial deletion, despite the lack of Erg overexpression in adenocarcinomas (Figure 9B). Together, these data suggest that by itself Erg overexpression exerts a weaker selective pressure during prostate cancer progression, whereas deletion of the interstitial genes, some of which are likely haploinsufficient, may play a more important role during progression from PIN to adenocarcinoma.

T-Δ-Erg/Pten-null tumors exhibit an EMT phenotype

To investigate the biological mechanisms underlying the more aggressive *T-Δ-Erg/Pten*-null tumors developed in *Pb-Cre;T-3Mb-Erg;Pten*$^{L/L}$ mice, we performed gene expression profiling using laser capture microdissected prostate epithelial cells to reduce stromal contamination. Only cells with round epithelial-like morphology were excised leaving behind spindle-shaped mesenchymal cells. As an internal control for stage specific differences between cancer lesions developed in control *Pb-Cre;Pten*$^{L/L}$ males (i.e., mainly HG-PIN) and *Pb-Cre;T-3Mb-Erg;Pten*$^{L/L}$ males (i.e., poorly differentiated adenocarcinoma and HG-PIN), we also excised HG-PIN lesions from *Pb-Cre;T-3Mb-Erg;Pten*$^{L/L}$ mice for analysis. Among the genes differentially regulated between these 3 groups, gene set enrichment analysis (GSEA) [39] revealed that multiple previously defined epithelial-to-mesenchymal transition (EMT) signatures were enriched in *T-Δ-Erg/Pten*-null tumors compared to control *Pten*-null HG-PIN lesions (Figure 10A). An enrichment of EMT signatures could also be found when comparing *T-Δ-Erg/Pten*-null HG-PIN lesions to *Pten*-null HG-PIN lesions, or when comparing *T-Δ-Erg/Pten*-null tumors to HG-PIN lesions developed in the same mice. These analyses suggested that the EMT signature in the *T-Δ-Erg/Pten*-null tumors was not simply due to a tumor stage difference (i.e., poorly differentiated adenocarcinoma versus HG-PIN), but was acquired progressively during prostate cancer progression when under the interstitial deletion background. We validated the EMT signature using IHC for E-Cadherin and Vimentin, which display epithelial and stromal compartment restricted expression, respectively (Figure 10B). E-Cadherin was highly expressed in the epithelial compartment in HG-PIN lesions in *Pb-Cre;Pten*$^{L/L}$, *Pb-Cre;T-ERG;Pten*$^{L/L}$ and *Pb-Cre;T-3Mb-Erg;Pten*$^{L/L}$ mice, but was downregulated in *T-Δ-Erg/Pten*-null tumors. Inversely, Vimentin displayed strict stromal-specific expression in all HG-PIN lesions yet was abundant within epithelial cells of the *T-Δ-Erg/Pten*-null tumors. In these *Pb-Cre*-based mice, a conditional Cre-reporter *Rosa26-STOP-YFP* (*R26Y*, Cre-mediated excision of a floxed *STOP* cassette in this allele leads to activation of the YFP reporter) was included to track *Pb-Cre*-expressing cells and their daughter cells (i.e., YFP$^+$ prostate epithelial cells). The presence of EMT features was also verified in immunofluorescent (IF) analyses where the epithelial marker K8 and the lineage marker YFP (for genetic marking) overlapped with Vimentin only in tumor cells but not in HG-PIN lesions. This data suggested that although the EMT program was already upregulated in *T-Δ-Erg/Pten*-null HG-PIN lesions at the transcript level, changes in the expression of key EMT markers at the protein level appeared at later tumor stages. Lastly, to rule out a possibility in which the poorly differentiated tumors with mesenchymal features developed in *Pb-Cre;T-3Mb-Erg;Pten*$^{L/L}$ mice were due to a desmoplastic response in the stroma (as a response to invasive prostate cancers developing nearby), similar to what was reported recently for the *Pb-Cre;T-ETV1;Pten*$^{L/L}$ mouse model [19], we stained these tumors for YFP expression and found that they were indeed YFP$^+$, thus confirming that these large poorly differentiated tumors developed in *Pb-Cre;T-3Mb-Erg;Pten*$^{L/L}$ mice were derived from *Pb-Cre*-mediated recombination and therefore of epithelial origin.

Multiple interstitial genes are candidate prostate cancer tumor suppressors

We next examined whether any interstitial genes could function as tumor suppressors during prostate carcinogenesis to explain the more aggressive nature of the *T-Δ-Erg/Pten*-null tumors. To do this, we first generated an "Interstitial genes" gene set composed of protein-coding genes between *TMPRSS2* and *ERG* and then performed GSEA using this gene set. We found that this gene set was significantly downregulated in *T-Δ-Erg/Pten*-null tumors when compared to either *Pten*-null HG-PINs (Figure 11A) or *T-Δ-Erg/Pten*-null HG-PINs (Figure 11B). Among the downregulated interstitial genes, *ETS2* overexpression has previously been shown to decrease proliferation and invasive ability of VCaP prostate cancer cells [31]; however, other genes such as *BRWD1* and *BACE2* have so far not been implicated in prostate cancer development. Based on the availability of usable antibodies, we further analyzed expression of several interstitial genes, including *Ets2*, *Hmgn1*, and *Bace2*, in *T-Δ-Erg/Pten*-null HG-PIN lesions compared to adenocarcinoma at the protein level (Figure 11C). *Bace2* was included as it is the most significantly downregulated gene in the above GSEA analysis (Figure 11A-B). Although *Hmgn1* failed to show up in the GSEA analysis, since it has been implicated in prostate cancer as a potential tumor suppressor [27, 28], we also included it in our validation. Expression at the protein level from these genes was abundantly detected in nuclei and cytoplasm of epithelial cells in HG-PIN lesions. In advanced tumors, expression levels were dramatically decreased, although weak cytoplasmic staining could still be observed (Figure 11C). Interestingly, in our GSEA analysis, although the "Interstitial genes" gene set was not significantly enriched in any of the two groups when we compared HG-PIN lesions from *Pb-Cre;T-3Mb-Erg;Pten*$^{L/L}$ mice to those from *Pb-Cre;Pten*$^{L/L}$ control mice, the above-described interstitial genes such as *Ets2*, *Bace2* and *Brwd1* all exhibited a trend of downregulation in *T-Δ-Erg/Pten*-null HG-PINs. Lastly, using a previously published human prostate cancer cohort [40], we analyzed whether deletion of interstitial genes predicted biochemical relapse to androgen deprivation therapy. Interestingly, only 4 of 17 interstitial genes including *ETS2*, *BRWD1*, *HMGN1*, and *BACE2* were significant for prostate cancer progression (when downregulated), regardless of patient fusion status (Figure 11D). Patients possessing downregulation of the remaining set of interstitial genes did not exhibit differences in disease-free survival compared to those with normal expression levels. Similarly, ERG overexpression was not associated with therapy failure (Figure 11D). Together, these analyses suggest that multiple genes within the *TMPRSS2-ERG* interstitial region might function as tumor suppressors.

Haploinsufficiency of *Ets2* contributes to prostate cancer progression

To directly test whether any interstitial gene could indeed function as a tumor suppressor in prostate cancer, we focused on *Ets2* for which a conditional kockout allele is available (*Ets2*^{L}) [41]. We crossed these mice with *Pten*$^{L/L}$ line to generate *Ets2*$^{L/+}$*;Pten*$^{L/L}$ mice. We then performed the regeneration assay upon *ex vivo* exposure of their prostate cells with *Ad-CMV-Cre*. Similar to Figure 8, *Ad-CMV-Cre*-infected *Pten*$^{L/L}$ control cells formed largely normal ducts with occasional areas of hyperplasia (Figure 12A). In contrast, *Ad-CMV-Cre*-infected *Ets2*$^{L/+}$*;Pten*$^{L/L}$ prostate cells formed small proliferating lesions invading into the lumen, consistent with HG-PIN (Figure 12A). This phenotype was notably weaker than that of the regenerated outgrowths from *Ad-CMV-Cre*-infected *T-3Mb-Erg;Pten*$^{L/L}$ prostate cells (Figure 8), suggesting that other deleted interstitial gene(s) may further contribute to the prostate cancer phenotype. Lastly, we generated *Pb-Cre;Ets2*$^{L/+}$*;Pten*$^{L/L}$ and matched control *Pb-Cre;Pten*$^{L/L}$ male mice. At 6-month of age, we found that although the anterior lobes of both mice developed HG-PIN lesions of similar severity, but the phenotype from the dorsolateral and ventral lobes of the *Pb-Cre;Ets2*$^{L/+}$*;Pten*$^{L/L}$ male was notably stronger. Haploinsufficiency of *Ets2* resulted in larger HG-PIN lesions in both the dorsolateral and ventral lobes while the latter also contained significantly more stromal proliferation and inflammatory infiltrate (Figure 12B). These data are thus consistent with that from our regeneration assay and further confirmed that Ets2 is a tumor suppressor for prostate cancer.

Candidate #3: *TEL/ETV6*

Test ETV6 as a potential tumor suppressor in prostate cancer

ETV6 (also known as TEL) is another ETS family transcription factor and it undergoes hemizygous deletion in about 25% of prostate cancers, suggesting it may function as a tumor suppressor in prostate cancer [12].

Furthermore, a partial deletion of *ETV6* was observed in a hormone naïve metastatic lymph node sample from a *TMPRSS2-ERG* fusion-positive prostate cancer patient [12]. This gene was therefore also included in our original proposal as a candidate tumor suppressor to test in our genetic screen. We investigated a potential tumor suppressor role of this ETS factor in prostate tumorigenesis by breeding a conditional knockout allele of *Etv6* (*Etv6*^{L}) [from Dr. Stuart Orkin's group [42]] to the *Pb-Cre;Pten*$^{L/L}$ background. We found that although *Etv6*-loss alone did not appear to affect prostate cells significantly, it cooperated with full *Pten*-loss (e.g., in *Pb-Cre;Etv6*$^{L/+}$*;Pten*$^{L/L}$ males), leading to development of locally invasive prostate adenocarcinoma [e.g., loss in smooth muscle actin (SMA) staining and presence of invasive ducts (Figure 13)] by 12-months of age. Biallelic *Etv6* loss did not appear to be more aggressive than single copy loss so far (Figure 13). To determine the molecular changes upon *Etv6* loss, we performed laser microdissection of HG-PIN lesions from this model and compared their expression profiling to that of *Pten* loss alone. By GSEA, we found that one of the most profound changes was actually strong negative enrichment of many gene sets for target genes of the histone mark H3K27Me3, which include a gene set generated from prostate cancer PC3 cell line by ChIP-Chip analysis (Figure 14). This would indicate a potential increase in the polycomb complex 2 (PRC2) activity and in the level of the H3K27Me3 histone mark. We performed antibody staining for the H3K27Me3 mark on protate sections from various male mice. We found that even loss of one copy of *Etv6* under the wild-type background already led to global increase in the H3K27Me3 staining intensity (Figure 15). We also observed this increase under the *Pten* loss background (Figure 15), thus confirmed our microarray analysis observation. Thus our study suggests that loss of *Etv6* in prostate cells may increase the activity of the PRC2 complex, this could be due to increased expression of components in the PRC2 complex, including EZH2, EED or SUZ12, which would then lead to increased H3K27Me3 repressive mark and subsequently downregulation of the PRC2 target genes. To determine whether this correlation could be identified in patient tumor samples, we again analyzed the MSKCC cohort [40]. In fact, we found that most of the prostate cancer cases with *ETV6* mRNA downregulation also have increased *EZH2* mRNA, but not those of other PRC2 members, such as *EED* and *SUZ12* (Figure 15). In addition, we found most of PRC2 target genes either from literature, or from that ChIP-Chip study in PC3 cells, also exhibited downregulation (Figure 16). Thus, we provided definitive evidence to show that ETV6 is a tumor suppressor in prostate cancer. Since previous studies showed that *ERG* overexpression may upregulate *EZH2* and promote EZH2-mediated dedifferentiation [43], loss of *ETV6* may cooperate with *TMPRSS2-ERG* via further downregulation of PRC2 targets.

KEY RESEARCH ACCOMPLISHMENTS:

1. Characterized several *Tmprss2-ETS* knockin mouse models we generated and published our initial work in *Genes and Development*.
2. Demonstrated a genetic interaction between *Nkx3.1*-loss and *Tmprss2-ERG* fusion *in vivo* and provided genetic evidence to show that this interaction is not sufficient to cooperate with *Tmprss2-ETS* fusions for the development of prostate cancer.
3. Obtained genetic evidence to support that the interstitial deletion in *TMPRSS2-ERG* fusion positive cases (with deletion) also contributes to development of advanced prostate cancer.
4. Validated *ETS2* in the interstitial region as a tumor suppressor in prostate cancer.
5. Obtained the genetic evidence to support that ETV6 is a tumor suppressor in prostate cancer.
6. Demonstrated that loss of ETV6 potentially contributes to prostate tumorigenesis via downregulation of PRC2 targets.

CONCLUSION:

In conclusion, we have thoroughly characterized three *Tmprss2-ETS* knockin mouse models we generated. We found that although ectopic expression of ERG or ETV1 sensitizes prostate cells for cooperation with oncogenic

pathways, such as activation of the PI3K pathway (due to *Pten* loss), they do not appear to cooperate with the oncogenic pathway due to *Nkx3.1* loss. In addition to these observations, we found that genes deleted in the interstitial region between *Tmprss2* and *Erg* appear to cooperate with *Pten*-loss, or both *Pten*-loss and ectopic *Tmprss2-Erg* expression (at the early stage), leading to development of invasive prostate cancer. We validated *ETS2*, another ETS family TF gene in the interstitial region as a tumor suppressor in prostate cancer. Furthermore, by focusing on another ETS family transcription factor, ETV6, which is deleted in some prostate cancer cases (including *TMPRSS2-ERG* fusion positive case), we found that ETV6 is also a tumor suppressor in prostate cancer. Although loss of *Etv6* alone did not seem to affect prostate cells, loss of one copy of *Etv6* was sufficient to cooperate with *Pten*-loss, leading to development of invasive prostate cancer. Mechanistic study showed that loss of ETV6 may contribute to prostate cancer development via downregulation of PRC2 targets. Since both ETS2 and ETV6 are ETS family TFs that are normally expressed in prostate epithelial cells (whereas ETS factors involved in gene fusions, such as ERG and ETV1, are not expressed in normal prostate epithelial cells), our study suggests that there may exist a network of ETS family TFs and oncogenic ETS TFs (e.g., ERG and ETV1) may contribute to prostate tumorigenesis by disrupting the normal functions (e.g., via competition) of tumor suppressive ETS TFs (e.g., ETS2 and ETV6).

PUBLICATIONS, ABSTRACTS, AND PRESENTATIONS:

Manuscript already published:

1. Baena E, Shao Z, Linn DE, Glass K, Hamblen MJ, Fujiwara Y, Kim J, Nguyen M, Zhang X, Godinho FJ, Bronson RT, Mucci LA, Loda M, Yuan GC, Orkin SH, Li Z. ETV1 directs androgen metabolism and confers aggressive prostate cancer in targeted mice and patients. ***Genes Dev***. 2013;27(6):683-98. PMCID: PMC3613614.

Manuscript under consideration:

1. Linn DE, Bronson RT, Li Z. Genetic interaction between Tmprss2-ERG gene fusion and Nkx3.1-loss does not enhance prostate tumorigenesis in mouse models. *In revision with* ***PLoS One,*** 2015.

Manuscript in preparation:

1. Linn DE, Penney KL, Bronson RT, Mucci LA, Li Z. Haploinsufficiency of interstitial genes between TMPRSS2 and ERG contributes to prostate tumorigenesis. *Manuscript in preparation*, 2015.

Presentation:

Li Z. Tumor suppressors in prostate cancers with TMPRSS2-ERG gene fusions. DF/HCC SPORE in Prostate Cancer Meeting, May 2014.

INVENTIONS, PATENTS AND LICENSES:

Nothing to report.

REPORTABLE OUTCOMES:

Nothing to report.

OTHER ACHIEVEMENTS:

Funding received based on work supported by this award:
Dana-Farber/Harvard Cancer Center sponsored A. David Mazzone Research Awards Program: Castration-Resistant Luminal Cells in the Prostate (08/01/2012 - 07/31/2014).

REFERENCES:

1. Tomlins, S.A., et al., *Recurrent fusion of TMPRSS2 and ETS transcription factor genes in prostate cancer.* Science, 2005. **310**(5748): p. 644-8.
2. Shah, R.B. and A.M. Chinnaiyan, *The discovery of common recurrent transmembrane protease serine 2 (TMPRSS2)-erythroblastosis virus E26 transforming sequence (ETS) gene fusions in prostate cancer: significance and clinical implications.* Adv Anat Pathol, 2009. **16**(3): p. 145-53.
3. Carver, B.S., et al., *ETS rearrangements and prostate cancer initiation.* Nature, 2009. **457**(7231): p. E1; discussion E2-3.
4. Klezovitch, O., et al., *A causal role for ERG in neoplastic transformation of prostate epithelium.* Proc Natl Acad Sci U S A, 2008. **105**(6): p. 2105-10.
5. Tomlins, S.A., et al., *Distinct classes of chromosomal rearrangements create oncogenic ETS gene fusions in prostate cancer.* Nature, 2007. **448**(7153): p. 595-9.
6. Tomlins, S.A., et al., *Role of the TMPRSS2-ERG gene fusion in prostate cancer.* Neoplasia, 2008. **10**(2): p. 177-88.
7. Carver, B.S., et al., *Aberrant ERG expression cooperates with loss of PTEN to promote cancer progression in the prostate.* Nat Genet, 2009. **41**(5): p. 619-24.
8. King, J.C., et al., *Cooperativity of TMPRSS2-ERG with PI3-kinase pathway activation in prostate oncogenesis.* Nat Genet, 2009. **41**(5): p. 524-6.
9. Han, B., et al., *Fluorescence in situ hybridization study shows association of PTEN deletion with ERG rearrangement during prostate cancer progression.* Mod Pathol, 2009.
10. Holcomb, I.N., et al., *Comparative analyses of chromosome alterations in soft-tissue metastases within and across patients with castration-resistant prostate cancer.* Cancer Res, 2009. **69**(19): p. 7793-802.
11. Choi, N., et al., *Adult murine prostate basal and luminal cells are self-sustained lineages that can both serve as targets for prostate cancer initiation.* Cancer Cell, 2012. **21**(2): p. 253-65.
12. Demichelis, F., et al., *Distinct genomic aberrations associated with ERG rearranged prostate cancer.* Genes Chromosomes Cancer, 2009.
13. Lapointe, J., et al., *Genomic profiling reveals alternative genetic pathways of prostate tumorigenesis.* Cancer Res, 2007. **67**(18): p. 8504-10.
14. Shen, M.M. and C. Abate-Shen, *Molecular genetics of prostate cancer: new prospects for old challenges.* Genes Dev, 2010. **24**(18): p. 1967-2000.
15. Kunderfranco, P., et al., *ETS transcription factors control transcription of EZH2 and epigenetic silencing of the tumor suppressor gene Nkx3.1 in prostate cancer.* PLoS ONE, 2010. **5**(5): p. e10547.
16. Bhatia-Gaur, R., et al., *Roles for Nkx3.1 in prostate development and cancer.* Genes Dev, 1999. **13**(8): p. 966-77.
17. Tanaka, M., et al., *Nkx3.1, a murine homolog of Ddrosophila bagpipe, regulates epithelial ductal branching and proliferation of the prostate and palatine glands.* Dev Dyn, 2000. **219**(2): p. 248-60.
18. Kim, M.J., et al., *Cooperativity of Nkx3.1 and Pten loss of function in a mouse model of prostate carcinogenesis.* Proc Natl Acad Sci U S A, 2002. **99**(5): p. 2884-9.
19. Baena, E., et al., *ETV1 directs androgen metabolism and confers aggressive prostate cancer in targeted mice and patients.* Genes Dev, 2013. **27**(6): p. 683-98.
20. Thangapazham, R., et al., *Loss of the NKX3.1 tumorsuppressor promotes the TMPRSS2-ERG fusion gene expression in prostate cancer.* BMC Cancer, 2014. **14**: p. 16.

21. Hermans, K.G., et al., *TMPRSS2:ERG fusion by translocation or interstitial deletion is highly relevant in androgen-dependent prostate cancer, but is bypassed in late-stage androgen receptor-negative prostate cancer.* Cancer Res, 2006. **66**(22): p. 10658-63.
22. Iljin, K., et al., *TMPRSS2 fusions with oncogenic ETS factors in prostate cancer involve unbalanced genomic rearrangements and are associated with HDAC1 and epigenetic reprogramming.* Cancer Res, 2006. **66**(21): p. 10242-6.
23. Liu, W., et al., *Comprehensive assessment of DNA copy number alterations in human prostate cancers using Affymetrix 100K SNP mapping array.* Genes Chromosomes Cancer, 2006. **45**(11): p. 1018-32.
24. Mehra, R., et al., *Comprehensive assessment of TMPRSS2 and ETS family gene aberrations in clinically localized prostate cancer.* Mod Pathol, 2007. **20**(5): p. 538-44.
25. Perner, S., et al., *TMPRSS2:ERG Fusion-Associated Deletions Provide Insight into the Heterogeneity of Prostate Cancer.* Cancer Res, 2006. **66**(17): p. 8337-41.
26. Yoshimoto, M., et al., *Three-color FISH analysis of TMPRSS2/ERG fusions in prostate cancer indicates that genomic microdeletion of chromosome 21 is associated with rearrangement.* Neoplasia, 2006. **8**(6): p. 465-9.
27. Rubinstein, Y.R., et al., *Chromosomal protein HMGN1 modulates the expression of N-cadherin.* Febs J, 2005. **272**(22): p. 5853-63.
28. Jaggi, M., et al., *N-cadherin switching occurs in high Gleason grade prostate cancer.* Prostate, 2006. **66**(2): p. 193-9.
29. Birger, Y., et al., *Increased tumorigenicity and sensitivity to ionizing radiation upon loss of chromosomal protein HMGN1.* Cancer Res, 2005. **65**(15): p. 6711-8.
30. Sussan, T.E., et al., *Trisomy represses Apc(Min)-mediated tumours in mouse models of Down's syndrome.* Nature, 2008. **451**(7174): p. 73-5.
31. Grasso, C.S., et al., *The mutational landscape of lethal castration-resistant prostate cancer.* Nature, 2012. **487**(7406): p. 239-43.
32. Mushinski, J.F., et al., *Inhibition of tumor cell motility by the interferon-inducible GTPase MxA.* J Biol Chem, 2009. **284**(22): p. 15206-14.
33. Attard, G., et al., *Duplication of the fusion of TMPRSS2 to ERG sequences identifies fatal human prostate cancer.* Oncogene, 2008. **27**(3): p. 253-63.
34. Mehra, R., et al., *Characterization of TMPRSS2-ETS gene aberrations in androgen-independent metastatic prostate cancer.* Cancer Res, 2008. **68**(10): p. 3584-90.
35. Ittmann, M., et al., *Animal models of human prostate cancer: the consensus report of the New York meeting of the Mouse Models of Human Cancers Consortium Prostate Pathology Committee.* Cancer Res, 2013. **73**(9): p. 2718-36.
36. Lukacs, R.U., et al., *Isolation, cultivation and characterization of adult murine prostate stem cells.* Nat Protoc, 2010. **5**(4): p. 702-13.
37. Kumar-Sinha, C., S.A. Tomlins, and A.M. Chinnaiyan, *Recurrent gene fusions in prostate cancer.* Nat Rev Cancer, 2008. **8**(7): p. 497-511.
38. Park, K., et al., *TMPRSS2:ERG gene fusion predicts subsequent detection of prostate cancer in patients with high-grade prostatic intraepithelial neoplasia.* J Clin Oncol, 2014. **32**(3): p. 206-11.
39. Subramanian, A., et al., *Gene set enrichment analysis: a knowledge-based approach for interpreting genome-wide expression profiles.* Proc Natl Acad Sci U S A, 2005. **102**(43): p. 15545-50.
40. Taylor, B.S., et al., *Integrative genomic profiling of human prostate cancer.* Cancer Cell, 2010. **18**(1): p. 11-22.
41. Tynan, J.A., et al., *Ets2-dependent microenvironmental support of mouse mammary tumors.* Oncogene, 2005. **24**(46): p. 6870-6.
42. Hock, H., et al., *Tel/Etv6 is an essential and selective regulator of adult hematopoietic stem cell survival.* Genes Dev, 2004. **18**(19): p. 2336-41.
43. Yu, J., et al., *An integrated network of androgen receptor, polycomb, and TMPRSS2-ERG gene fusions in prostate cancer progression.* Cancer Cell, 2010. **17**(5): p. 443-54.

APPENDICES:

Baena et al., *Genes Dev.* 27:683-98 is attached at the end of this file.

Supporting data: include Figures 1-16 (starting from next page).

SUPPORTING DATA: **Figures 1-16**

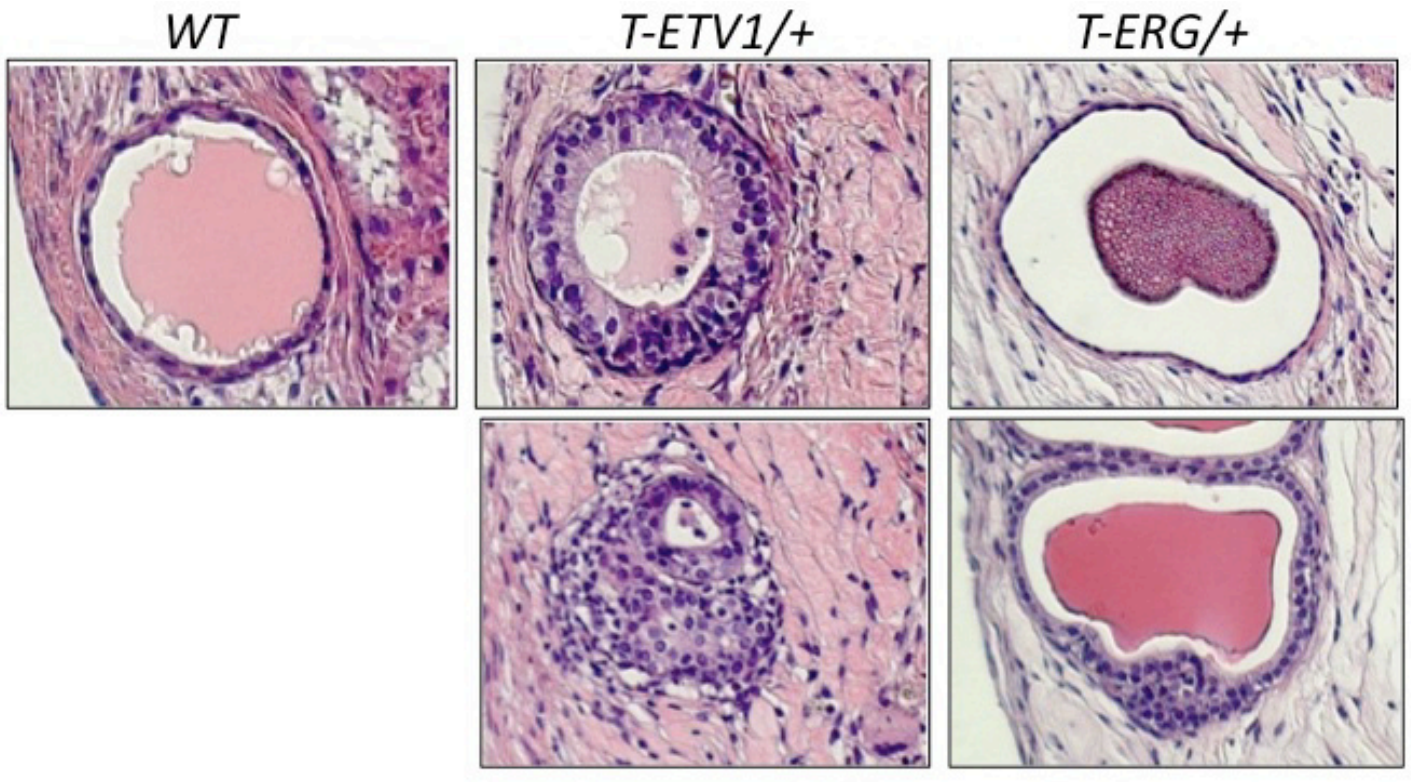

Figure 1. Renal capsule reconstitution of transplanted prostate cells. Prostate cells with the indicated genotypes were infected by lentivirus expressing shRNA for *Pten* before transplantation. *Pten* knockdown appears to cooperate with *T-ETV1* knockin (middle) moderately; but it only appears to cooperate with *T-ERG* knockin (right) very weakly, if any.

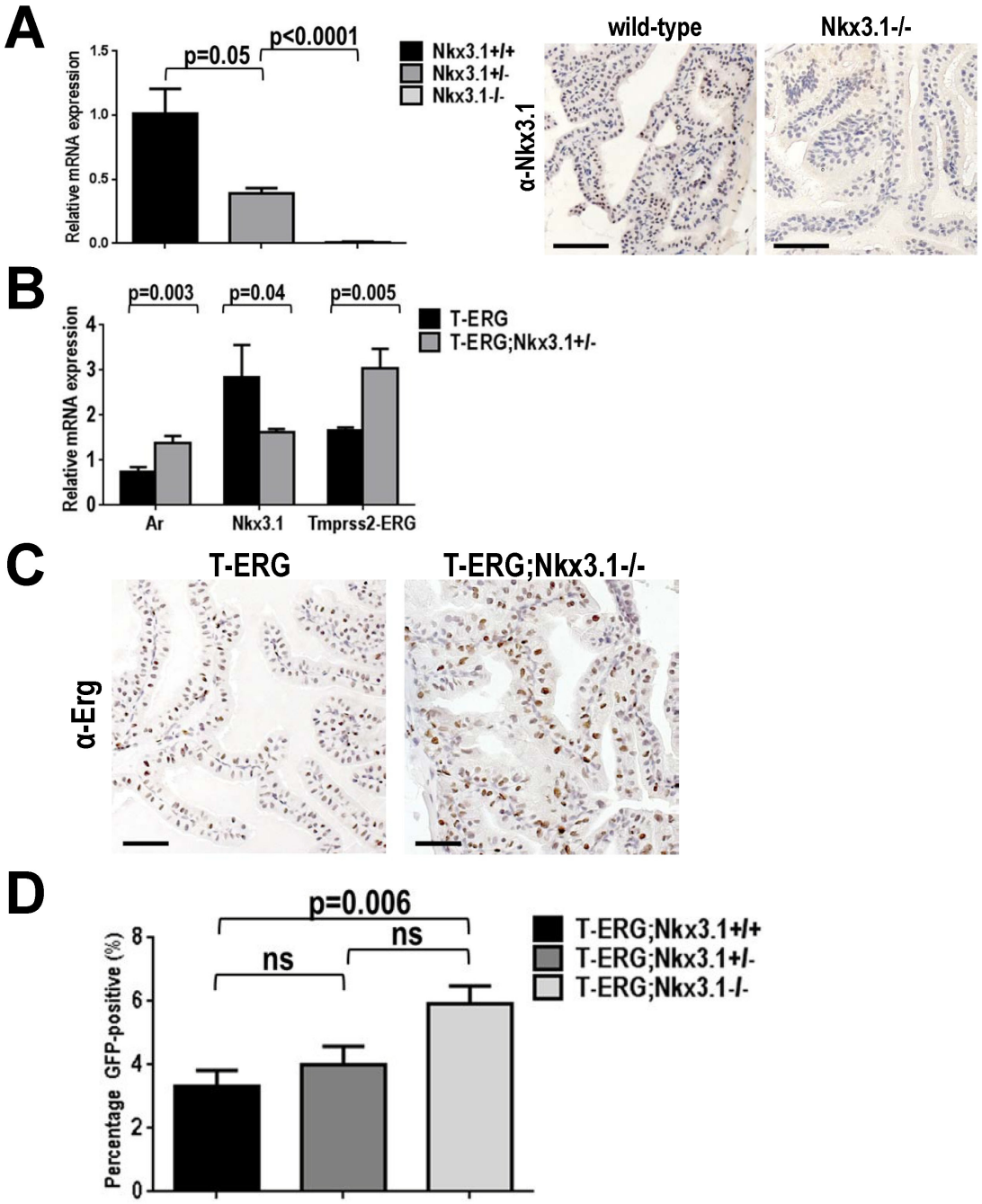

Figure 2. *Nkx3.1*-loss modestly increases the *Tmprss2* promoter activity *in vivo*.

A. Progressive *Nkx3.1* transcript loss was confirmed in wild type (black) and heterozygous (dark gray) and homozygous (light gray) *Nkx3.1* knockout mice by real-time RT-PCR (left). Immunohistochemical (IHC) staining using a mouse-specific Nkx3.1 antibody also validated Nkx3.1 protein loss.

B. Real-time RT-PCR showing slight but statistically significant increase in the *Tmprss2-ERG* expression in *T-ERG;Nkx3.1*$^{+/-}$ double heterozygous males.

C. Immunohistochemical (IHC) staining showing increase in ectopic ERG expression at the protein level from the *T-ERG* knockin allele under the *Nkx3.1*-null background (*T-ERG;Nkx3.1*$^{-/-}$).

D. FACS analysis showing progressive increase in the percentage of GFP^{+} cells in the prostates of *T-ERG;Nkx3.1*$^{+/-}$ and *T-ERG;Nkx3.1*$^{-/-}$ males, compared to those of males with *T-ERG* alone.

Statistics: *p* values from Student t-test are indicated; ns = not significant. Scale bars represent 50μm.

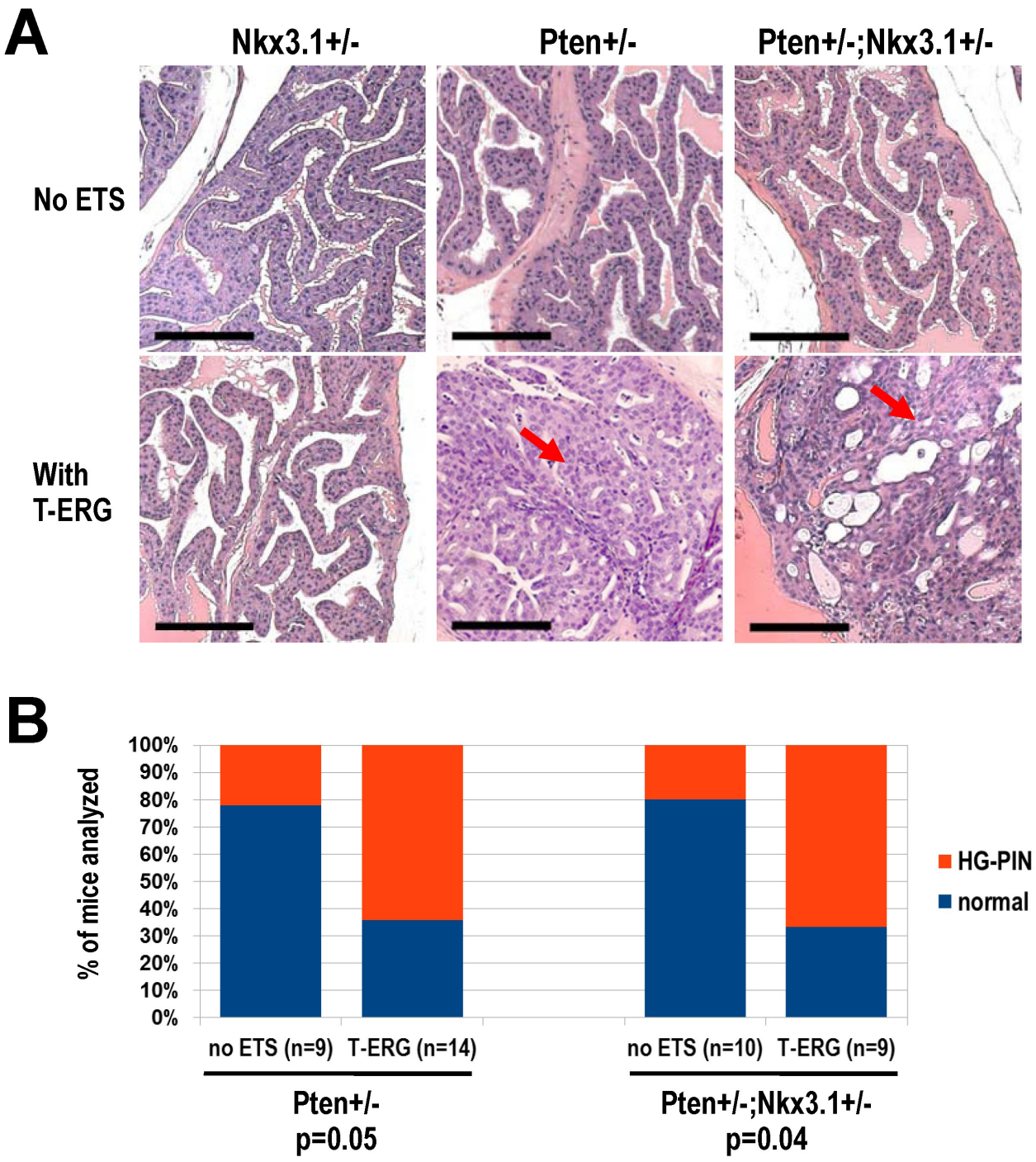

Figure 3. Heterozygous *Nkx3.1*-loss does not strongly cooperate with *Pten*-loss and *Tmprss2-ERG* expression.

A. Representative histology of male mice with the indicated combinations of *Nkx3.1*$^{+/-}$, *Pten*$^{+/-}$, and *T-ERG* knockin. Red arrows: HG-PIN lesions due to cooperation between *Pten*$^{+/-}$ and *T-ERG*. Scale bars represent 100μm.

B. Histology summary of aged *Pten*$^{+/-}$ (left) and *Pten*$^{+/-}$*;Nkx3.1*$^{+/-}$ (right) male mice with or without the *T-ERG* knockin allele. Notable cooperation was detected with *T-ERG* (p=0.05 under the *Pten*$^{+/-}$ background and p=0.04 under the *Pten*$^{+/-}$*;Nkx3.1*$^{+/-}$ background). HG-PIN in any prostate lobe was diagnosed by a trained rodent pathologist.

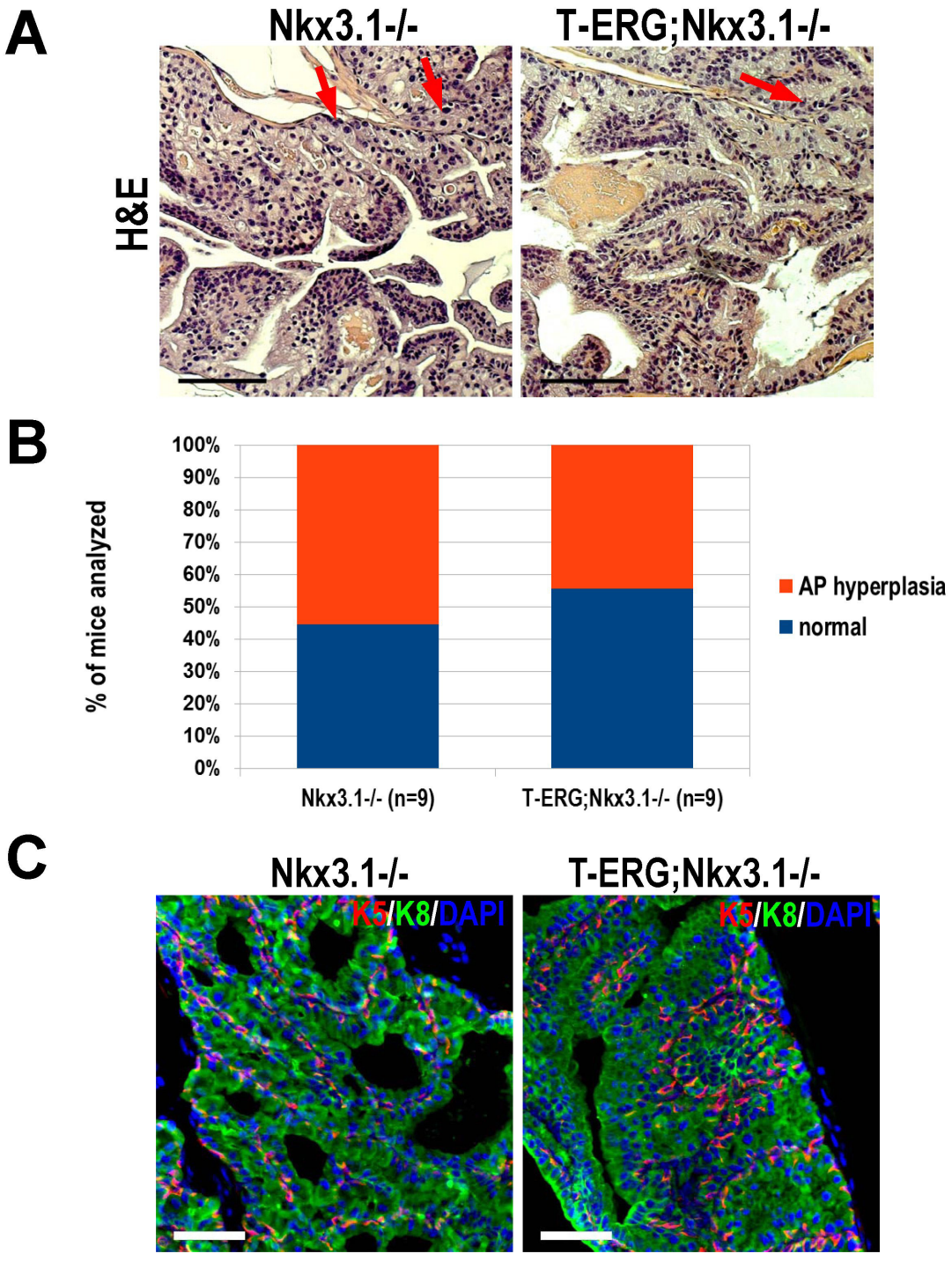

Figure 4. Total *Nkx3.1*-loss does not cooperate with *Tmprss2-ERG* gene fusion to promote prostate tumorigenesis.

A. Representative histology of *Nkx3.1*$^{-/-}$ (left) and *T-ERG;Nkx3.1*$^{-/-}$ (right) mouse prostates stained with H&E. Scarce pleomorphic nuclei are evident (red arrows). Scale bars represent 100µm.

B. Graphical summary of histological findings of *Nkx3.1*$^{-/-}$ and *T-ERG;Nkx3.1*$^{-/-}$ male mice. There was no significant difference in anterior lobe (AP) hyperplasia frequency (p=0.63). Histology was diagnosed by a trained rodent pathologist.

C. IF staining for respective basal keratin 5 (K5, red) and luminal keratin 8 (K8, green) to visualize prostate architecture in *Nkx3.1*$^{-/-}$ and *T-ERG;Nkx3.1*$^{-/-}$ mice. Nuclei counterstained with DAPI (blue). Scale bars represent 50µm.

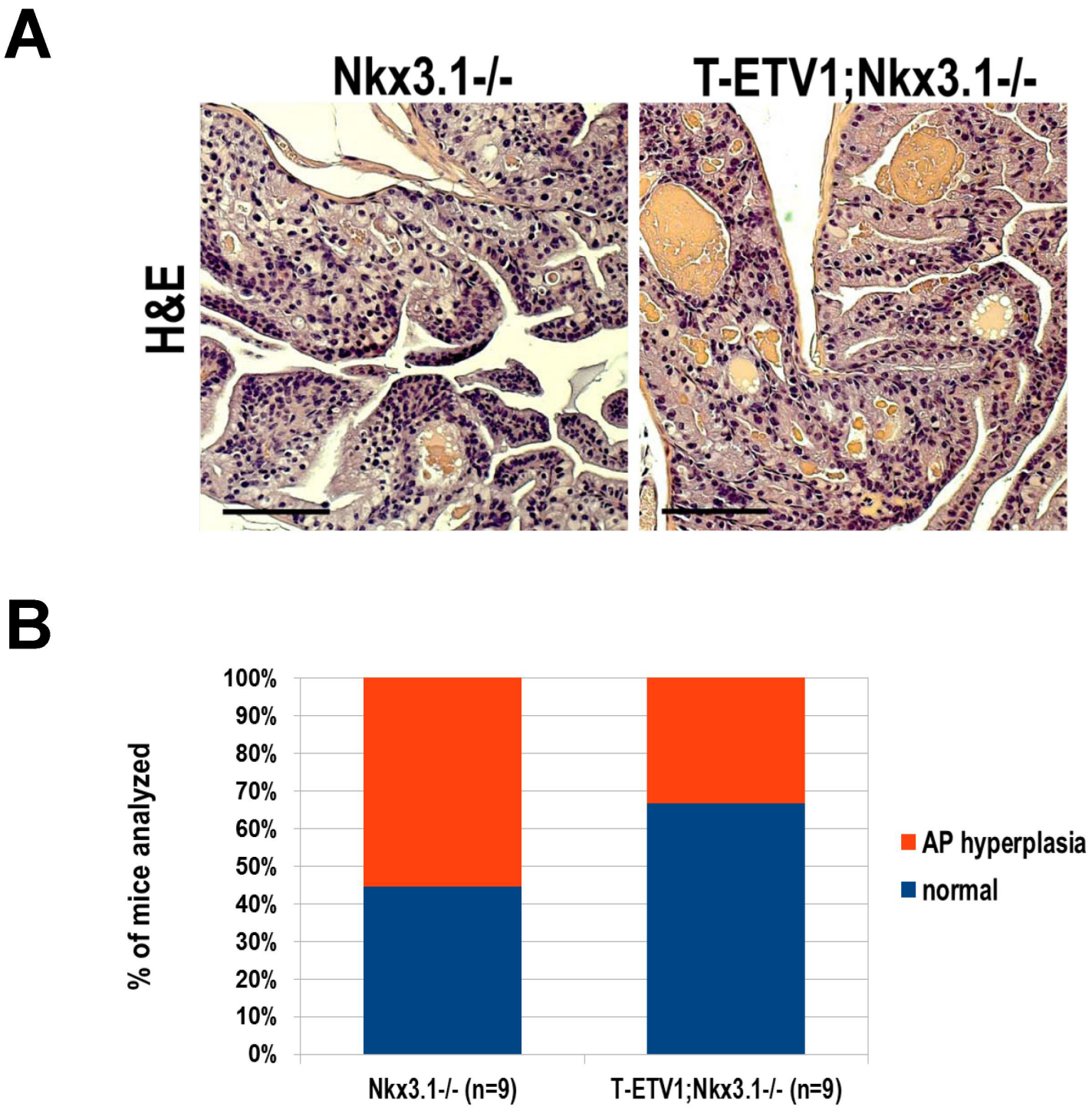

Figure 5. *Nkx3.1*-loss does not cooperate with *Tmprss2-ETV1* expression.
A. Representative histology of *T-ETV1;Nkx3.1*$^{-/-}$ and *Nkx3.1*$^{-/-}$ prostates in aged mice. H&E stained anterior prostate (AP) is shown. Scale bar represents 100μm.
B. Graphical summary of histology results from all animals analyzed as shown in A.

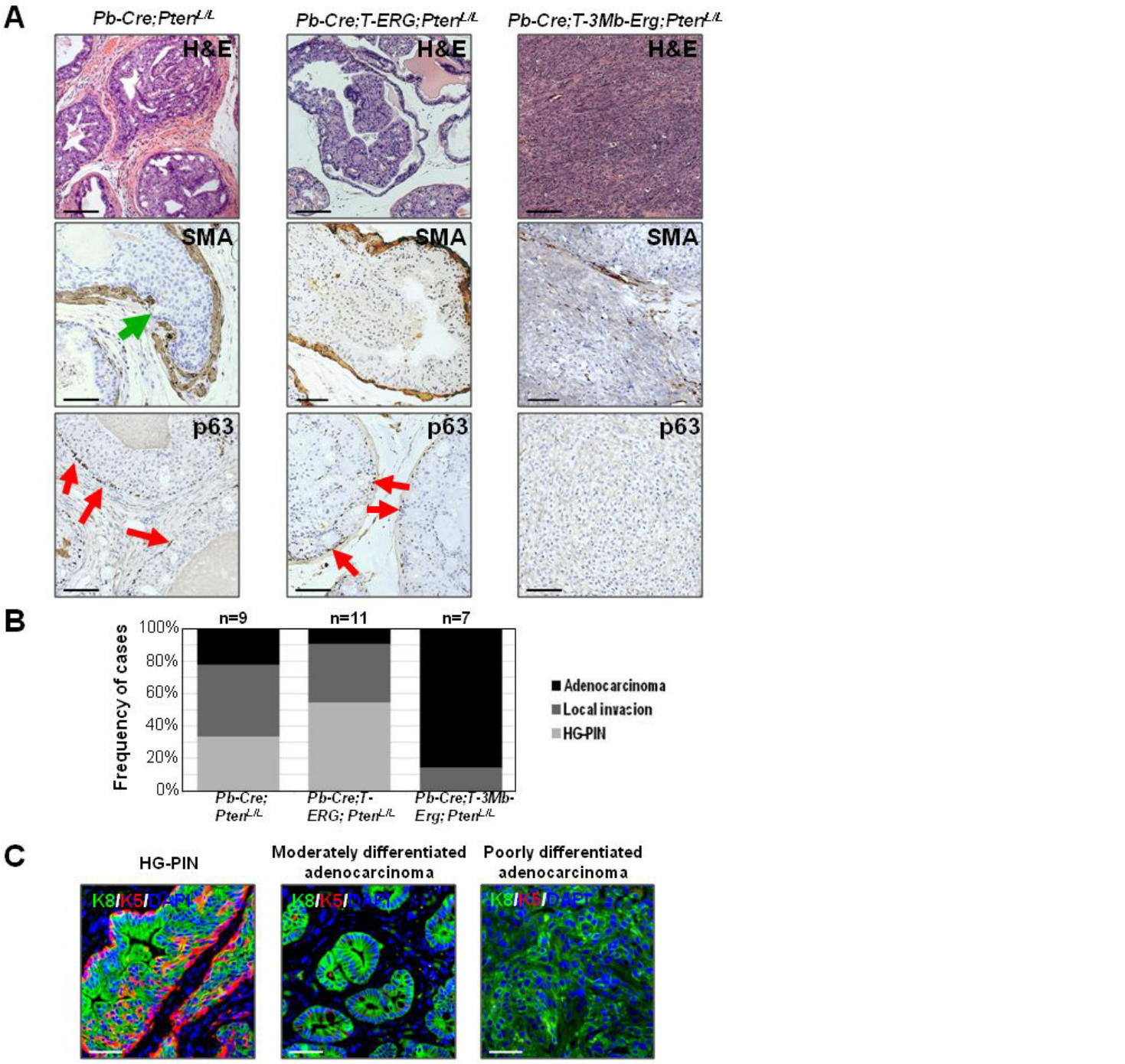

Figure 6. *Tmprss2-Erg* gene fusion generated through interstitial deletion more strongly cooperates with *Pten*-loss.

A. Representative haematoxylin and eosin (H&E) staining (top row), SMA IHC staining (middle row), and p63 IHC staining (bottom row) of prostate sections from mice with the indicated genotypes. Green arrow denotes discontinuous SMA staining and emergence of epithelial cells through basement membrane. Loss of basal marker p63 was used to validate adenocarcinoma. Red arrows denote p63-expressing ($p63^{+}$) basal cells. Scale bars are 100μm for H&E and 50μm for SMA and p63 staining.

B. Graphical summary of dominant histological lesions observed in aged mouse models of *Tmprss2-Erg* fusions with (*T-3Mb-Erg*) or without (*T-ERG*) interstitial deletion.

C. Progressive lesions developed in *Pb-Cre;T-3Mb-Erg;Pten*$^{L/L}$ mice. IF staining for luminal marker K8 (green), basal marker K5 (red), and DAPI (blue) showing progress loss of $K5^{+}$ basal cells in moderately and poorly differentiated adenocarcinomas. Scale bars are 50μm.

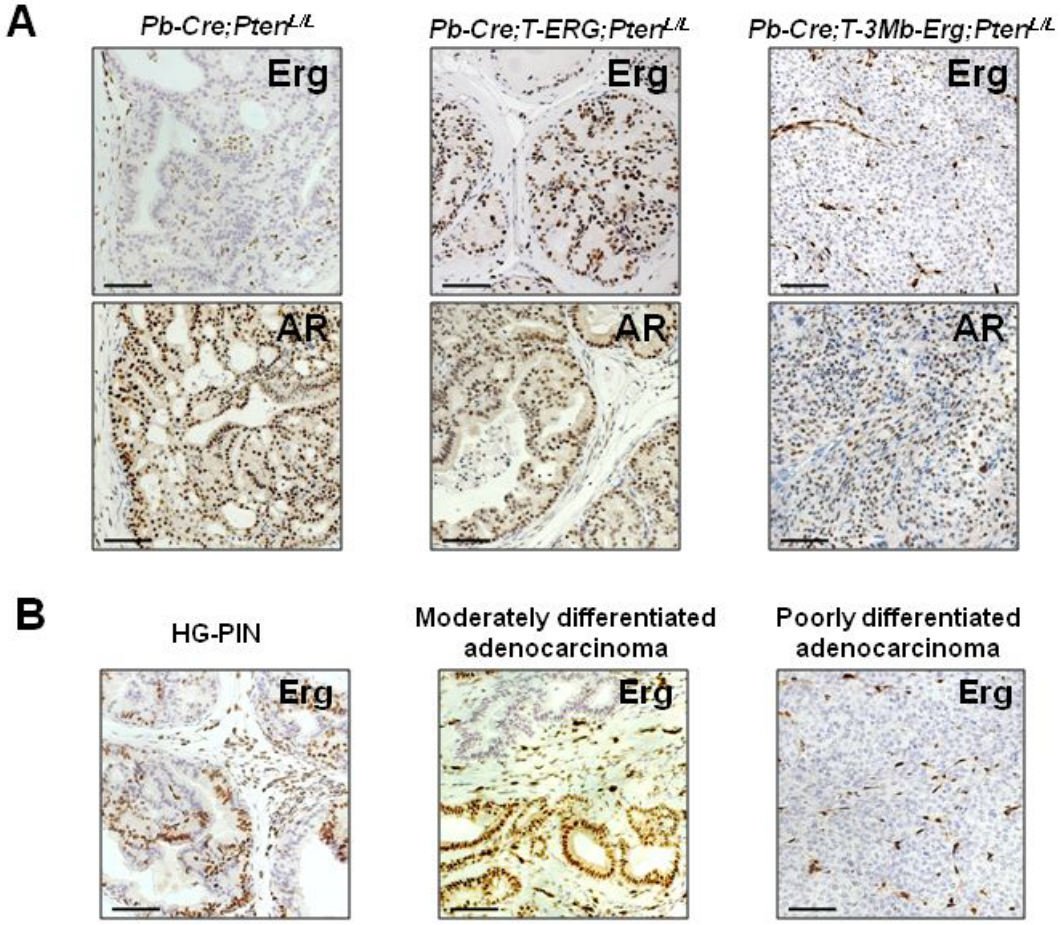

C

Genotype	Tissue type	Erg positivity (%)
Pb-Cre;T-ERG;Pten$^{L/L}$	HG-PIN	1160/1245 = 93.2%
Pb-Cre;T-3Mb-Erg;Pten$^{L/L}$	HG-PIN	1514/3104 = 48.8%
	MD adenocarcinoma	732/2306 = 31.7%
	PD adenocarcinoma	3/1569 = 0.002%

Figure 7. Erg overexpression required for early PIN formation but not for advanced tumor progression.
A. IHC staining depicting Erg (top row) and AR (bottom row) expression in typical prostate lesions from various *Tmprss2-Erg* models. Erg-positive endothelial cells (i.e., brown cells in section from *Pb-Cre;Pten$^{L/L}$* control) serve as an internal control for Erg staining in all models. Scale bars are 100μm.
B. Progressive lesions developed in *Pb-Cre;T-3Mb-Erg;Pten$^{L/L}$* mice. IHC staining for Erg showing progressive loss of Erg positivity in advanced cancer lesions. Scale bars are 50μm.
C. Summary of percentage of Erg-positive epithelial cells in *T-ERG;Pten*-null and *T-Δ-Erg;Pten*-null lesions.

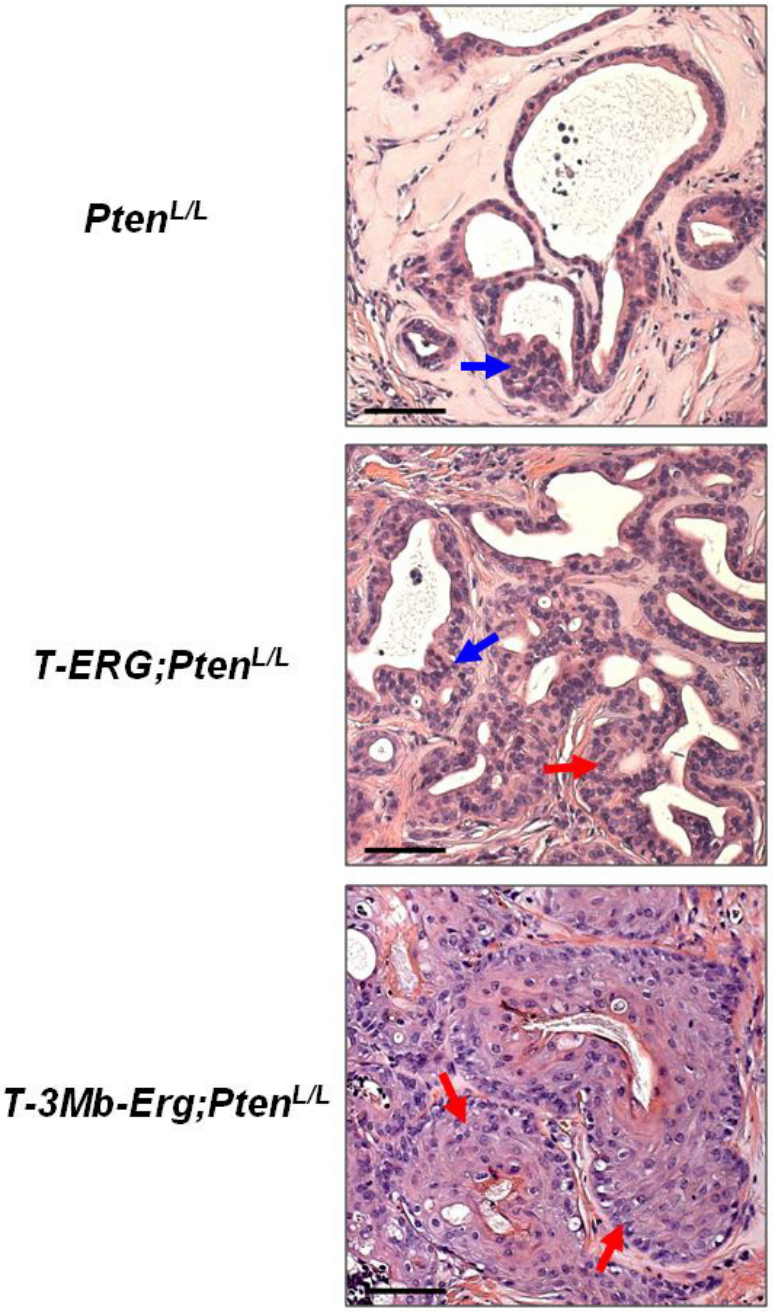

Figure 8. Prostate regeneration assay showing cooperation of ectopic Erg expression with *Pten*-loss. Prostate regeneration assay using *Pten*$^{L/L}$, *T-ERG;Pten*$^{L/L}$ or *T*-Δ-*Erg;Pten*$^{L/L}$ cells infected with Cre-expressing adenovirus prior to implantation. Blue arrows denote low-grade PIN (LG-PIN) while red arrows denote high-grade (HG-PIN) lesions. Scale bars are 50μm.

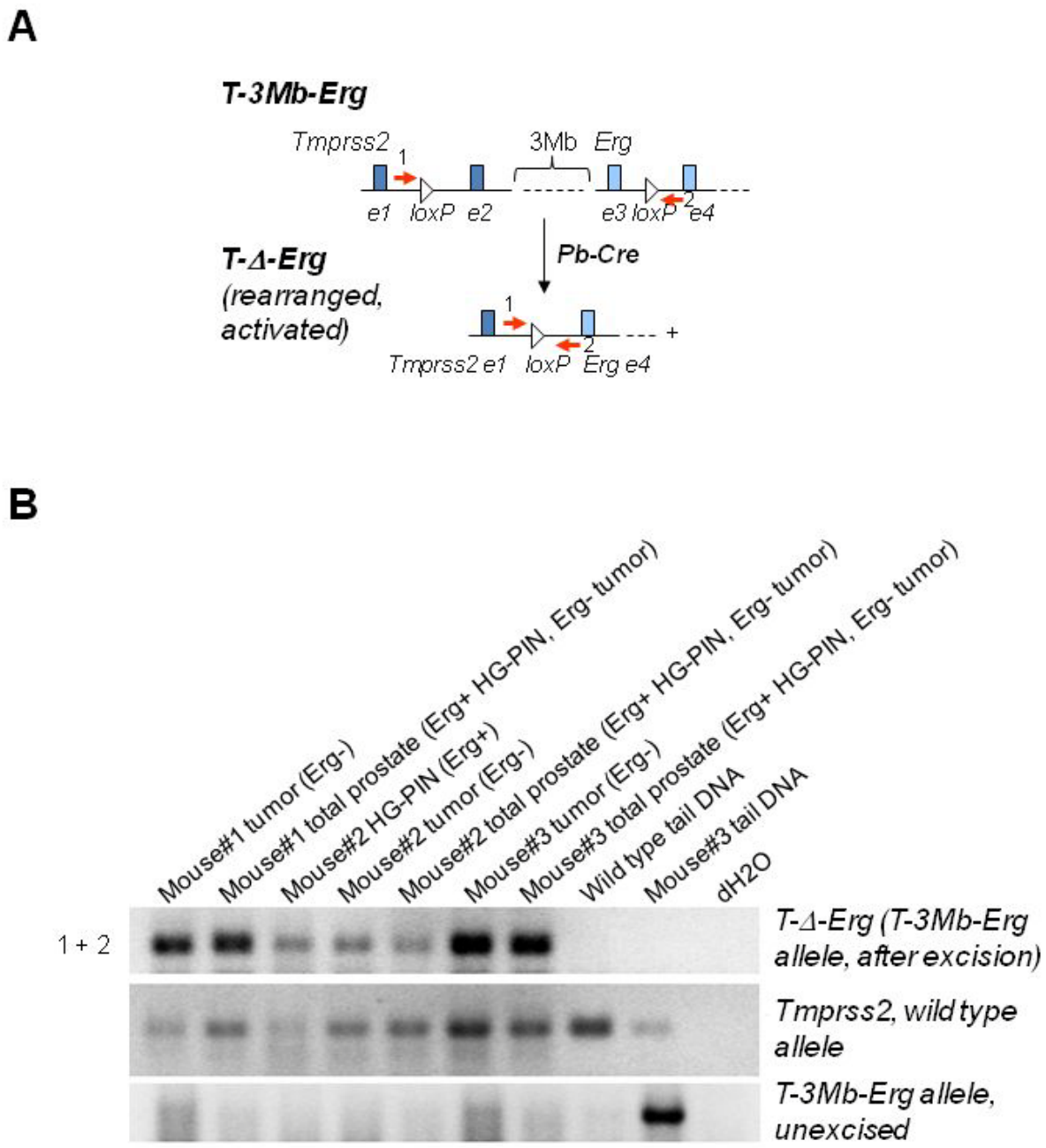

Figure 9. Confirmation of Cre-mediated deletion in *T-Δ-Erg;Pten*-null lesions

A. Schematic diagram showing PCR strategy (primers 1+2) to detect Cre-mediated excision of the 3Mb interstitial region and generation of the *Tmprss2-Erg* fusion at the same time.

B. PCR analysis of genomic DNA prepared from HG-PIN lesions (Erg^{+}) or large poorly differentiated adenocarcinomas (Erg^{-}) isolated from *Pb-Cre;T-3Mb-Erg;*$Pten^{L/L}$ prostates by laser-capture microdissection confirmed Cre-mediated excision and creation of the *Tmprss2-Erg* gene fusion (detected by primers 1 and 2); primers specific for the wild type *Tmprss2* allele and the unexcised *T-3Mb-Erg* allele were used as controls. All three mice (Mouse #1-3) were *Pb-Cre;T-3Mb-Erg;*$Pten^{L/L}$ males.

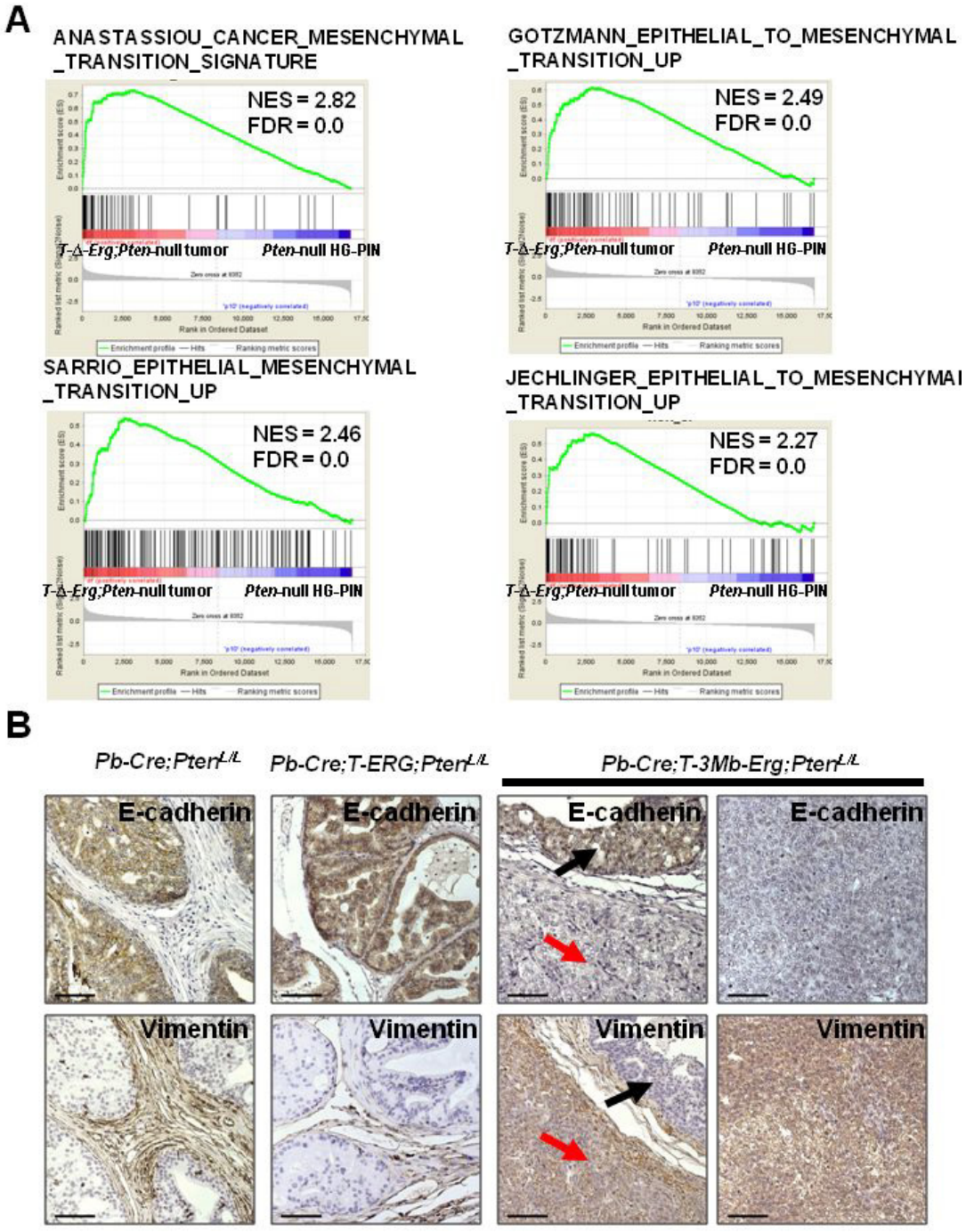

Figure 10. *T*-Δ-*Erg/Pten*-null tumors exhibit an EMT phenotype.
A. GSEA results showing highly significant (FDR<0.25) enrichment of multiple EMT gene sets in *T*-Δ-*Erg/Pten*-null tumors in relation to HG-PIN lesions in *Pb-Cre;Pten*$^{L/L}$ control males. The gene sets are from the c2 CGP (chemical and genetic perturbations) collection of MSigDB (http://www.broadinstitute.org/gsea/msigdb/index.jsp).
B. IHC confirmation of EMT features in *T*-Δ-*Erg/Pten*-null tumors using E-cadherin (top rows) and Vimentin (bottom rows) staining. Control *Pten*-null and *T-ERG/Pten*-null HG-PINs (left panels), *T*-Δ-*Erg/Pten*-null HG-PIN (middle panel, black arrows), and *T*-Δ-*Erg/Pten*-null tumors (middle panel, red arrows; right panel) are shown. Scale bars are 50μm.

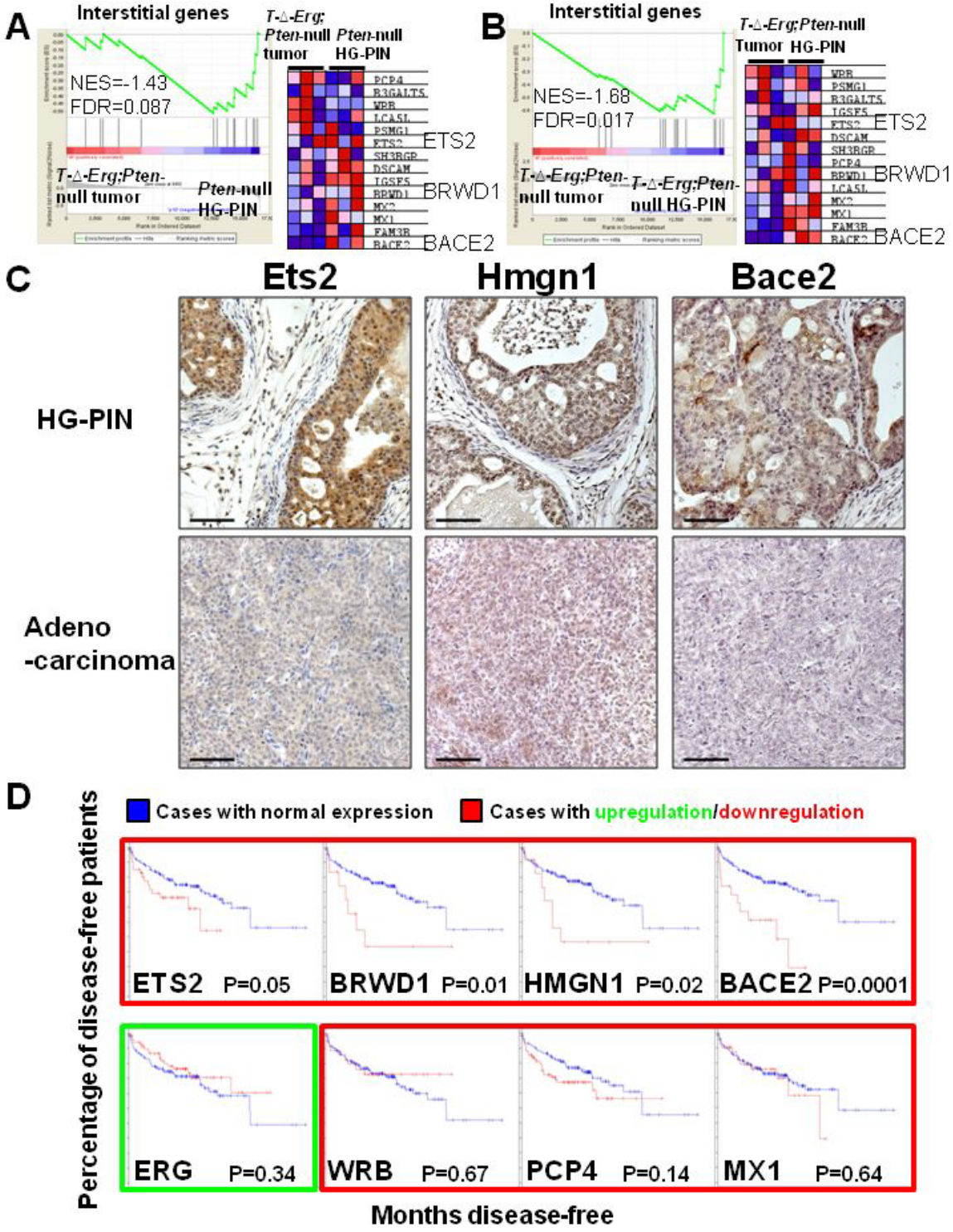

Figure 11. Multiple interstitial genes are candidate prostate cancer tumor suppressors.

A-B. GSEA for the "Interstitial genes" showing significant (FDR<0.25) negative enrichment (i.e., downregulation) of this gene set in *T*-Δ-*Erg/Pten*-null tumors in relation to *Pten*-null HG-PINs (A) or *T*-Δ-*Erg/Pten*-null HG-PINs (B). In A and B, Enrichment plots are shown on the left, heat maps are shown on the right.

C. Expression of select interstitial genes, *Ets2*, *Hmgn1*, and *Bace2* were significantly lower in adenocarcinoma (bottom row) compared to HG-PIN lesions (top row) in *Pb-Cre;T-3Mb-Erg;Pten*$^{L/L}$ mice. Scale bars are 50μm.

D. Kaplan-Meier curves of human patient data reveals that downregulation of several interstitial genes (top row) predict biochemical relapse from androgen deprivation therapy, whereas some do not (bottom row). Blue lines depict patients with normal expression while patients with downregulation are red lines.

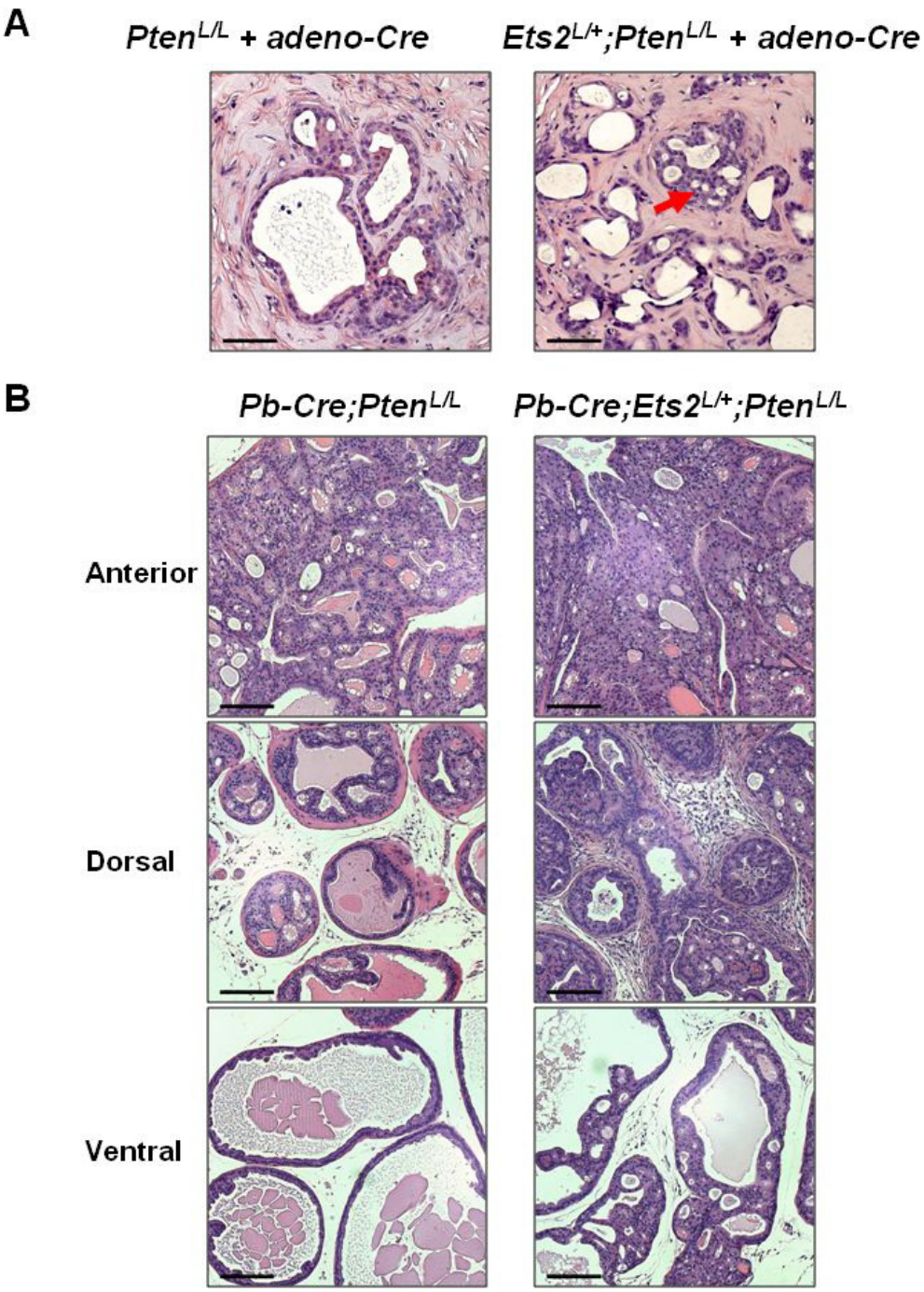

Figure 12. Haploinsufficiency of *Ets2* contributes to prostate cancer progression under the *Pten*-null background.

A. Prostate regeneration assay using $Pten^{L/L}$ or $Ets2^{L/+};Pten^{L/L}$ prostate cells infected with *Ad-CMV-Cre* adenovirus prior to implantation. Red arrow denotes a lesion resembling HG-PIN. Scale bars are 50μm.

B. H&E staining showing enhanced Prostate cancer phenotype in a 6-month old *Pb-Cre;*$Ets2^{L/+};Pten^{L/L}$ male compared to its matched *Pb-Cre;*$Pten^{L/L}$ control male, particularly in the dorsolateral and ventral lobes. Scale bars are 100μm.

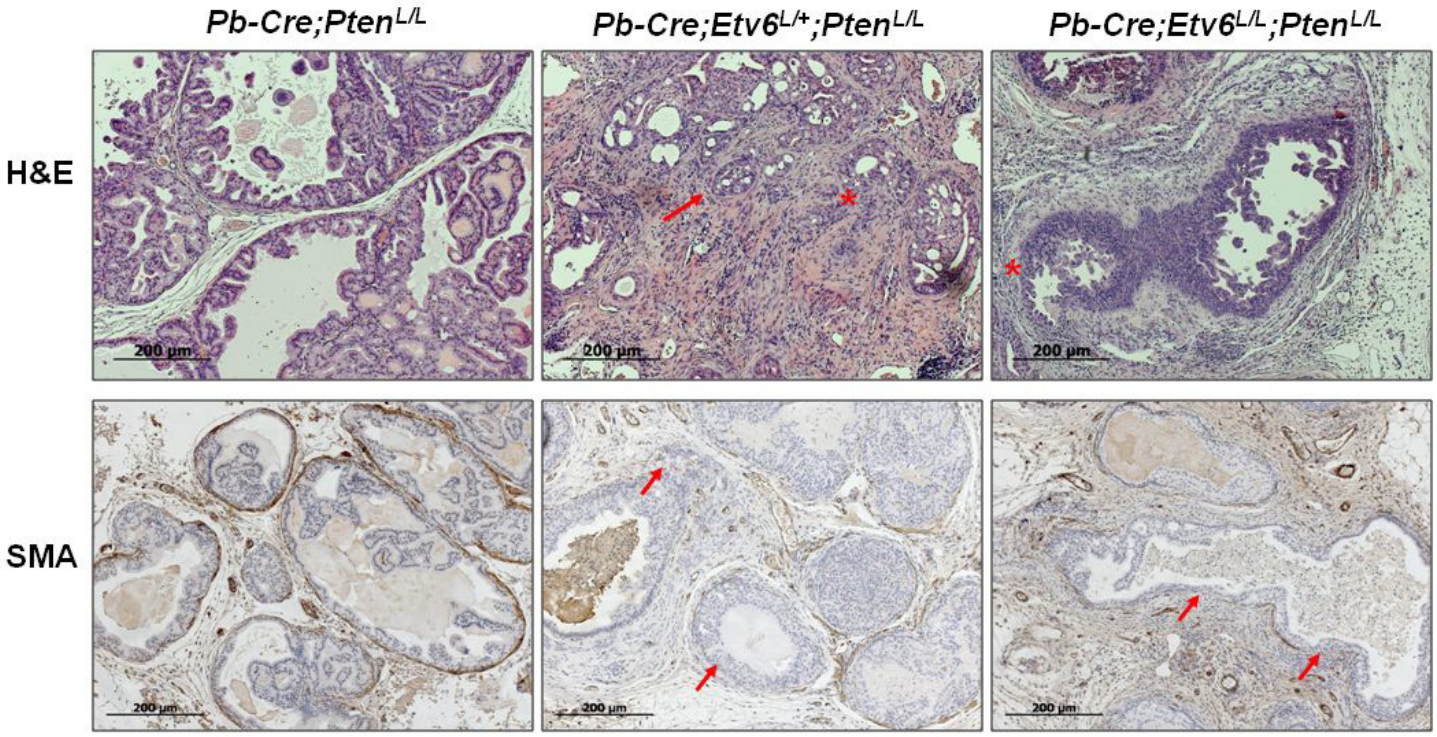

Figure 13. *Etv6*-loss cooperates with *Pten*-loss to drive development of invasive prostate cancer.
Top row shows H&E staining of prostate sections from male mice with the indicated genotypes. Arrow: invasive ducts; Stars: locally invasive prostate cancers. Lower row shows IHC staining of smooth muscle actin (SMA), which is a basal marker. Arrows: regions with loss of SMA+ basal cells (a sign of invasive prostate cancer).

Negative enrichment of many gene sets for H3K27ME3 targets in *PbCre;Etv6*$^{L/L}$;*Pten*$^{L/L}$ HGPINs vs. *PbCre;Pten*$^{L/L}$ HGPINs - due to increase in PRC2 activity (lead to increased H3K27ME3)?

	GS follow link to MSigDB	GS DETAILS	SIZE	ES	NES	NOM p-val	FDR q-val	FWER p-val	RANK AT MAX	LEADING EDGE
1	MEISSNER_BRAIN_HCP_WITH_H3K4ME3_AND_H3K27ME3	Details	1028	-0.18			1.000	0.000	3858	tags=28%, list=23%, signal=35%
2	ZWANG_TRANSIENTLY_UP_BY_2ND_EGF_PULSE_ONLY	Details	1292	-0.37			1.000	0.000	4936	tags=47%, list=30%, signal=61%
3	MIKKELSEN_MCV6_HCP_WITH_H3K27ME3	Details	415	-0.48	-2.95	0.000	0.000	0.000	5409	tags=61%, list=32%, signal=88%
4	MIKKELSEN_MEF_HCP_WITH_H3K27ME3	Details	566	-0.47	-2.94	0.000	0.000	0.000	4927	tags=55%, list=29%, signal=76%
5	MARTENS_TRETINOIN_RESPONSE_UP	Details	714	-0.40	-2.48	0.000	0.000	0.000	5180	tags=52%, list=31%, signal=72%
6	MIKKELSEN_NPC_HCP_WITH_H3K27ME3	Details	326	-0.42	-2.46	0.000	0.000	0.000	5054	tags=53%, list=30%, signal=75%
7	SCHLESINGER_H3K27ME3_IN_NORMAL_AND_METHYLATED_IN_CANCER	Details	25	-0.66	-2.39	0.000	0.000	0.000	4213	tags=68%, list=25%, signal=91%
8	SHEN_SMARCA2_TARGETS_DN	Details	289	-0.41	-2.36	0.000	0.000	0.002	4514	tags=51%, list=27%, signal=69%
9	MIKKELSEN_MEF_HCP_WITH_H3_UNMETHYLATED	Details	199	-0.43	-2.36	0.000	0.000	0.002	4995	tags=54%, list=30%, signal=76%
10	MIKKELSEN_MCV6_ICP_WITH_H3K27ME3	Details	71	-0.49	-2.32	0.000	0.000	0.004	5164	tags=58%, list=31%, signal=83%
11	KONDO_PROSTATE_CANCER_WITH_H3K27ME3	Details	170	-0.43	-2.31	0.000	0.000	0.005	5023	tags=52%, list=30%, signal=74%
12	ROLEF_GLIS3_TARGETS	Details	37	-0.57	-2.31	0.000	0.000	0.006	2998	tags=49%, list=18%, signal=59%
13	BENPORATH_PRC2_TARGETS	Details	589	-0.36	-2.29	0.000	0.000	0.008	5233	tags=49%, list=31%, signal=69%
14	MIKKELSEN_IPS_WITH_HCP_H3K27ME3	Details	94	-0.46	-2.29	0.000	0.000	0.009	4686	tags=52%, list=28%, signal=72%
15	MIKKELSEN_IPS_HCP_WITH_H3_UNMETHYLATED	Details	74	-0.50	-2.28	0.000	0.000	0.009	5840	tags=69%, list=35%, signal=105%
16	MEISSNER_BRAIN_HCP_WITH_H3_UNMETHYLATED	Details	32	-0.59	-2.27	0.000	0.000	0.010	4980	tags=66%, list=30%, signal=93%
17	MEISSNER_NPC_HCP_WITH_H3K4ME2_AND_H3K27ME3	Details	336	-0.38	-2.23	0.000	0.001	0.025	5369	tags=52%, list=32%, signal=76%
18	ZHOU_PANCREATIC_ENDOCRINE_PROGENITOR	Details	14	-0.73	-2.22	0.000	0.001	0.032	3784	tags=86%, list=23%, signal=111%
19	MIKKELSEN_MEF_LCP_WITH_H3K27ME3	Details	65	-0.48	-2.19	0.000	0.001	0.046	4788	tags=62%, list=29%, signal=86%
20	MIKKELSEN_ES_ICP_WITH_H3K27ME3	Details	40	-0.53	-2.17	0.000	0.002	0.061	4506	tags=55%, list=27%, signal=75%
21	MIKKELSEN_MEF_ICP_WITH_H3K27ME3	Details	191	-0.39	-2.16	0.000	0.002	0.065	5771	tags=59%, list=35%, signal=89%
22	BENPORATH_SUZ12_TARGETS	Details	940	-0.33	-2.16	0.000	0.002	0.065	5233	tags=47%, list=31%, signal=65%
23	RICKMAN_HEAD_AND_NECK_CANCER_F	Details	53	-0.49	-2.16	0.000	0.002	0.069	3801	tags=45%, list=23%, signal=58%
24	BENPORATH_ES_WITH_H3K27ME3	Details	1022	-0.33	-2.10	0.000	0.003	0.124	5214	tags=47%, list=31%, signal=64%

Gene Set: KONDO_PROSTATE_CANCER_WITH_H3K27ME3
Top 200 genes with high histone H3 trimethylation mark at K27 (H3K27me3) in PC3 cells (prostate cancer), by ChIP-chip assay on an 88K microarray (all promoters)

Figure 14. GSEA analysis showing downregulation of multiple gene sets for H3K27Me3 target genes in prostate HG-PIN lesions with *Etv6*-loss (negative correlation).

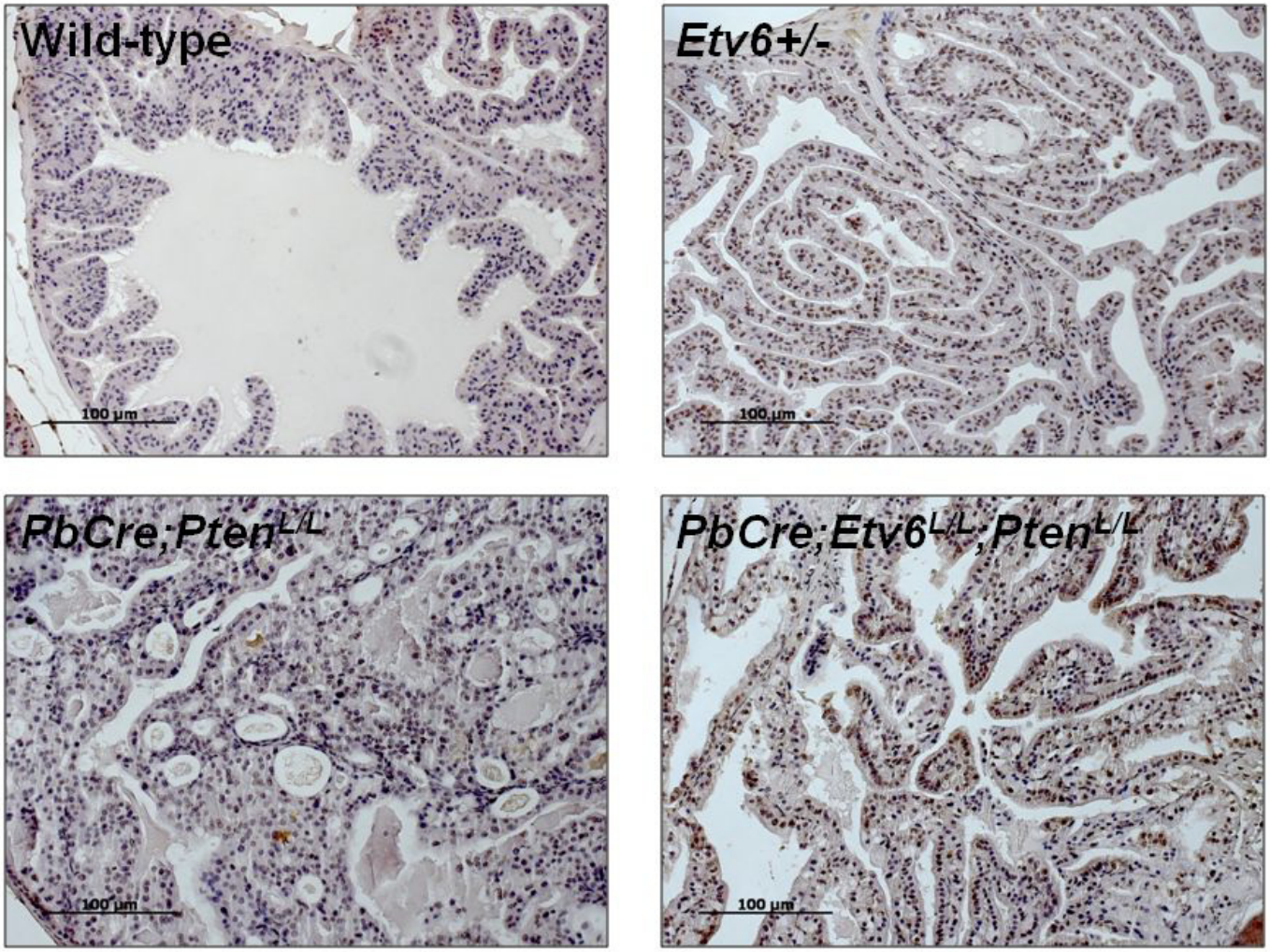

Figure 15. IHC staining showing increased H3K27Me3 histone mark signal (brown cells) upon *Etv6*-loss.

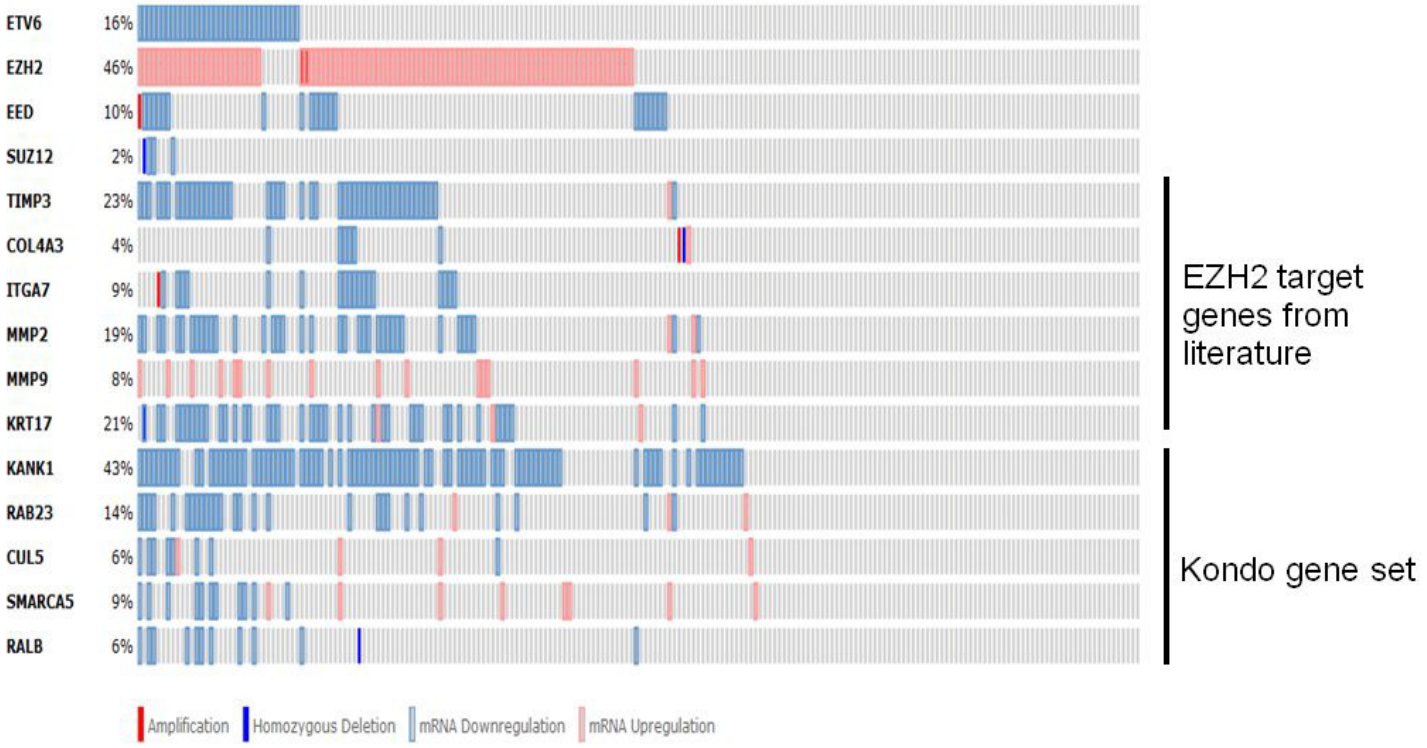

Figure 16. cBioPortal analysis showing downregulation of EZH2 target genes in prostate cancer cases (from the MSKCC cohort) with downregulation of *ETV6* and upregulation of *EZH2*.

ETV1 directs androgen metabolism and confers aggressive prostate cancer in targeted mice and patients

Esther Baena,[1,2] Zhen Shao,[1,2,3,9] Douglas E. Linn,[4,9] Kimberly Glass,[3] Melanie J. Hamblen,[1,2,5] Yuko Fujiwara,[1,2,5] Jonghwan Kim,[1,2] Minh Nguyen,[1,2] Xin Zhang,[4] Frank J. Godinho,[1,2,5] Roderick T. Bronson,[6] Lorelei A. Mucci,[7] Massimo Loda,[8] Guo-Cheng Yuan,[3] Stuart H. Orkin,[1,2,5,10] and Zhe Li[1,2,4,10]

[1]Division of Hematology and Oncology, Boston Children's Hospital, Boston, Massachusetts 02115, USA; [2]Department of Pediatric Oncology, Dana-Farber Cancer Institute, Harvard Medical School, Boston, Massachusetts 02115, USA; [3]Department of Biostatistics and Computational Biology, Dana-Farber Cancer Institute, Harvard School of Public Health, Boston, Massachusetts 02115, USA; [4]Division of Genetics, Brigham and Women's Hospital, Boston, Massachusetts 02115, USA; [5]Howard Hughes Medical Institute, Boston, Massachusetts 02115, USA; [6]Pathology, Harvard Medical School, Boston, Massachusetts 02115, USA; [7]Department of Epidemiology, Harvard School of Public Health, Brigham and Women's Hospital, Boston, Massachusetts 02115, USA; [8]Center for Molecular Oncologic Pathology, Dana-Farber Cancer Institute, Brigham and Women's Hospital, Boston, Massachusetts 02115, USA

Distinguishing aggressive from indolent disease and developing effective therapy for advanced disease are the major challenges in prostate cancer research. Chromosomal rearrangements involving ETS transcription factors, such as ERG and ETV1, occur frequently in prostate cancer. How they contribute to tumorigenesis and whether they play similar or distinct in vivo roles remain elusive. Here we show that in mice with ERG or ETV1 targeted to the endogenous *Tmprss2* locus, either factor cooperated with loss of a single copy of *Pten*, leading to localized cancer, but only ETV1 appeared to support development of invasive adenocarcinoma under the background of full Pten loss. Mechanistic studies demonstrated that ERG and ETV1 control a common transcriptional network but largely in an opposing fashion. In particular, while ERG negatively regulates the androgen receptor (AR) transcriptional program, ETV1 cooperates with AR signaling by favoring activation of the AR transcriptional program. Furthermore, we found that ETV1 expression, but not that of ERG, promotes autonomous testosterone production. Last, we confirmed the association of an ETV1 expression signature with aggressive disease and poorer outcome in patient data. The distinct biology of ETV1-associated prostate cancer suggests that this disease class may require new therapies directed to underlying programs controlled by ETV1.

[*Keywords*: ERG; ETS transcription factor; ETV1; Pten; androgen receptor; metabolism]

Supplemental material is available for this article.

Received November 27, 2012; revised version accepted February 20, 2013.

Prostate cancer is a heterogeneous disease. Recent studies show little benefit from prostate-specific antigen (PSA) screening and radical prostatectomy for men with lower-risk disease (Wilt et al. 2012). A central challenge in management is identification of those men with prostate cancer whose disease will eventually progress to the lethal castration-resistant stage. Understanding molecular events leading to castration-resistant prostate cancer (CRPC) is critical for the development of improved therapies for such patients.

Chromosomal rearrangements involving genes encoding ETS transcription factors (notably, ERG and ETV1) are found in ~50% of human prostate cancer cases and likely constitute the most frequent gene rearrangements in human malignancies (Tomlins et al. 2005; Gopalan et al. 2009). The translocations place the coding regions of *ERG* or *ETV1* under the control of androgen-responsive promoters, such as *TMPRSS2*, thereby activating expression in response to androgens. *TMPRSS2* has been reported as the principal 5′ fusion partner of *ERG*, whereas more heterogeneous 5′ fusion partners, such as *TMPRSS2*, *SCL45A3*, or *ACSL3*, have been described for *ETV1* (Tomlins et al. 2007; Attard et al. 2008b). The majority of these 5′ fusion

[9]These authors contributed equally to this work.
[10]Corresponding authors
E-mail stuart_orkin@dfci.harvard.edu
E-mail zli4@rics.bwh.harvard.edu
Article is online at http://www.genesdev.org/cgi/doi/10.1101/gad.211011.112. Freely available online through the *Genes & Development* Open Access option.

partners are also androgen-responsive genes. As ETS proteins, ERG and ETV1 are involved in regulation of cell growth, proliferation, differentiation, and apoptosis through activation or repression of target genes (Oikawa and Yamada 2003). Although functional overlap among different members of the ETS family exists, individual ETS factors also serve distinct roles. Thus, the expression pattern of ETS members through development varies, along with their repertoire of target genes, biological processes regulated, and oncogenic potentials (Seth and Watson 2005; Kunderfranco et al. 2010; Wei et al. 2010; Hollenhorst et al. 2011).

Clinical studies of the prevalence and prognostic significance of ETS fusions in prostate cancer have yielded discrepant results, possibly related to differences in the genetics of the evaluated populations and diversity in methods used. Several studies suggest that ETS fusions are associated with a worse prognosis (Demichelis et al. 2007; Nam et al. 2007; Attard et al. 2008a), whereas others have failed to confirm the correlation (Gopalan et al. 2009; Hermans et al. 2009; Minner et al. 2011). Cases with ETS fusions are generally grouped together for patient stratification. However, considering all ETS translocations as a single entity risks obscuring possible differences in the contribution of each to disease outcome. For example, effects of *TMPRSS2-ERG*, the most common translocation, may bias findings of aggregate studies. Studies to date have not specifically addressed the biology of individual ETS fusions and their associated outcomes.

In this study, we used knock-in mouse modeling and comprehensive genome-wide approaches to characterize the functional specificities of ERG and ETV1 in prostate cancer. Our data indicate that ERG and ETV1 regulate a common set of genes, such as androgen receptor (AR) target genes, but in an opposing direction. In particular, ETV1, but not ERG, up-regulates expression of AR target genes as well as genes involved in steroid biosynthesis and metabolism. This ETV1-driven oncogenic program predisposes prostate cells for cooperation with other oncogenic events, such as PTEN loss, leading to more aggressive disease in murine models and human patients. Our findings further establish different biological subtypes of human prostate cancer based on distinct ETS factor-driven signatures.

Results

Tmprss2-ETV1 *cooperates with total Pten loss, leading to invasive adenocarcinoma*

As a step toward defining the roles of ETS fusions in prostate cancer, several groups have generated transgenic mouse strains that express ERG or ETV1 ectopically under the control of the *Probasin* (*Pb*) promoter (*Pb-ERG* or *Pb-ETV1*) (Tomlins et al. 2007, 2008; Klezovitch et al. 2008; Carver et al. 2009; King et al. 2009; Shin et al. 2009). Interpretation of results has varied. Prostatic intraepithelial neoplasia (PIN)-like lesions have been described in prostates of *Pb-ERG* and *Pb-ETV1* transgenic males (Tomlins et al. 2007, 2008; Klezovitch et al. 2008; Shin et al. 2009). However, others have reported that *Pb-ERG* transgenic males are normal (Carver et al. 2009; King et al. 2009). Discrepant findings may be related to mouse strain differences, to different transgene integration sites, or in the precise portions of the ETS cDNAs that were expressed. We reasoned that mice engineered to express ETS factors from an endogenous promoter in the proper chromosomal configuration might provide a more relevant biological context. Moreover, prior transgenic models cannot address potential contributions of haploinsufficiency or loss of genes deleted between *TMPRSS2* and *ERG* to prostate tumorigenesis, such as occurs in patients with a *TMPRSS2-ERG* fusion generated through an interstitial deletion of chromosome 21.

We engineered knock-in mouse models to recapitulate *TMPRSS2-ETS* fusions (with or without the interstitial deletion) in prostate cancer. We used two strategies. In the first strategy, we knocked in N terminus-truncated human *ERG* or *ETV1* cDNA, together with an *ires-GFP* cassette, into exon 2 of the mouse *Tmprss2* locus (referred to as *T-ERG* or *T-ETV1* hereafter), which shares ~80% homology as well as at least two conserved AR-binding sites with those of the human *TMPRSS2* (Fig. 1A; Supplemental Fig. S1; Jacquinet et al. 2000). The resultant fusion transcripts recapitulate the *TMPRSS2-ERGa* or *TMPRSS2-ETV1a* fusions in patients (Tomlins et al. 2005). In the second strategy, we used sequential gene targeting to introduce *lox*P sites into the *Tmprss2* and *Erg* loci on the same chromosome (Fig. 1A; Supplemental Fig. S2A,B). Cre-mediated recombination deletes the ~3-Mb intragenic region and generates the *Tmprss2-Erg* fusion gene (Supplemental Fig. S2C,D), which approximates the *TMPRSS2-ERGa* fusion subtype (Tomlins et al. 2005). Since most genes in this interstitial region are syntenic between humans and mice (Supplemental Fig. S2E), this unique knock-in model also permits assessment of the contribution of the interstitial deletion to prostate cancer development (referred to as *T-3Mb-Erg* or *T-Δ-Erg* before or after Cre-mediated excision of the interstitial region, respectively) (Fig. 1A). In all three knock-in alleles (i.e., *T-ETV1*, *T-ERG*, and *T-Δ-Erg*) we confirmed expression of their corresponding fusion transcripts in prostates (Fig. 1B). By immunohistochemistry (IHC), we detected moderate expression of Erg protein in the knock-in prostates (Fig. 1C). Despite multiple efforts, we were unable to validate an antibody that faithfully detects ETV1 protein by IHC. Therefore, we used IHC staining for GFP as a surrogate for ETV1 expression, as the knock-in GFP reporter is under the same transcriptional control (Fig. 1A). With this approach, we detected robust GFP (ETV1) expression in prostate epithelial cells but not in stromal cells (Fig. 1D). In all three knock-in strains, prostates appeared largely normal, and we did not observe prostatic intraepithelial neoplasia (PIN) lesions or cancer (Fig. 1E). However, in a portion of *T-ETV1* males (four out of 11), in particular those at old ages (≥18 mo; three out of three), we observed varying degrees of inflammation (Fig. 1E). In addition, pathological analysis in several exceptional *T-Δ-Erg* males (four out of 21 but in none of the *T-ERG*

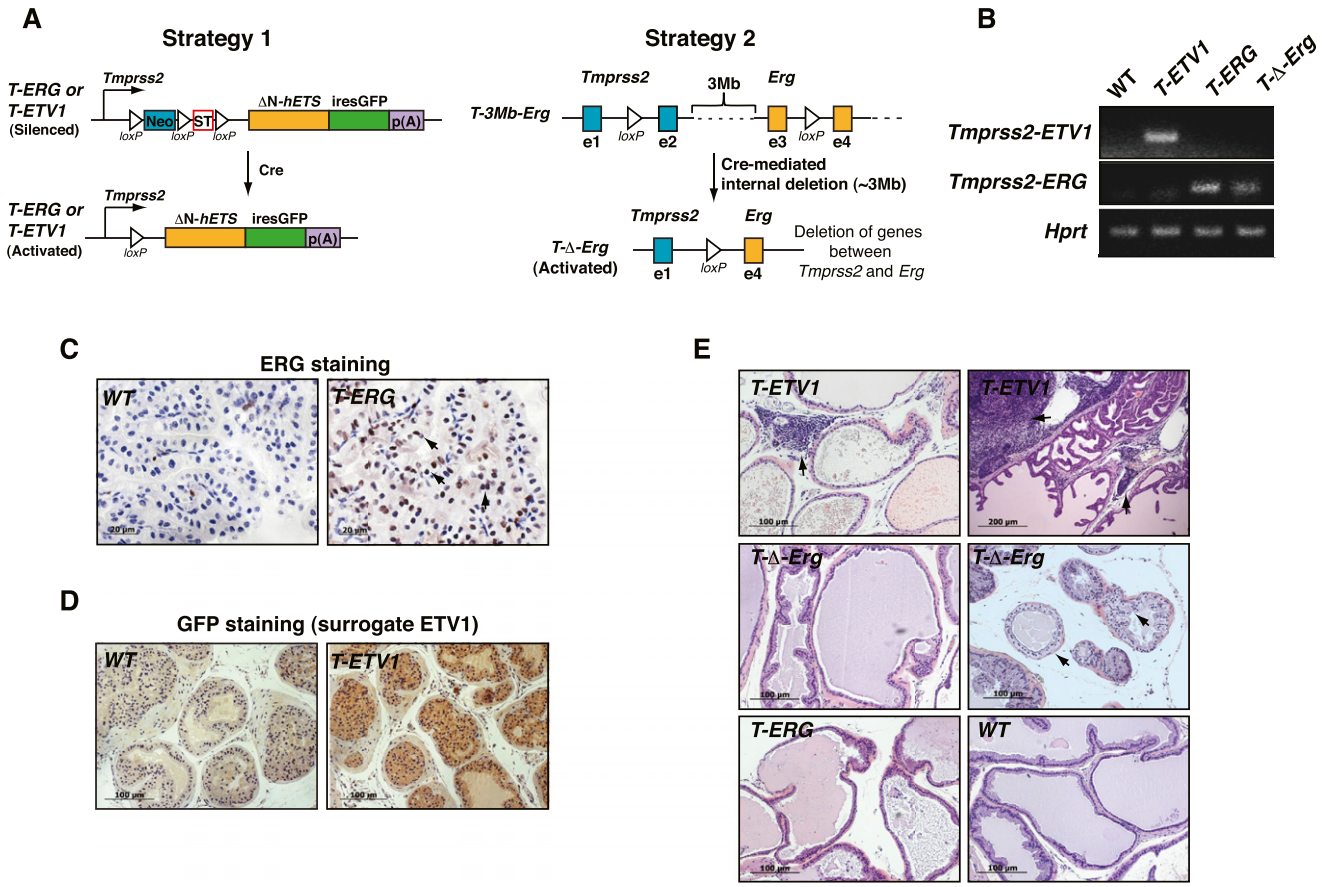

Figure 1. *Tmprss2-ERG* (with or without interstitial deletion) and *Tmprss2-ETV1* expression are insufficient to initiate prostate tumorigenesis. (*A*) Targeting strategies for engineering *Tmprss2-ERG* and *Tmprss2-ETV1* knock-ins. Strategy 1 is based on direct knock-in of N terminus-truncated human *ERG* or *ETV1* cDNA (ΔN-*hETS*) into the murine *Tmprss2* locus. Strategy 2 is based on the introduction of *loxP* sites to murine *Tmprss2* and *Erg* loci by sequential gene targeting in mouse embryonic stem cells so that the 3-Mb interstitial region can be deleted by Cre-mediated recombination and meanwhile generate the *Tmprss2-Erg* gene fusion. Details of gene targeting are shown in Supplemental Figures S1 and S2. (*B*) RT–PCR showing expression of the *Tmprss2-ETV1* fusion transcripts in *T-ETV1* knock-in prostates and expression of the *Tmprss2-ERG* fusion transcripts in *T-ERG* and *T-Δ-Erg* knock-in prostates but not in wild-type (WT) prostates. (*C*) IHC staining showing moderate ERG expression (arrows) in the anterior lobes of a *T-ERG* knock-in male but not in the wild-type male. (*D*) IHC staining showing homogeneous GFP expression (as surrogate for ETV1) in the anterior lobes of a *T-ETV1* knock-in male but not in the wild-type male. (*E*) Hemotoxylin and eosin (H&E) staining showing normal prostate histology from all three knock-ins (showing ventral lobes except those of *T-ETV1*). Arrows in *T-ETV1* pictures indicate inflammation in *T-ETV1* knock-in males ([*left*] slight inflammation in the lateral lobe of a young knock-in male; [*right*] extensive inflammation in the anterior lobe of a 30-mo-old knock-in male). (*Right*) Arrows in the *T-Δ-Erg* picture indicate abnormal-looking (lightly stained "foamy"-looking cytoplasm, randomly distributed nuclei) prostate cells,observed in four out of 21 of *T-Δ-Erg* males. Bars, 100 μm (200 μm in *top right* picture). All animals analyzed in *C–E* were ~10 mo of age unless otherwise indicated.

males) revealed some hyperplasia and foci of cells with lightly stained cytoplasm and loss of polarity (Fig. 1E). Despite these minor phenotypes, we conclude that expression of ERG or ETV1 from the endogenous *Tmprss2* promoter, even in the presence of the interstitial deletion (for Erg fusion), is insufficient to initiate prostate tumorigenesis.

Overexpression of ERG or ETV1 from the *Pb* promoter or through lentiviral transduction in prostate cells has been previously reported to cooperate with activation of the PI3K pathway to drive a more aggressive prostate cancer phenotype (Carver et al. 2009; King et al. 2009; Zong et al. 2009). To determine whether this is also the case when ETV1 or ERG is expressed from the endogenous *Tmprss2* promoter, we bred mice containing the knock-in alleles with *Pten*$^{+/-}$ mice. We found that within the time frame monitored (up to 15 mo of age), prostates of all aged *T-ETV1;Pten*$^{+/-}$, *T-ERG;Pten*$^{+/-}$, and *T-Δ-Erg;Pten*$^{+/-}$ double-mutant males developed PIN lesions that stain positive for phosphorylated AKT (pAKT), whereas prostates of *Pten*$^{+/-}$-alone mice appeared largely normal (Fig. 2A; Supplemental Fig. S3). In the above cohort, PIN lesions from double-mutant males maintained relatively uniform and high levels of ETV1 (GFP) or ERG expression (Fig. 2B); this is particularly notable for ERG, as in the prostates of *ERG* knock-in alone, ERG expression was

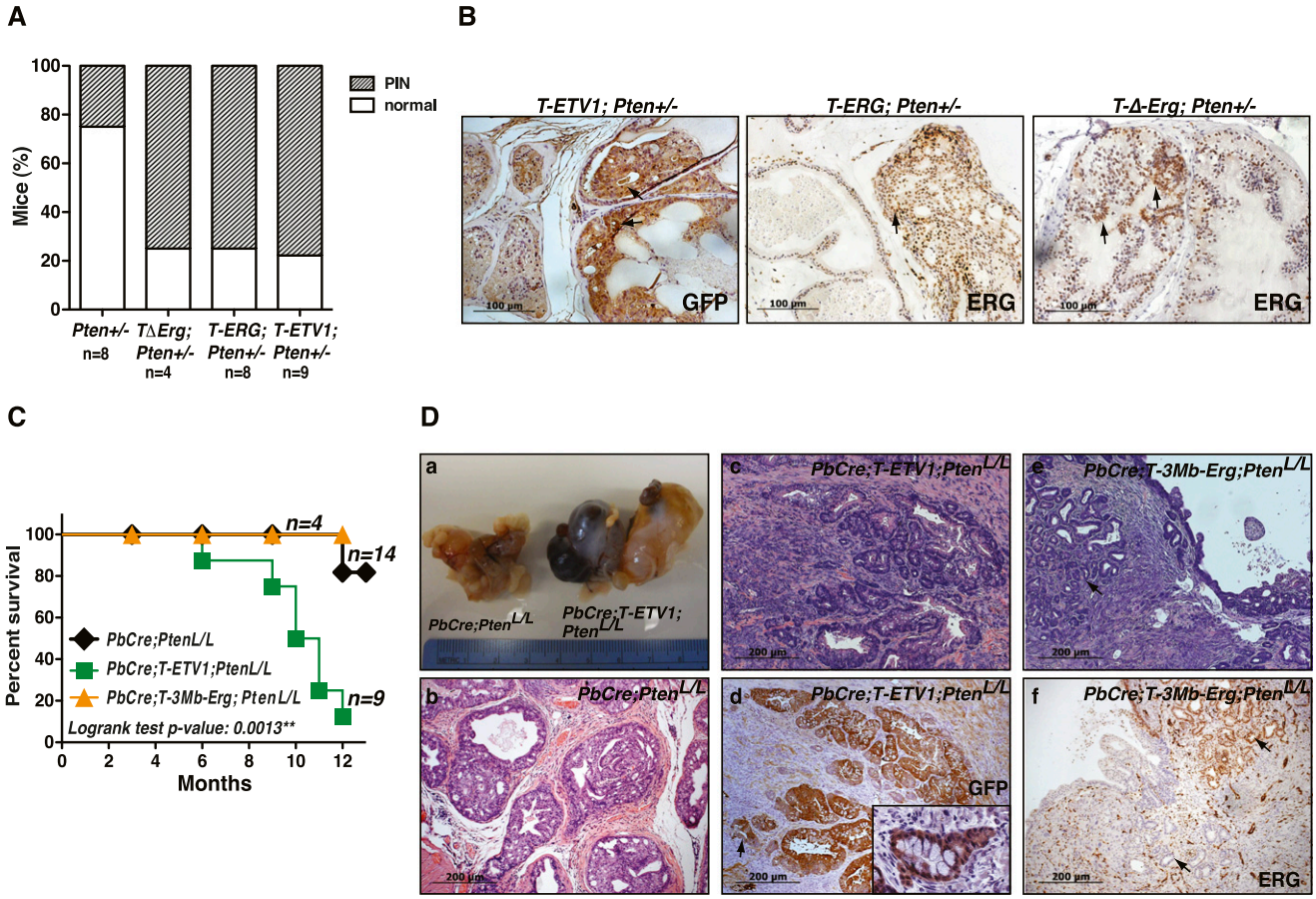

Figure 2. Cooperation of *Tmprss2-ERG* and *Tmprss2-ETV1* gene fusions with *Pten* loss. (*A*) Bar graph summarizing histology of prostates from $Pten^{+/-}$, *T-Δ-Erg*;$Pten^{+/-}$, *T-ERG*;$Pten^{+/-}$, and *T-ETV1*;$Pten^{+/-}$ males. All males were at 6–15 mo of age when checked. The youngest $Pten^{+/-}$, *T-Δ-Erg*;$Pten^{+/-}$, *T-ERG*;$Pten^{+/-}$, and *T-ETV1*;$Pten^{+/-}$ males in which PIN lesions were detected were at 13, 9.5, 6.5, and 6 mo of age, respectively. (*B*) IHC staining showing GFP expression (as a surrogate for ETV1 expression) in the PIN lesion of a *T-ETV1*;$Pten^{+/-}$ male (*left*) and ERG expression in the PIN lesions of a *T-ERG*;$Pten^{+/-}$ male (*middle*) and a *T-Δ-Erg*;$Pten^{+/-}$ male (*right*). Note, in all cases, GFP or ERG staining in PIN lesions (arrows) is stronger than that in normal-appearing prostate cells. Bars, 100 μm. (*C*) Kaplan-Meier survival curve. All males were monitored for survival for at least 1 yr. The four *PbCre;T-3Mb-Erg*;$Pten^{L/L}$ males all survived to 1 yr and were euthanized for histology. The majority of *PbCre*;$Pten^{L/L}$ control males were still alive even after 15 mo. Log-rank test: (**) $P = 0.0013$ for *PbCre;T-ETV1*;$Pten^{L/L}$ in relation to *PbCre*;$Pten^{L/L}$ controls. (*D*) Cancer phenotypes in *PbCre*;$Pten^{L/L}$ males with or without ETS fusions. (Panel *a*) Gross appearance of prostates from a 10-mo-old *PbCre;T-ETV1*;$Pten^{L/L}$ male showing large tumor and prostatic cyst (*right*) and a 13-mo-old *PbCre*;$Pten^{L/L}$ control male (*left*). (Panel *b*) Typical localized prostate cancer seen in a control *PbCre*;$Pten^{L/L}$ male. (Panel *c*) Invasive prostate adenocarcinoma seen in a *PbCre;T-ETV1*;$Pten^{L/L}$ male. (Panel *d*) GFP staining (as a surrogate for ETV1 expression) in invasive prostate adenocarcinoma cells (brown) in a *PbCre;T-ETV1*;$Pten^{L/L}$ male (a magnified view of GFP^+ invasive prostate cancer cells is shown in the *inset*). (Panel *e*) Invasive prostate adenocarcinoma cells (arrow) detected in an aged *PbCre;T-3Mb-Erg*;$Pten^{L/L}$ male. (Panel *f*) IHC staining of Erg (brown) revealing Erg^+ and Erg^- invasive prostate tumor cells (arrows; from the same male as in panel *e*) within the same section. Bars, 200 μm.

initially relatively weak and heterogeneous (Fig. 1C). Thus, overexpression of ETV1 or ERG correlates with the observed localized premalignant phenotype.

To test cooperation of *Tmprss2-ETS* with total loss of Pten, we used *Pb-Cre* (Wu et al. 2001) to inactivate a conditional knockout allele of *Pten* (Lesche et al. 2002) and generated *Pb-Cre;T-3Mb-Erg*;$Pten^{L/L}$ males and *Pb-Cre;T-ETV1*;$Pten^{L/L}$ males. Prostate cancer development in these models was tracked by pAKT expression (Supplemental Fig. S4). Under our housing and genetic background (mixed C57/BL6-129), *Pb-Cre*;$Pten^{L/L}$ males developed localized PIN lesions that slowly progressed to prostate adenocarcinomas. In contrast, the Pten loss-driven prostate cancer phenotype in *Pb-Cre;T-ETV1*;$Pten^{L/L}$ males was markedly enhanced. The majority of *Pb-Cre;T-ETV1*;$Pten^{L/L}$ males died before 1 yr of age, possibly due in part to large prostatic cyst formation (Supplemental Fig. S5). In contrast, the majority of *Pb-Cre*;$Pten^{L/L}$ and *Pb-Cre;T-3Mb-Erg*;$Pten^{L/L}$ males survived to at least 1 yr of age (Fig. 2C). On histology, we observed aggressive GFP^+ (from the *T-ETV1* allele) prostate adenocarcinoma cells invading into stroma in *Pb-Cre;T-ETV1*;$Pten^{L/L}$ prostates (Fig. 2D, panels c,d). Prostate cancer cells metastasized locally to the urogenital area (e.g., in lymphatic vessel)

(Supplemental Fig. S6A). In addition, we noted marked stromal responses, including sarcomatous-like lesions and regions with bone-like differentiation (Supplemental Fig. S6B). Since such lesions were negative for GFP (i.e., ETV1 expression) and pAKT (Supplemental Fig. S6C), we reasoned that they may represent a desmoplastic response in the stroma due to invasive prostate cancers developing nearby, as observed in other cancers (Dvorak 1986), rather than cancers arising from an epithelial-to-mesenchymal transition.

In younger *Pb-Cre;T-3Mb-Erg;Pten*$^{L/L}$ males (4–7 mo), the prostate phenotype appeared indistinguishable from that of *Pb-Cre;Pten*$^{L/L}$ controls. The four oldest *Pb-Cre;T-3Mb-Erg;Pten*$^{L/L}$ males in this cohort all survived to 1 yr of age and were euthanized for histological examination. In these mice, we observed regions of invasive prostate adenocarcinoma not typically seen in *Pb-Cre;Pten*$^{L/L}$ control males at the same age in our cohort (Fig. 2D, panel e). However, we noted that whereas some cancer cells stained strongly for Erg expression, many were negative. In particular, we detected foci of invasive adenocarcinoma with strong Erg expression, accompanied by adjacent foci of invasive adenocarcinoma with similar histology but with little or no Erg expression (Fig. 2D, panel f). We also observed regions with invasive adenocarcinoma that were largely negative for Erg in epithelial cells (Supplemental Fig S7). The dynamic expression pattern suggests that Erg expression is up-regulated and selected for in PIN lesions under the *Pten*$^{+/-}$ background but may not be strictly needed in invasive cancers under the total *Pten* loss background. In contrast, ETV1 expression appeared consistently homogeneous in invasive cancer cells, suggesting that its overexpression is required for cooperation with total *Pten* loss for the development of invasive adenocarcinomas (Fig. 2D, panel d).

In summary, we found that while both *Tmprss2-ETV1* and *Tmprss2-ERG* cooperate with loss of a single copy of *Pten* in the development of localized prostate cancer, only *Tmprss2-ETV1* appears to cooperate with full loss of *Pten*, leading to invasive prostate adenocarcinoma and decreased survival.

ERG and ETV1 regulate distinct programs in immortalized nontumorigenic prostate cells

The genetically engineered knock-in mice distinguished ETV1 from ERG in supporting invasive adenocarcinoma. To gain mechanistic insights into this difference, we performed an integrated genomic analysis to identify their respective target genes. First, we ectopically expressed ETV1 or ERG in immortalized human nontumorigenic prostate epithelial cells, RWPE-1 cells. Thus, RWPE-1 cells were engineered to express full-length *ERG* or *ETV1* cDNA carrying a substrate tag that permits in vivo biotinylation by coexpressed *Escherichia coli* biotin ligase BirA (bioERG and bioETV1) (Supplemental Fig. S8A,B). RWPE-1 cells overexpressing bioERG (R.ERG) or bioETV1 (R.ETV1) proliferated normally compared with controls (Supplemental Fig. S8C). Microarray expression profiling data strongly overlapped with those previously reported (ERG [Gupta et al. 2010] and ETV1 [Tomlins et al. 2007] in RWPE-1 cells [Supplemental Fig. S8D,E]) and yielded two findings. First, a set of genes was uniquely regulated by either ERG or ETV1. Second, both factors also regulated a common set of genes but in a largely opposing fashion (Fig. 3A). This latter observation is depicted by the quantitative two-dimensional comparison of the ERG and ETV1 data sets, which illustrates a statistically significant correlation between ERG-driven up-regulated genes and ETV1-driven down-regulated genes and vice versa (Fig. 3B). Gene ontology (GO) and Ingenuity pathway analysis (IPA) implicated genes up-regulated upon ERG expression and down-regulated upon ETV1 expression that are associated with cell proliferation. In contrast, genes down-regulated on ERG expression and up-regulated by ETV1 are correlated with cell motility and lipid metabolism (Supplemental Fig. S9). As revealed by quantitative RT–PCR of select common genes, ETV1 expression induced up-regulation of genes involved in AR signaling (*TMPRSS2* and *SOX9*) or invasion and lipid metabolism (*VIMENTIN*, *ADRB2*, and *ACSL3*) as well as down-regulation of cell cycle genes (*E2F1* and *BRCA1*) (Fig. 3C). In contrast, these genes exhibited largely an opposite expression pattern in ERG-expressing RWPE-1 cells (Fig. 3C). Thus, these data point to distinct regulatory programs driven by ERG and ETV1 in nontumorigenic prostate cells.

ERG and ETV1 have shared and distinct chromatin targets

To interrogate further similarities and differences of ERG and ETV1 transcriptional programs, we performed ChIP (chromatin immunoprecipitation)-on-chip analysis. We identified ERG ChIP targets in VCaP cells (harboring *TMPRSS2-ERG*) by an anti-ERG antibody. As a ChIP-quality antibody for ETV1 is not available, we used the bio-ChIP approach (Supplemental Fig. S10A; de Boer et al. 2003; Wang et al. 2006; Kim et al. 2008) on LNCaP cells (harboring *ETV1* fusions) ectopically expressing bioETV1 and the *E. coli* biotin ligase BirA (Supplemental Fig. S10B). On comparison of ERG and ETV1 ChIP targets (Supplemental Table S1), we identified three subsets: ERG–ETV1 common targets, ERG-only targets, and ETV1-only targets (Fig. 4A), which are consistent with reported ChIP-seq (ChIP combined with deep sequencing) data in RWPE-1 cells (Hollenhorst et al. 2011). Bound regions for each factor were typically in close proximity to the transcription start sites (TSSs) (Supplemental Fig. S10C,D). We confirmed that ERG–ETV1 common target regions were occupied by both ERG and ETV1. As anticipated, ETS-binding motifs are the most statistically significant enriched motifs within the predicted targets (Fig. 4B). Further analysis of the defined target subsets revealed clear differences of motif enrichment at common versus unique targets (Fig. 4B; Supplemental Fig. S10E), consistent with expression profiling data indicating distinct biological processes regulated by ERG and ETV1 in prostate cells (Supplemental Figs. S9A,B, S10F).

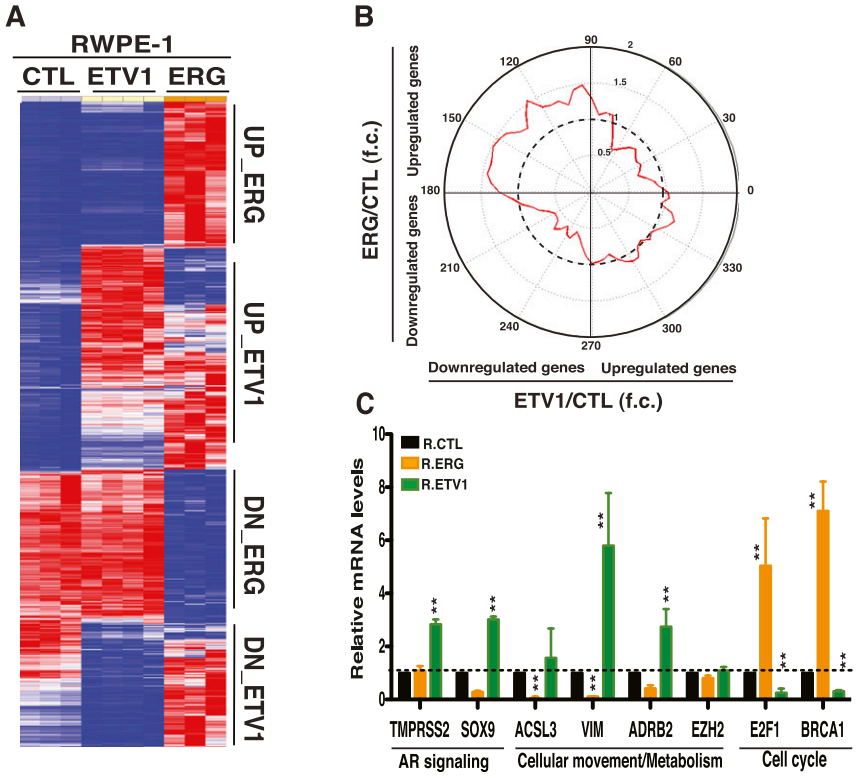

Figure 3. ERG and ETV1 regulate a common program in immortalized nontumorigenic RWPE-1 prostate cells but in an opposing fashion. (*A*) Expression profiling of ERG-overexpressing (R.ERG) and ETV1-overexpressing (R.ETV1) RWPE-1 cells compared with BirA-expressing controls (CTL). Heat map generated by hierarchical clustering and by applying Pearson correlation and the complete linkage rule. The heat map shows differentially expressed genes (fold change, >1.5; false discovery rate [FDR], <0.05). (Red) Highest expression; (blue) lowest expression. (*B*) Bidimensional plot comparing expression profiles of genes differentially expressed (fold change, >1.5) in R.ERG versus R.CTL and in R.ETV1 versus R.CTL RWPE-1 cells. The red line represents the distribution of genes. The dotted line corresponds to a gene density fold change of 1. (*C*) RT–PCR analysis of select genes associated with prostate cancer pathways upon ERG or ETV1 overexpression in RWPE-1 cells. $n = 3$ per group. Error bars, SEM; *t*-test: (**) $P < 0.01$. If no *P*-value is indicated, $P > 0.05$.

Interestingly, IPA analysis indicated that nuclear receptor signaling pathways, including those associated with estrogen, androgen, and glucocorticoid receptor signaling, were significantly enriched in ERG–ETV1 common targets (Fig. 4C). In contrast, the ERG-only subset correlated with the cell cycle network. Intriguingly, the lipid metabolism biological network as well as the Oncostatin M and IL-3 signaling pathways, which have been correlated with increased cell motility and invasiveness (Dentelli et al. 1999; Holzer et al. 2004), were enriched in the ETV1-only subset (Fig. 4C). Taken together, our combined gene expression and ChIP-on-chip analyses argue that ERG and ETV1 control distinct transcriptional programs in prostate cells.

ERG and ETV1 interact differentially with the AR signaling pathway

The AR pathway is a critical driver of tumorigenic prostate development in both androgen-dependent (AD) and castration-resistant stages (Wang et al. 2009). Our data suggest that genes associated with AR signaling belong to the ERG–ETV1 common target category (Fig. 4C; Supplemental Fig. S11A). To address potential cross-talk of ERG and ETV1 common targets with the AD program, we defined an improved androgen-driven signature from AD VCaP and LNCaP cell lines that mitigates differences among diverse expression-based gene sets (Supplemental Fig. S12). Gene set enrichment analysis (GSEA) (Subramanian et al. 2005) revealed that this signature was significantly depleted after *ETV1* knockdown in LNCaP cells (Fig. 5A) but enhanced in VCaP cells upon *ERG* silencing (Fig. 5B). This finding was confirmed by quantitative RT–PCR for select AR-driven genes in LNCaP and VCaP cells (Figure 5C,D). ChIP analysis further demonstrated that, while androgen stimulated AR and ETV1 binding to the enhancers and promoters of two established AR targets, *PSA* and *TMPRSS2*, androgen decreased ERG occupancy to these AR target genes (Supplemental Fig. S11B,C). These data indicate that ETV1 cooperates with activation of AR signaling, while ERG negatively modulates the AR transcriptional program.

To determine whether ERG and ETV1 also regulate AR signaling differentially in vivo, we examined GFP expression in *T-ERG* and *T-ETV1* males, as the reporter serves as a surrogate for the in vivo activity of the *Tmprss2* promoter in these identically engineered mice. GFP expression was readily detected in *T-ETV1* prostates but barely detected in *T-ERG* prostates (Fig. 5E). In contrast, GFP expression was detected in estrogen receptor-positive mammary epithelial cells (Sleeman et al. 2007) of both *T-ERG* and *T-ETV1* females (Supplemental Fig. S13). These data indicate that *Tmprss2* is indeed an estrogen and androgen dual-responsive promoter and that its promoter activity is down-regulated in *T-ERG* prostate cells.

To ascertain whether elevated AR signaling up-regulates the *Tmprss2* promoter activity in vivo, we bred *T-ERG* and *T-ETV1* mice to transgenic mice that express a mutated version of AR (E231G) expressed from the *Pb* promoter (*Pb-AR*) (Han et al. 2005). In *Pb-AR;T-ERG* double-transgenic males, we detected a strong GFP signal in the prostate (Fig. 5E). The *Pb-AR* transgene is most

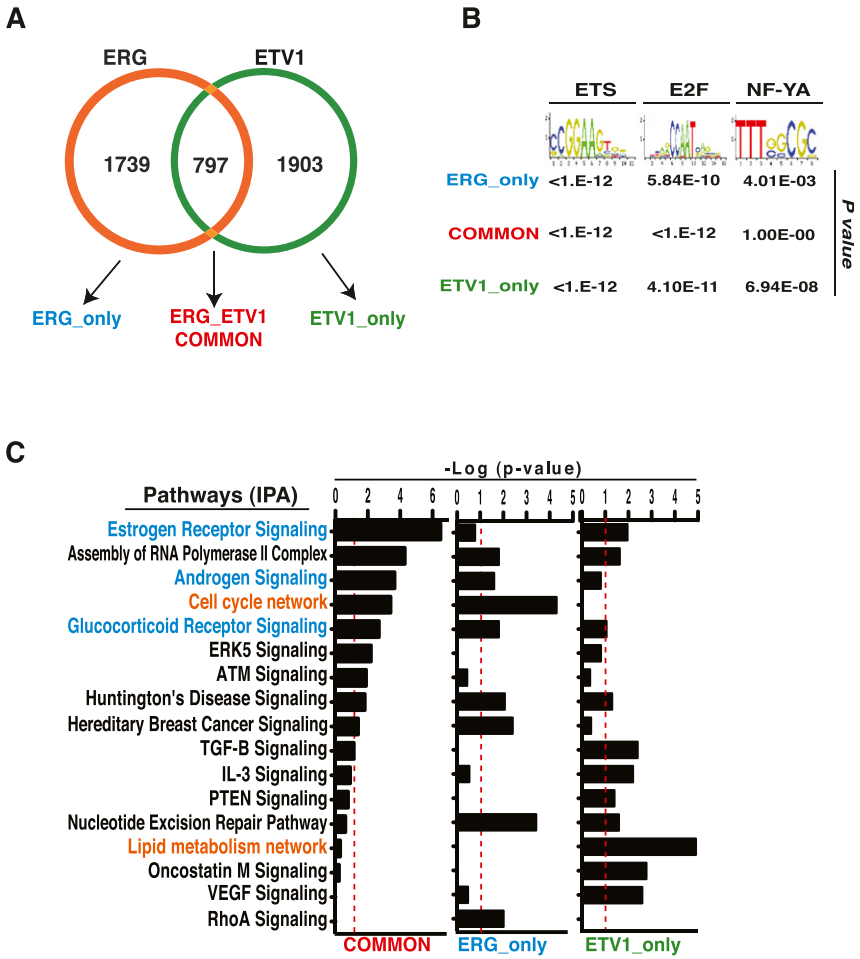

Figure 4. ERG and ETV1 drive specific transcriptional programs. (*A*) Venn diagram of targets occupied by ERG and ETV1. The intensity of binding at each probe was calculated by model-based analysis of tiling array (MAT) (Johnson et al. 2006). MAT scores were then normalized by quantile–quantile normalization (Bolstad et al. 2003) between ETV1 and ERG ChIP-on-chip experiments. Target loci were defined as the peaks associated with *P*-value < 10^{-4}. (*B*) Enrichment of ETS-binding motifs and other indicated motifs in all ChIP target subsets. The Fisher exact test was applied. (*C*) IPA analysis of ChIP-defined target gene sets implicating common target genes in nuclear receptor signaling pathways and ETV1 unique targets in lipid metabolism network. The significance of enrichment of each gene set is shown as −Log (*P*-value).

active in the ventral prostate lobes (Han et al. 2005). In accord with this, we observed stronger staining for ERG in the ventral lobes of *Pb-AR;T-ERG* prostates, compared with barely detectable ERG staining in *T-ERG* prostates (Fig. 5F). Furthermore, we measured expression levels of select AR targets in mouse prostates. In the *Pb-AR* background, most AR targets were down-regulated in *T-ERG* males, whereas AR targets were typically up-regulated in *T-ETV1* males, thus illustrating the opposite regulation of AR signaling by ERG and ETV1 in vivo (Fig. 5G). Despite elevated AR signaling, prostates of *Pb-AR*-alone as well as those of *Pb-AR;T-ERG* and *Pb-AR;T-ETV1* males appeared largely normal. Taken together, human prostate cancer cell and mouse model data indicate that differential regulation of the AR pathway by ETV1 and ERG occurs not only in vitro, but, importantly, also under the physiological setting.

ETV1 directs androgen metabolism in prostate epithelial cells

In addition to the opposing regulation of common targets by ETV1 and ERG, we hypothesized that unique targets controlled by ETV1 might contribute to the aggressive phenotype seen in association with ETV1 expression. To gain mechanistic insights into programs selectively regulated by ETV1 we sorted GFP$^+$ (thus, ETV1-expressing) prostate luminal cells from *T-ETV1* knock-in males and compared them with luminal cells from wild-type prostates by microarray expression profiling (Fig. 6A,B). We confirmed the luminal cell expression pattern in both sorted samples (Supplemental Fig. S14). By GSEA, we identified several cancer-associated metabolic pathways that were enriched in *T-ETV1* luminal cells (Supplemental Fig. S15A). Of note, cholesterol and steroid biosynthesis pathways, both of which are strongly related to prostate tumorigenesis (Twiddy et al. 2010; Zadra et al. 2010), were most highly enriched (Fig. 6C,D). On analysis of a patient cohort with CRPCs metastatic to bone (Stanbrough et al. 2006), we observed that genes associated with the steroid hormone biosynthesis pathway and androgen and estrogen metabolism are significantly enriched in tumors with higher *ETV1* expression (Supplemental Fig. S15A). *HSD17B7*, a gene shared by steroid biosynthesis and steroid hormone biosynthesis pathways, was up-regulated in both *T-ETV1* luminal cells and *ETV1*-high bone metastases (Supplemental Fig. S15B). *HSD17B7* as well as other HSD17B enzyme genes (*HSD17B4* and *HSD17B10*) are ChIP targets of ETV1 in prostate cancer cells and are components of the lipid metabolism

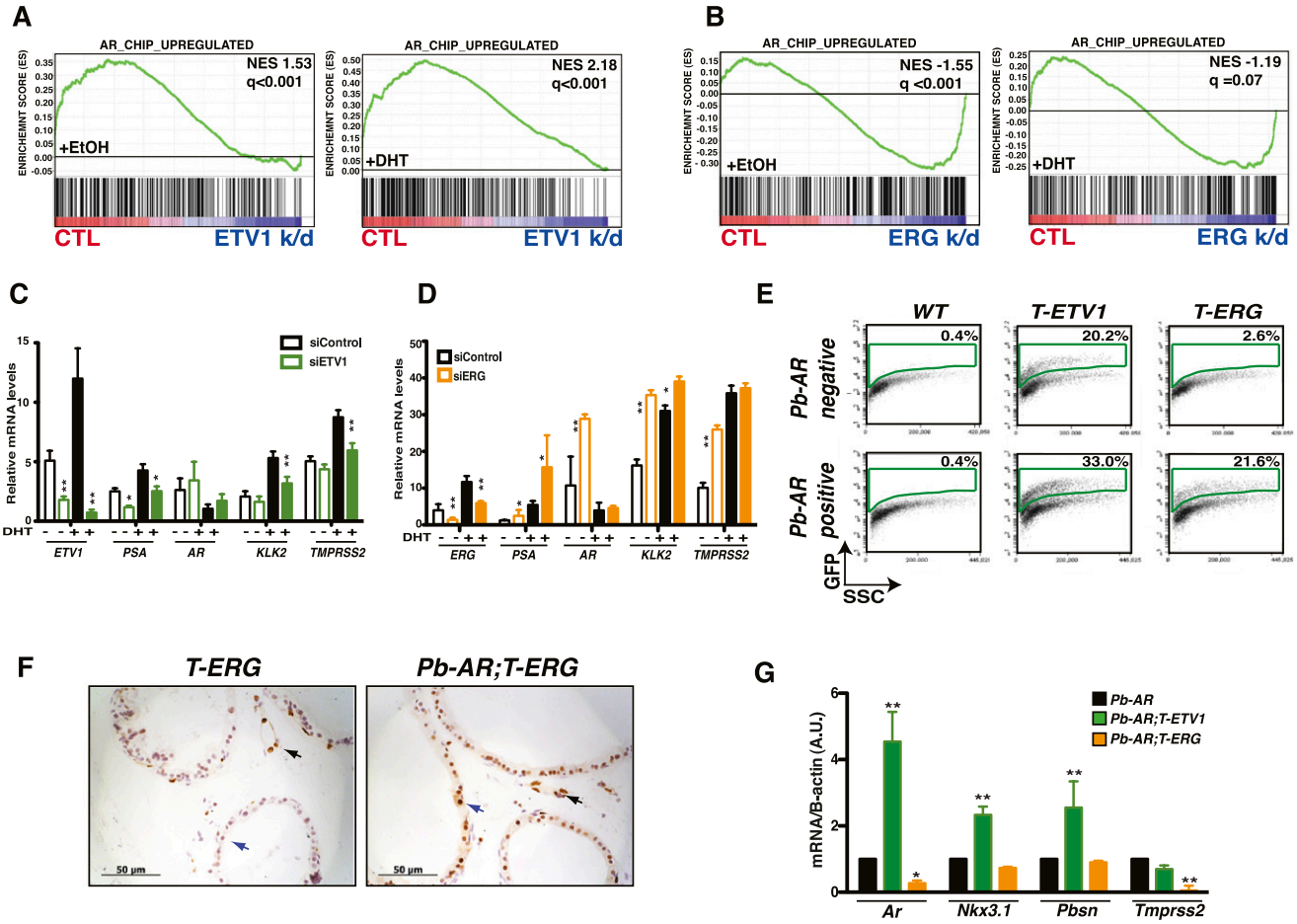

Figure 5. ERG and ETV1 regulate AR signaling in an opposite manner. (*A*) Androgen-induced genes are depleted in *ETV1*-silenced LNCaP cells upon 16-h androgen stimulation ([*left*] no androgen stimulation; [*right*] with androgen stimulation). The androgen-induced signature was obtained from the common AR ChIP targets in LNCaP and VCaP cells that were up-regulated in them upon androgen stimulation. (*B*) Androgen-induced genes are significantly enriched in *ERG*-silenced VCaP cells upon 16-h androgen stimulation compared with controls ([*left*] no androgen stimulation; [*right*] with androgen stimulation). (*C*,*D*) *ETV1* silencing specifically decreases expression of AR-associated genes (*C*), whereas *ERG* silencing increases their expression (*D*). Mean, $n = 3$; error bars, SEM; *t*-test: (*) $P < 0.05$; (**) $P < 0.01$. If no *P*-value is indicated, $P > 0.05$. (*E*) Flow cytometry analysis demonstrating robust GFP$^+$ population in the *T-ETV1* prostates but not in the *T-ERG* prostates. However, in the presence of the *Pb-AR* transgene, GFP expression can be readily detected in *Pb-AR;T-ERG* prostates; in addition, GFP expression in *Pb-AR;T-ETV1* prostates appear to be further elevated. (*F*) IHC staining showing weak ERG staining in the ventral lobe of a *T-ERG* knock-in male (blue arrow; compared with strong Erg staining in the endothelial cells [black arrow]) but much stronger ERG staining in the ventral lobe of a *Pb-AR;T-ERG* male (blue arrow; almost comparable with ERG staining in endothelial cells in the same section [black arrow]). Bars, 50 μm. (*G*) Real-time PCR quantification showing up-regulation of most AR target genes in *Pb-AR;T-ETV1* prostates and slight down-regulation of them in *Pb-AR;T-ERG* prostates in relation to those of *Pb-AR*-alone prostates. Mean, $n = 3$; error bars, SEM; *t*-test: (*) $P < 0.05$, (**) $P < 0.01$. If no *P*-value is indicated, $P > 0.05$.

network enriched in ETV1-only ChIP targets (Fig. 4C; Supplemental Fig. S15C). By independent ChIP analysis, we validated ETV1, but not ERG, binding to the *HSD17B7* and *HSD17B4* promoters (Fig. 6E; Supplemental Fig. S15D). Expression of *HSD17B7* in LNCaP cells was reduced upon ETV1 depletion (Fig 6F). In ETV1-overexpressing RWPE-1 cells, *HSD17B7* expression trended upward (although not statistically significant) (Supplemental Fig. S16A). We also confirmed higher *Hsd17b7* expression in lineage-depleted *T-ETV1* prostate cells (Fig. 6G). Since HSD17B7 is critical in converting less active forms of estrogen and androgen to more active forms (Fig. 6H; Krazeisen et al. 1999), and *Tmprss2* is an androgen and estrogen dual-responsive gene, we reasoned that up-regulation of the steroid biosynthesis pathway by ETV1 may provide prostate cells with an intrinsic source of steroids. If this supposition were correct, such cells might be intrinsically castration-resistant. To test this prediction, *T-ETV1* knock-in males as well as *T-ERG* and wild-type control males were castrated. We observed that almost half of prostate cells from the castrated *T-ETV1* mice were GFP$^+$. In addition, we also detected a small population of GFP^{low} prostate cells from the castrated *T-ERG* males (Supplemental Fig. S16B), consistent with a recent study and possibly reflecting the existence of a subpopulation of *Tmprss2*$^+$ prostate cells that are intrinsically castration-

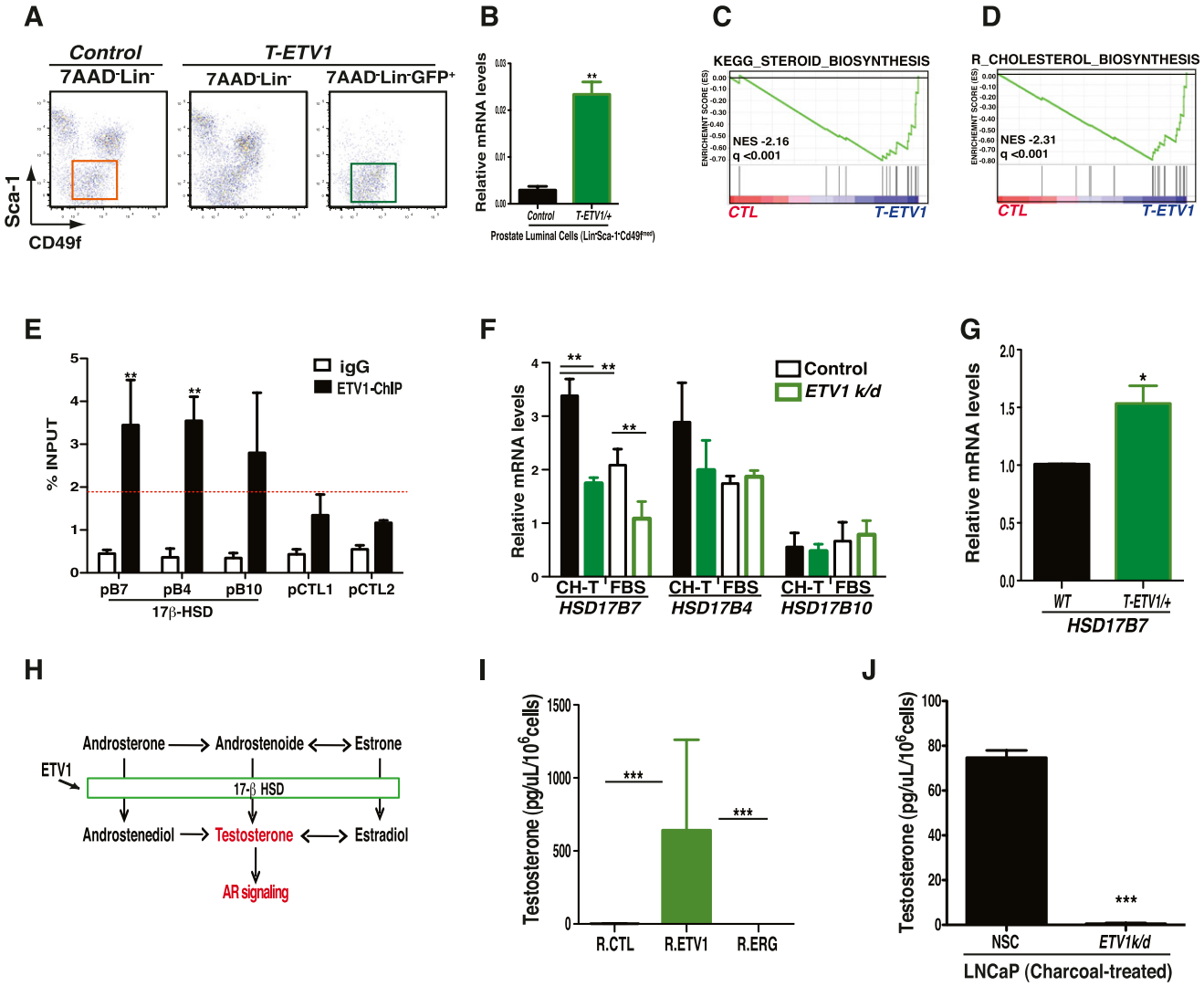

Figure 6. ETV1 regulates steroid metabolism in prostate cells. (*A*, *right* plot) Flow cytometry profiles and gating strategies showing GFP$^+$ prostate luminal cells (Lin$^-$Sca-1$^-$CD49f^{med}) sorted from *T-ETV1* knock-in males used for microarray analysis. (*Left* plot) The Lin$^-$Sca-1$^-$CD49f^{med} prostate luminal cells sorted from wild-type (WT) control males were used as the control. (*B*) Real-time PCR quantification confirming ectopic *ETV1* expression in sorted GFP$^+$ prostate luminal cells from *T-ETV1* knock-in mice (mean, $n = 3$ samples per group; error bars, SEM). (*C*,*D*) Steroid and cholesterol biosynthesis pathways are the top pathways significantly enriched in *T-ETV1* knock-in prostate luminal cells compared with controls. Note that a critical enzyme in the steroid biosynthesis pathway, HSD17B7, is also a key enzyme in the steroid hormone biosynthesis pathway, which is enriched in metastatic prostate cancers (Supplemental Fig. S15). (*E*) ChIP-PCR validation of ETV1 binding to *HSD17B7* (*pB7*), *HSD17B4* (*pB4*), and *HSD17B10* (*pB10*) promoters (mean, $n = 5$; error bars, SEM). (pCTL1 and pCTL2) Nonspecific promoter control regions. (*F*) Only HSD17B7 levels significantly decreased upon knockdown of ETV1 (k/d) (mean, $n = 3$, error bars, SEM) under both the androgen-deprivation condition ([CH-T] charcoal-treated) and the regular condition in the presence of serum (FBS). Conversely, *HSD17B7* expression increased upon ETV1 overexpression in RPWE-1 cells (Supplemental Fig. S16A). *t*-test: (**) $P < 0.01$. If no *P*-value is indicated, $P > 0.05$. (*G*) *T-ETV1* knock-in prostate cells exhibit increased *Hsd17b7* expression levels compared with wild-type controls (mean, $n = 3$; error bars, SEM). *t*-test: (*) *P*-value < 0.05. (*H*) Schematic diagram showing the key role of 17-β HSD enzymes, including HSD17B7, in converting androgen and estrogen from their less active forms to active forms. (*I*) ETV1 overexpression in RWPE-1 cells promoted the elevation of the endogenous testosterone level, while no changes were observed upon ERG overexpression (mean, $n = 4$; error bars, SEM). Testosterone levels per 10^6 cells (R.ETV1 mean = 642.16 pg/μL; R.ERG mean = 0.49 pg/μL; R.CTL mean = 1.89 pg/μL). *t*-test: (***) $P < 0.001$. (*J*) Testosterone levels were reduced in androgen-deprived (charcoal-treated) LNCaP cells upon stable ETV1 silencing (k/d) as compared with controls (mean, $n = 3$; error bars, SEM). (NSC) Nonsilencing shRNA control. Testosterone levels per 10^6 cells (NSC mean = 74.69 pg/μL; R.ERG mean = 0.49 pg/μL; *ETV1k/d* mean = 0.56 pg/μLr). *t*-test: (***) $P < 0.001$.

resistant (Casey et al. 2012). As expected, the castration-resistant GFP$^+$ cells in *T-ETV1* males exhibited higher *Hsd17b7* levels than controls (Supplemental Fig. S16C).

To determine whether increased ETV1 expression enhances steroid production, we directly measured by liquid chromatography/mass spectrometry (LC/MS) the levels

of endogenous testosterone in control, ETV1-expressing, and ERG-expressing human RWPE-1 cells. Remarkably, ETV1-expressing RWPE-1 cells showed much higher levels (>300-fold higher) of endogenous testosterone compared with ERG-expressing and control RWPE-1 cells (Fig. 6I; Supplemental Fig. S17A,B). Conversely, *ETV1* knockdown in LNCaP cells reduced testosterone production under conditions of androgen deprivation (Fig. 6J). To further characterize this observation, we quantified the intraprostatic levels of testosterone in wild-type, *T-ETV1*, and *T-ERG* mice under noncastrated and castrated conditions. As expected, noncastrated mice showed very low concentrations of testosterone in their prostate cells. Interestingly, castrated *T-ETV1* mice indeed exhibited higher testosterone levels than those of castrated wild-type and *T-ERG* prostate samples (Supplemental Fig. S17C). These results indicate that ETV1 expression directly regulates androgen production in prostate cells.

ETV1-only gene sets associate with an aggressive phenotype in patients

Data to this point suggest that ETV1 and its unique oncogenic program contribute to invasive prostate cancer. To relate these findings to patients, we analyzed data from a patient cohort that includes 22 primary localized and 29 metastatic samples, of which ~50% carried the *TMPRSS2-ERG* fusion (ETV1 rearrangement status not characterized) (Stanbrough et al. 2006). In this cohort, samples exhibiting higher *ERG* expression correlated with localized tumors, whereas high *ETV1* expression enriched for metastases (Fig. 7A). We repeated the analysis with an independent cohort of 150 prostate tumor samples from patients at Memorial Sloan-Kettering Cancer Center (MSKCC) (Taylor et al. 2010). A correlation between high *ETV1* expression and metastases and the presence of more localized prostate tumors in the high *ERG* expression group were confirmed in this second cohort (Fig. 7B). Samples with high *ERG* or high *ETV1* expression did not overlap, consistent with a strong tendency to mutual exclusivity in both primary and metastatic samples (Supplemental Fig. S18A,B). We next interrogated whether *ERG* and *ETV1* cooperate similarly with *PTEN* deletion in the MSKCC cohort by analyzing the outcome of patients carrying deletion of *PTEN* and overexpression of *ERG* or *ETV1*. High *ERG* expression with *PTEN* loss failed to correlate with the worse outcome (Fig. 7C). In contrast, high *ETV1* expression cooperated with *PTEN* loss, as shown by much poorer disease-free survival (Fig. 7D). These data are consistent with a previous report correlating greater disease recurrence with high *ETV1* levels (Shin et al. 2009).

We next evaluated for the first time whether ERG- and ETV1-specific gene signatures serve as tumor biomarkers or as a predictor of aggressive behavior. We analyzed ERG and ETV1 signatures defined in our analysis of ERG and ETV1 ChIP and expression profiling data in the Swedish watchful waiting and MSKCC cohorts (Setlur et al. 2008; Taylor et al. 2010), including 362 localized prostate cancer samples and 150 patients with localized and metastatic prostate cancer, respectively. Of note, ETV1-specific signatures, comprised of genes directly bound by ETV1 and up-regulated upon ETV1 expression, are associated with a high Gleason score (>7) in both cohorts and with lethality in the MSKCC cohort, again highlighting a correlation between ETV1 expression and a worse disease prognosis (Fig. 7E; Supplemental Fig. S18C). Taken together, data from three independent patient cohorts concur in validating that ETV1 drives a transcriptional program in prostate cells that is distinct from that of ERG. Moreover, our data suggest for the first time that the ETV1-driven program dictates a poorer outcome in patients with prostate cancer.

Discussion

Our multidisciplinary studies reveal distinct transcription programs regulated by ERG and ETV1 in prostate cells. In particular, we show that they control overlapping gene targets but largely in an opposing fashion; they also control unique targets and pathways. Overall, the networks regulated by ERG are associated with cell cycle and DNA replication, whereas those controlled by ETV1 are related to synthesis of lipids and other metabolic pathways. These networks are distinct and contribute to different pathogenic consequences. These conclusions are validated by findings in novel knock-in mouse models and by patient outcome analysis.

AR signaling is a common pathway regulated by ERG and ETV1 but in an opposite manner

AR signaling is central to prostate development and tumorigenesis. Indeed, AR has recently been implicated in double-strand breaks that favor the formation of translocations involving androgen-driven promoters and ETS family members (Lin et al. 2009; Haffner et al. 2010). We observed a complex relationship between ERG- or ETV1-regulated networks and AR signaling. In agreement with prior findings, we observed negative regulation of AR signaling by ERG (Yu et al. 2010). In contrast, ETV1 cooperates with AR signaling by favoring activation of the AR transcriptional program (Fig. 5). Upon androgen stimulation, ETV1 recruitment to the established *PSA* and *TMPRSS2* regulatory elements correlates with AR binding, suggesting coordinate regulation of androgen-driven genes by ETV1 and AR.

We validated divergent regulation of AR signaling by ERG and ETV1 in vivo in knock-in mice. As *Tmprss2* is an AR target, the transcriptional output from the *Tmprss2* promoter serves as a reporter for AR activity. In *T-ERG* knock-in mice, ERG expression appears to down-regulate AR target genes, including *Tmprss2*, which would lead to down-regulation of its own expression, thus forming a negative regulatory loop, consistent with prior findings (Yu et al. 2010). In contrast, in *T-ETV1* knock-in males, ETV1 expression positively cooperated with AR signaling, leading to further enhancement of expression of AR targets, including *Tmprss2*, which would then support robust expression of ETV1 and the GFP reporter, reflecting a

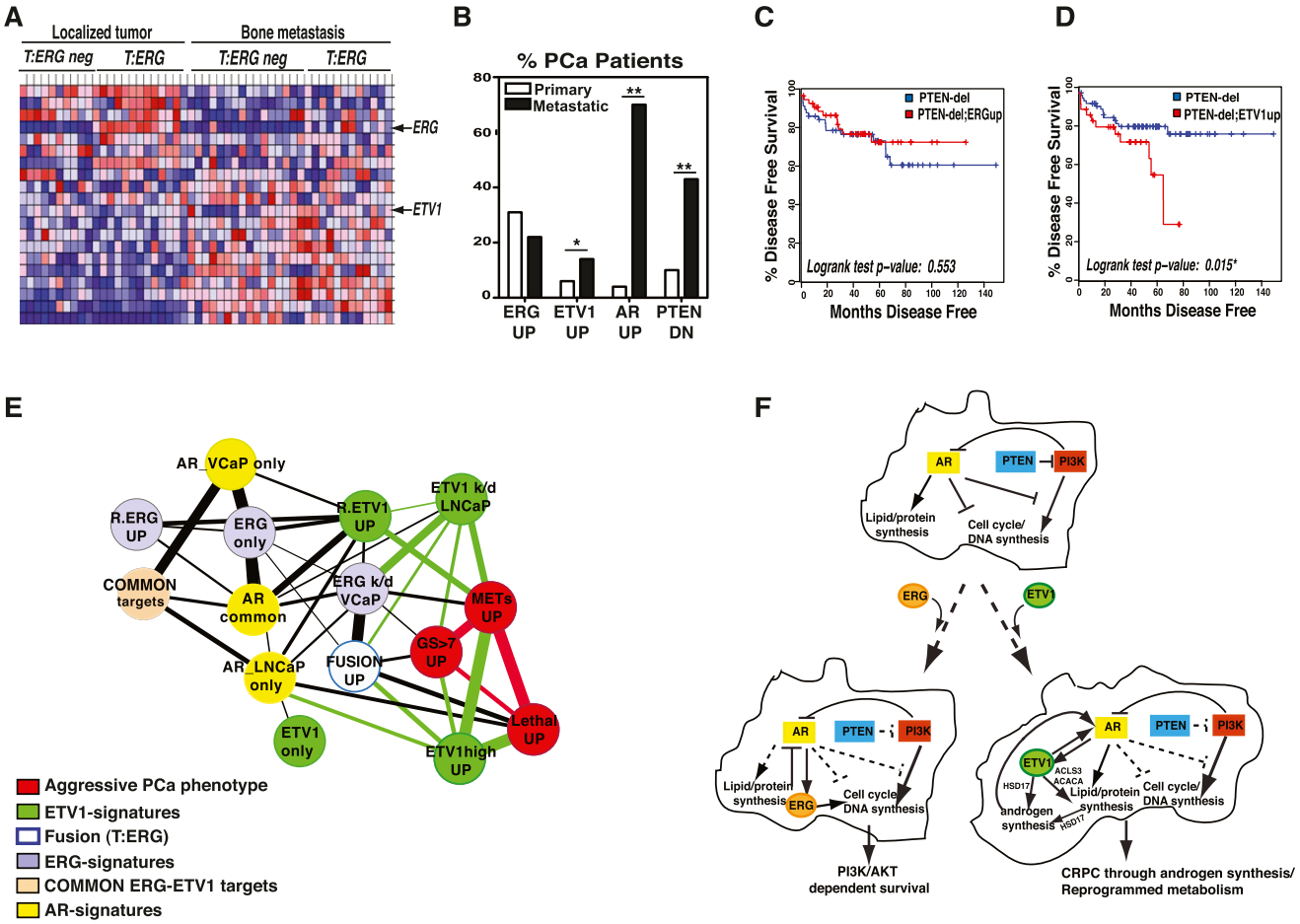

Figure 7. ETV1, rather than ERG, expression and the program it drives are associated with advanced prostate cancer in multiple patient cohorts. (*A*) Heat map showing ERG and ETV1 expression pattern in localized and bone metastatic prostate cancer samples using the Beth-Israel (BI) cohort data set (Stanbrough et al. 2006). Heat map generated by hierarchical clustering and by applying Pearson correlation and the complete linkage rule. Heat map showing differentially expressed select genes (fold change, >2; FDR, <0.05). (*B*) Graph showing ERG and ETV1 expression along prostate cancer progression from localized to metastatic samples in the MSKCC cohort (Taylor et al. 2010). The graph reveals that the number of patients carrying *ETV1* overexpression (fold change, >3), *PTEN* deletion, and AR alterations (amplification and expression fold change, >3) increased in metastatic samples compared with localized prostate tumors, while patients carrying high levels of *ERG* (fold change, >3) did not increase over time (also in Supplemental Fig. S18B). *t*-test: (*) *P*-value < 0.05; (**) *P*-value < 0.01. If no *P*-value is indicated, $P > 0.05$. (*C*) Disease-free survival plot showing that among all patients in the MSKCC cohort with *PTEN* deletion ($n = 21$), those with *ERG* overexpression ($n = 4$) exhibited no survival difference from the rest of patient with *PTEN* deletion. $P = 0.553$ by log-rank test. (*D*) Disease-free survival plot showing that among all patients in the MSKCC cohort with *PTEN* deletion ($n = 21$), those with *ETV1* overexpression ($n = 8$) exhibited much worse survival compared with remaining patients with *PTEN* deletion. (*) $P = 0.015$ by log-rank test. (*E*) Correlation between ERG- and ETV1-associated gene sets with patient prognosis. Overlap between genes enriched in patient samples associated with indolent or aggressive prostate cancer from the MSKCC cohort (Taylor et al. 2010) and ETV1 or ERG gene sets defined in Figures 3 and 4. ETV1-associated genes are enriched in patients with a higher Gleason score in the Swedish cohort (also in Supplemental Fig. S18C; Setlur et al. 2008). "UP" represents those genes up-regulated in the shown category with a fold change of >1.5. The significance of overlap of these gene sets was calculated by the Fisher exact test and visualized as connecting line width (cutoff, $P = 0.01$). (Red) Aggressive prostate cancer-associated; (green) ETV1-associated gene sets; (blue) *TMPRSS2-ERG* fusion-associated gene sets; (purple) ERG signature-associated gene sets; (yellow) AR-associated gene sets; (orange) common targets of ERG and ETV1. (*F*) Model illustrating the differential contribution by ERG and ETV1 to prostate tumorigenesis under the PTEN loss background. See the text for details.

positive regulatory loop. These mechanistic differences account for the striking difference in GFP intensity in the two knock-in strains, which were identically engineered (Fig. 5E). Of note, the negative loop in the *T-ERG* knock-in is overridden by elevated AR signaling in vivo. Indeed, the only consistent association between the *TMPRSS2-ERG* fusion and clinical parameters identified thus far is the association of this fusion (in particular when ERG expression was measured by IHC) with a high level of AR signaling (Minner et al. 2011; Hoogland et al. 2012). Last, in human prostate tumors with *ETV1* fusions, several 5′ fusion partners other than *TMPRSS2* are also involved.

Since the majority of these 5′ fusion partners are also androgen-responsive genes (Tomlins et al. 2007; Attard et al. 2008b), we reason that a similar positive regulatory loop may be operative in such tumors to enhance AR signaling and ETV1 expression. In addition, AR has been reported to regulate the endogenous *ETV1* locus as well (Cai et al. 2007), suggesting a positive feedback between both the endogenous and rearranged ETV1, thus predisposing affected prostate cells for prostate cancer development.

ETV1, but not ERG, reprograms metabolic pathways in normal prostate epithelial cells

Among the unique genes up-regulated by ETV1, those encoding for enzymes involved in cholesterol and steroid biosynthesis and in cancer-associated metabolic pathways (e.g., glycolysis) (Supplemental Fig. S15A) are of particular interest. In particular, we were able to demonstrate increased production of endogenous testosterone upon ETV1 expression in both human prostate cells and *T-ETV1* knock-in mice (upon castration) (Fig. 6I,J; Supplemental Fig. S17C). Due to the increased testosterone level, we anticipated observing higher levels of androstenedione or dihydrotestosterone as well; however, none were detected, possibly due to technical limitations. However, decreased levels of estrone were detected in ETV1-expressing RWPE-1 cells, probably due to the promotion of testosterone synthesis (Supplemental Fig. S17B).

Although ETV1-expressing prostate cells appear ostensibly normal (Fig. 1E), their metabolic programs resemble those of cancer cells. Increased aerobic glycolysis has been observed only in advanced disease, whereas increased sterol and protein synthesis are common features of both primary and advanced prostate cancer (Swinnen et al. 2000; Rossi et al. 2003; Ettinger 2004; Bauer et al. 2005). In particular, activation of lipid metabolism has been described in most localized and metastatic prostate tumors, underscoring its potential role in prostate cancer progression (Twiddy et al. 2010; Zadra et al. 2010). Arachidonic acid metabolism and Toll-like receptor signaling inflammatory pathways (De Marzo et al. 2007) are enriched in both CRPCs with higher ETV1 expression and *T-ETV1* mouse prostate cells, correlating with the extended areas of inflammation observed in *T-ETV1* prostates (Fig. 1E). Thus, we speculate that this unique ETV1-controlled program, in concert with positive cooperation with AR signaling, may reprogram prostate cells for malignant progression in association with additional oncogenic events (Fig. 7F).

TMPRSS2-ETV1 *and* TMPRSS2-ERG *fusions make distinct contributions to prostate tumorigenesis*

Although both *Tmprss2-ERG* and *Tmprss2-ETV1* cooperate with loss of a single copy of *Pten* in leading to localized PIN lesions, similar to those demonstrated previously in mice overexpressing *ERG* or *ETV1* under the *Probasin* or viral promoters (Carver et al. 2009; King et al. 2009; Zong et al. 2009) or in mice expressing *ERG* from an extended human *TMPRSS2* promoter (Casey et al. 2012), our mechanistic and animal model studies suggest they do so differently (Fig. 7F). Ectopic ERG expression likely represses the differentiation program of prostate cells (e.g., represses AR and AR targets and up-regulates Ezh2 and its targets, as suggested previously) (Yu et al. 2010). Interestingly, it has been reported that *Pten* loss leads to a castration-like phenotype by suppressing androgen-responsive gene expression through modulation of AR transcriptional activity. Moreover, conditional deletion of AR further promotes proliferation of prostate cells with *Pten* loss (Mulholland et al. 2011). We speculate that *TMPRSS2-ERG* may act in a similar fashion by down-regulating AR and, consequently, promoting cell proliferation. Indeed, the ERG expression pattern in our murine models (Figs. 1C, 2B,D) suggests that ERG may be required primarily at early stages of the disease but may be not as functionally relevant at late stages. This may explain our observation that ERG cooperates with Pten haploinsufficiency (i.e., under a more sensitized $Pten^{+/-}$ background), whereas its contribution under the total *Pten* loss background appears far less. The high levels of ERG expression often observed in localized fusion-positive human prostate cancers may be a secondary consequence of high activity of AR signaling in such tumors in general (i.e., similar to what we observed in *Pb-AR;T-ERG* prostates) (Fig. 5E–G) rather than a critical requirement of ERG overexpression at this stage. In contrast, ectopic ETV1 expression appears to enhance androgen signaling and reprogram the metabolism of prostate cells, processes critical for both early and advanced stages of the disease. Activation of the PI3K/AKT pathway drives anabolic metabolism and tumorigenesis (Ward and Thompson 2012). We propose that *TMPRSS2-ETV1* cooperates with *Pten* loss by further enhancing metabolic reprogramming, in particular, by favoring steroid biosynthesis, a pathway critical for invasive adenocarcinoma cells. The cooperation between ETV1 and *Pten* loss is also consistent with the recent finding that combined loss of Pten and COP1, a ubiquitin ligase that negatively regulates ETV1 levels, leads to more invasive prostate adenocarcinomas (Vitari et al. 2011).

In aged *PbCre;T-3Mb-Erg;*$Pten^{L/L}$ males, we also observed invasive prostate cancer (Fig. 2E). Interestingly, in such invasive cancers, we observed a mosaic pattern of Erg expression (Fig. 2E). Several possibilities can explain this observation. Erg-expressing prostate cells may send signals to Erg-negative cells so that high levels of Erg expression are not needed in all cells of the invasive cancer. Alternatively, Erg may not be critical for the development of advanced cancer, and another genetic or epigenetic change may contribute to advanced disease. One potential genetic change is haploinsufficiency of one or more deleted genes in the interstitial region. Interestingly, *ETS2*, a gene residing within the interstitial region, was recently proposed to be a tumor suppressor contributing to aggressive prostate cancer cases carrying *TMPRSS2-ERG* fusions with deletion (Grasso et al. 2012). Whether haploinsufficiency of the deleted genes (e.g., *ETS2*) contributes to the advanced cancer phenotype awaits further investigation.

Distinct roles of ETV1 and ERG in prostate tumorigenesis have implications for prostate cancer therapy

Our analysis of gene expression and patient outcome data sets underscores the relevance of distinct features of ETV1-regulated pathways to invasive adenocarcinoma progression. ETV1-defined, but not ERG-defined, gene sets are associated with high Gleason score and metastasis (Fig. 7E; Supplemental Fig. S18C). Our observation that *ERG* expression does not correlate with the worse outcome is consistent with a recent meta-analysis describing no association of ERG with Gleason score, clinical outcome, or recurrence of the disease including 62 cohorts (Pettersson et al. 2012). Of note, ERG mRNA and protein level analysis (Markert et al. 2011; Pettersson et al. 2012) showed that *TMPRSS2-ERG* fusion status does not always correlate with the *TMPRSS2-ERG* transcriptional signature or ERG protein level in prostate cancer patients. Accordingly, most recent clinical studies have supported high ERG expression levels as a favorable prognosis biomarker (Bismar et al. 2012; Kimura et al. 2012; Suh et al. 2012). Consistent with our findings, however, *ETV1* expression at the transcript level has been associated with a greater Gleason score and recurrence of the disease (Attard et al. 2008b; Shin et al. 2009). Unfortunately, thus far, it has not been possible to study clinical relevance of ETV1 at the protein level due to the lack of satisfactory antibodies. Moreover, ETV1, rather than ERG, is among AR ChIP targets defined recently from primary CRPC patient samples (Sharma et al. 2013). Last, there is also a high overlap between ETV1-associated, castration-associated, and recurrent prostate tumor signatures (Supplemental Fig. S18E). Although *TMPRSS2-ETV1* fusions are only found in ~1%–2% of all prostate cancer cases, prostate tumors with elevated *ETV1* expression (5%–10% of all cases) are enriched in advanced disease (Fig. 7A,B), suggesting that the ETV1-driven oncogenic program may be selected for during prostate cancer progression.

In summary, our data suggest that ETV1 is a novel marker of aggressive prostate cancer, and the oncogenic program it drives may be an important therapeutic target for treating advanced prostate cancer. Metabolic enzymes (such as HSD17B7) that are regulated by ETV1 may be explored as therapeutic targets. Moreover, ETS factors have been described to modulate the Ras/MAPK pathway (Hollenhorst et al. 2011). Interestingly, ETV1 overexpression, but not that of ERG, is associated with Ras/MAPK activity in a range of tumors, including ETV1-dependent melanoma and gastrointestinal stromal tumor, where ETV1 is a master regulator of lineage (Chi et al. 2010; Jane-Valbuena et al. 2010). These observations raise the possibility that MAPK inhibitors may be explored to target ETV1-overexpressing tumors. In conclusion, our study suggests that tumors characterized by an ETV1 expression signature through either translocation or other mechanisms represent a distinct biological entity associated with aggressive prostate cancer. Future research should focus on exploring novel therapeutic approaches for this entity.

Materials and methods

Mouse lines

Tmprss2-ETS conditional knock-in mice were generated by standard gene targeting. *Pb-Cre* (*Pb-Cre4*) transgenic mice were acquired from the Mouse Models of Human Cancers Consortium (MMHCC) repository. *Pten* conditional knockout mice ($Pten^{L}$) and *Pb-AR* [FVB-Tg(Pbsn-Ar*E231G)] transgenic mice were acquired from JAX. $Pten^{+/-}$ mice were generated by crossing $Pten^{L/+}$ mice to *Gata1-Cre* mice. All studies were approved by the Institutional Animal Care and Use Committee (IACUC).

Pathology, immunostaining, and flow cytometry

Standard protocols were followed.

Cell lines

Cell lines were obtained from American Type Culture Collection and cultured accordingly. ERG or ETV1 overexpression and silencing experiments were performed by standard protocols.

RT–PCR

Real-time RT–PCR was performed according to standards protocols. All primer sequences are listed in Supplemental Table S2.

Gene expression microarray analysis

RWPE-1 stable cell clones (R.ERG, R.ETV1, and R.CTL) were grown under normal conditions. VCaP and LNCaP cells, 24 h after ERG or ETV1 RNAi, respectively, were grown in hormone-depleted conditions for 2 d, and then in the presence or absence of 10 nM DHT for 16 h. Mouse primary prostate cells were FACS-sorted and processed according to standard procedures. Affymetrix HG133 plus 2.0 or Mouse Genome 430 2.0 expression arrays were used for human or mouse samples, respectively. Gene Pattern software (Reich et al. 2006) was used for data normalization, extraction of expression values, and generation of GTC files for GSEA (Subramanian et al. 2005). A bidimensional comparison plot was used to compare differentially expressed genes ($P < 0.05$ by two-tailed *t*-test) in RWPE-1 cells upon overexpression of either ETV1 or ERG.

ChIP and ChIP-on-chip

BioChIP–chip for ETV1 was performed as described (Kim et al. 2008), and conventional ChIP–chip reaction for ERG was as described (Kim et al. 2004). Affymetrix Human Promoter 1.0R array hybridization was performed at the Dana-Farber Cancer Institute Microarray Core Facility. Peak identification was calculated by MAT score (Johnson et al. 2006). For ChIP-PCR experiments, conventional ChIP reactions were performed. Antibodies used were as follows: anti-AR (N20X), anti-ERG (C17X) and anti-rabbit IgG from Santa Cruz Biotechnology, and anti-ETV1 kindly provided by Dr. Litovchick. The online DAVID functional annotation tool (Huang et al. 2009) and the IPA tool (Ingenuity Systems, Inc.) were used to determine the enrichment for all "FAT" GO terms and canonical pathways/networks in each gene set.

Patient tumor data analysis

Gene sets associated with indolent and aggressive prostate cancer were extracted from the Swedish, MSKCC, Sharma, and

Glinsky cohorts (Glinsky 2004; Setlur et al. 2008; Taylor et al. 2010; Sharma et al. 2013) and analyzed for their mutual overlap between tumor cohort-derived signatures (differentially expressed genes: fold change, >1.5; false discovery rate [FDR], <0.05) and ERG- and ETV1-associated gene sets obtained in our studies. The overlap between gene sets was represented by a connectivity network, where the width of the connector edge was −log10(*P*-value). The *P*-value was derived from a hypergeometric distribution by using Fisher exact test to analyze the significance of the mutual overlap. Cytoscape software version 2.8 (Cline et al. 2007) was used for the visualization of gene sets overlapping the network.

Statistics

All statistics were based on a Student's *t*-test, unless otherwise indicated. Dot plots and histograms show data means, and error bars are standard error of the mean (SEM). All statistics were performed using the data analysis package within Microsoft Excel or the analysis tool within GraphPad Prism 5.0. Kaplan-Meier survival analysis was performed using GraphPad Prism 5.0.

Steroid metabolism measurement

Steroids from RWPE-1 and androgen-deprived LNCaP cells were extracted following Lemmen et al. (2002) and quantified by LC/MS at the Harvard FAS Center for Systems Biology.

Testosterone measurement

The intraprostatic testosterone levels were measured by a mouse testosterone ELISA kit (Calbiotech) based on the manufacturer's instructions. Briefly, mouse prostates were microdissected in cold PBS and lysed in RIPA buffer. Testosterone levels were calculated as the total amount per gram of total protein.

Accession number

The Gene Expression Omnibus accession number is GSE39388.

Acknowledgments

We thank Drs. Larisa Litovchick, Carmen Priolo, and Fatima Al-Shahrour for reagents, mouse surgical techniques, analysis support, and helpful discussions, and Dr. Maaike van Bragt for FACS analysis of knock-in mammary glands. This work was supported by a Career Development Award from Dana-Farber/Harvard Cancer Center Prostate Cancer SPORE (to Z.L.), a post-doctoral award from the Spanish Ministry of Science (EX2006-0958 to E.B.), and grants from the Department of Defense (PC060492 to S.H.O., PC100704 to Z.L., and PC080097 to E.B.) and NIH (U01CA105423 to S.H.O.). S.H.O. is an Investigator of Howard Hughes Medical Institute.

References

Attard G, Clark J, Ambroisine L, Fisher G, Kovacs G, Flohr P, Berney D, Foster CS, Fletcher A, Gerald WL, et al. 2008a. Duplication of the fusion of TMPRSS2 to ERG sequences identifies fatal human prostate cancer. *Oncogene* **27:** 253–263.

Attard G, Clark J, Ambroisine L, Mills IG, Fisher G, Flohr P, Reid A, Edwards S, Kovacs G, Berney D, et al. 2008b. Heterogeneity and clinical significance of ETV1 translocations in human prostate cancer. *Br J Cancer* **99:** 314–320.

Bauer DE, Hatzivassiliou G, Zhao F, Andreadis C, Thompson CB. 2005. ATP citrate lyase is an important component of cell growth and transformation. *Oncogene* **24:** 6314–6322.

Bismar TA, Dolph M, Teng L-H, Liu S, Donnelly B. 2012. ERG protein expression reflects hormonal treatment response and is associated with Gleason score and prostate cancer specific mortality. *Eur J Cancer* **48:** 538–546.

Bolstad BM, Irizarry RA, Astrand M, Speed TP. 2003. A comparison of normalization methods for high density oligonucleotide array data based on variance and bias. *Bioinformatics* **19:** 185–193.

Cai C, Hsieh C-L, Omwancha J, Zheng Z, Chen S-Y, Baert J-L, Shemshedini L. 2007. ETV1 is a novel androgen receptor-regulated gene that mediates prostate cancer cell invasion. *Methods Enzymol* **21:** 1835–1846.

Carver BS, Tran J, Gopalan A, Chen Z, Shaikh S, Carracedo A, Alimonti A, Nardella C, Varmeh S, Scardino PT, et al. 2009. Aberrant ERG expression cooperates with loss of PTEN to promote cancer progression in the prostate. *Nat Genet* **41:** 619–624.

Casey OM, Fang L, Hynes PG, Abou-Kheir WG, Martin PL, Tillman HS, Petrovics G, Awwad HO, Ward Y, Lake R, et al. 2012. TMPRSS2- driven ERG expression in vivo increases self-renewal and maintains expression in a castration resistant subpopulation. *PLoS ONE* **7:** e41668.

Chi P, Chen Y, Zhang L, Guo X, Wongvipat J, Shamu T, Fletcher JA, Dewell S, Maki RG, Zheng D, et al. 2010. ETV1 is a lineage survival factor that cooperates with KIT in gastrointestinal stromal tumours. *Nature* **467:** 849–853.

Cline MS, Smoot M, Cerami E, Kuchinsky A, Landys N, Workman C, Christmas R, Avila-Campilo I, Creech M, Gross B, et al. 2007. Integration of biological networks and gene expression data using Cytoscape. *Nat Protoc* **2:** 2366–2382.

de Boer E, Rodriguez P, Bonte E, Krijgsveld J, Katsantoni E, Heck A, Grosveld F, Strouboulis J. 2003. Efficient biotinylation and single-step purification of tagged transcription factors in mammalian cells and transgenic mice. *Proc Natl Acad Sci* **100:** 7480–7485.

De Marzo AM, Platz EA, Sutcliffe S, Xu J, Grönberg H, Drake CG, Nakai Y, Isaacs WB, Nelson WG. 2007. Inflammation in prostate carcinogenesis. *Nat Rev Cancer* **7:** 256–269.

Demichelis F, Fall K, Perner S, Andren O, Schmidt F, Setlur SR, Hoshida Y, Mosquera J-M, Pawitan Y, Lee C, et al. 2007. TMPRSS2:ERG gene fusion associated with lethal prostate cancer in a watchful waiting cohort. *Oncogene* **26:** 4596–4599.

Dentelli P, Del Sorbo L, Rosso A, Molinar A, Garbarino G, Camussi G, Pegoraro L, Brizzi MF. 1999. Human IL-3 stimulates endothelial cell motility and promotes in vivo new vessel formation. *J Immunol* **163:** 2151–2159.

Dvorak HF. 1986. Tumors: Wounds that do not heal. Similarities between tumor stroma generation and wound healing. *N Engl J Med* **315:** 1650–1659.

Ettinger SL. 2004. Dysregulation of sterol response element-binding proteins and downstream effectors in prostate cancer during progression to androgen independence. *Cancer Res* **64:** 2212–2221.

Glinsky GV. 2004. Gene expression profiling predicts clinical outcome of prostate cancer. *J Clin Invest* **113:** 913–923.

Gopalan A, Leversha MA, Satagopan JM, Zhou Q, Al-Ahmadie HA, Fine SW, Eastham JA, Scardino PT, Scher HI, Tickoo SK, et al. 2009. TMPRSS2-ERG gene fusion is not associated with outcome in patients treated by prostatectomy. *Cancer Res* **69:** 1400–1406.

Grasso CS, Wu Y-M, Robinson DR, Cao X, Dhanasekaran SM, Khan AP, Quist MJ, Jing X, Lonigro RJ, Brenner JC, et al. 2012. The mutational landscape of lethal castration-resistant prostate cancer. *Nature* **487:** 239–243.

Gupta S, Iljin K, Sara H, Mpindi JP, Mirtti T, Vainio P, Rantala J, Alanen K, Nees M, Kallioniemi O. 2010. FZD4 as a mediator of ERG oncogene-induced WNT signaling and epithelial-to-mesenchymal transition in human prostate cancer cells. *Cancer Res* **70:** 6735–6745.

Haffner MC, Aryee MJ, Toubaji A, Esopi DM, Albadine R, Gurel B, Isaacs WB, Bova GS, Liu W, Xu J, et al. 2010. Androgen-induced TOP2B-mediated double-strand breaks and prostate cancer gene rearrangements. *Nat Genet* **42:** 668–675.

Han G, Buchanan G, Ittmann M, Harris JM, Yu X, Demayo FJ, Tilley W, Greenberg NM. 2005. Mutation of the androgen receptor causes oncogenic transformation of the prostate. *Proc Natl Acad Sci* **102:** 1151–1156.

Hermans KG, Boormans JL, Gasi D, van Leenders GJHL, Jenster G, Verhagen PCMS, Trapman J. 2009. Overexpression of prostate-specific TMPRSS2(exon 0)-ERG fusion transcripts corresponds with favorable prognosis of prostate cancer. *Clin Cancer Res* **15:** 6398–6403.

Hollenhorst PC, Ferris MW, Hull MA, Chae H, Kim S, Graves BJ. 2011. Oncogenic ETS proteins mimic activated RAS/MAPK signaling in prostate cells. *Genes Dev* **25:** 2147–2157.

Holzer RG, Ryan RE, Tommack M, Schlekeway E, Jorcyk CL. 2004. Oncostatin M stimulates the detachment of a reservoir of invasive mammary carcinoma cells: Role of cyclooxygenase-2. *Clin Exp Metastasis* **21:** 167–176.

Hoogland AM, Jenster G, van Weerden WM, Trapman J, van der Kwast T, Roobol MJ, Schröder FH, Wildhagen MF, van Leenders GJ. 2012. ERG immunohistochemistry is not predictive for PSA recurrence, local recurrence or overall survival after radical prostatectomy for prostate cancer. *Mod Pathol* **25:** 471–479.

Huang DW, Sherman BT, Lempicki RA. 2009. Systematic and integrative analysis of large gene lists using DAVID bioinformatics resources. *Nat Protoc* **4:** 44–57.

Jacquinet EE, Rao NVN, Rao GVG, Hoidal JRJ. 2000. Cloning, genomic organization, chromosomal assignment and expression of a novel mosaic serine proteinase: Epitheliasin. *FEBS Lett* **468:** 93–100.

Jane-Valbuena J, Widlund HR, Perner S, Johnson LA, Dibner AC, Lin WM, Baker AC, Nazarian RM, Vijayendran KG, Sellers WR, et al. 2010. An oncogenic role for ETV1 in melanoma. *Cancer Res* **70:** 2075–2084.

Johnson WE, Li W, Meyer CA, Gottardo R, Carroll JS, Brown M, Liu XS. 2006. Model-based analysis of tiling-arrays for ChIP–chip. *Proc Natl Acad Sci* **103:** 12457–12462.

Kim J, Bhinge AA, Morgan XC, Iyer VR. 2004. Mapping DNA-protein interactions in large genomes by sequence tag analysis of genomic enrichment. *Nat Methods* **2:** 47–53.

Kim J, Chu J, Shen X, Wang J, Orkin SH. 2008. An extended transcriptional network for pluripotency of embryonic stem cells. *Cell* **132:** 1049–1061.

Kimura T, Furusato B, Miki J, Yamamoto T, Hayashi N, Takahashi H, Kamata Y, van Leenders GJ, Visakorpi T, Egawa S. 2012. Expression of ERG oncoprotein is associated with a less aggressive tumor phenotype in Japanese prostate cancer patients. *Pathol Int* **62:** 742–748.

King JC, Xu J, Wongvipat J, Hieronymus H, Carver BS, Leung DH, Taylor BS, Sander C, Cardiff RD, Couto SS, et al. 2009. Cooperativity of TMPRSS2-ERG with PI3-kinase pathway activation in prostate oncogenesis. *Nat Genet* **41:** 524–526.

Klezovitch O, Risk M, Coleman I, Lucas JM, Null M, True LD, Nelson PS, Vasioukhin V. 2008. A causal role for ERG in neoplastic transformation of prostate epithelium. *Proc Natl Acad Sci* **105:** 2105–2110.

Krazeisen A, Breitling R, Imai K, Fritz S, Möller G, Adamski J. 1999. Determination of cDNA, gene structure and chromosomal localization of the novel human 17β-hydroxysteroid dehydrogenase type 7(1). *FEBS Lett* **460:** 373–379.

Kunderfranco P, Mello-Grand M, Cangemi R, Pellini S, Mensah A, Albertini V, Malek A, Chiorino G, Catapano CV, Carbone GM. 2010. ETS transcription factors control transcription of EZH2 and epigenetic silencing of the tumor suppressor gene Nkx3.1 in prostate cancer. *PLoS ONE* **5:** e10547.

Lemmen JG, van den Brink CE, Legler J, van der Saag PT, van der Burg B. 2002. Detection of oestrogenic activity of steroids present during mammalian gestation using oestrogen receptor α- and oestrogen receptor β-specific in vitro assays. *J Endocrinol* **174:** 435–446.

Lesche R, Groszer M, Gao J, Wang Y, Messing A, Sun H, Liu X, Wu H. 2002. Cre/loxP-mediated inactivation of the murine Pten tumor suppressor gene. *Genesis* **32:** 148–149.

Lin C, Yang L, Tanasa B, Hutt K, Ju B-G, Ohgi KA, Zhang J, Rose DW, Fu X-D, Glass CK, et al. 2009. Nuclear receptor-induced chromosomal proximity and DNA breaks underlie specific translocations in cancer. *Cell* **139:** 1069–1083.

Markert EK, Mizuno H, Vazquez A, Levine AJ. 2011. Molecular classification of prostate cancer using curated expression signatures. *Proc Natl Acad Sci* **108:** 21276–21281.

Minner S, Enodien M, Sirma H, Luebke AM, Krohn A, Mayer PS, Simon R, Tennstedt P, Muller J, Scholz L, et al. 2011. ERG status is unrelated to PSA recurrence in radically operated prostate cancer in the absence of antihormonal therapy. *Clin Cancer Res* **17:** 5878–5888.

Mulholland DJ, Tran LM, Li Y, Cai H, Morim A, Wang S, Plaisier S, Garraway IP, Huang J, Graeber TG, et al. 2011. Cell autonomous role of PTEN in regulating castration-resistant prostate cancer growth. *Cancer Cell* **19:** 792–804.

Nam RK, Sugar L, Yang W, Srivastava S, Klotz LH, Yang L-Y, Stanimirovic A, Encioiu E, Neill M, Loblaw DA, et al. 2007. Expression of the TMPRSS2:ERG fusion gene predicts cancer recurrence after surgery for localised prostate cancer. *Br J Cancer* **97:** 1690–1695.

Oikawa T, Yamada T. 2003. Molecular biology of the Ets family of transcription factors. *Gene* **303:** 11–34.

Pettersson A, Graff RE, Bauer SR, Pitt MJ, Lis RT, Stack EC, Martin NE, Kunz L, Penney KL, Ligon AH, et al. 2012. The TMPRSS2:ERG rearrangement, ERG expression, and prostate cancer outcomes: A cohort study and meta-analysis. *Cancer Epidemiol Biomarkers Prev* **21:** 1497–1509.

Reich M, Liefeld T, Gould J, Lerner J, Tamayo P, Mesirov JP. 2006. GenePattern 2.0. *Nat Genet* **38:** 500–501.

Rossi S, Graner E, Febbo P, Weinstein L, Bhattacharya N, Onody T, Bubley G, Balk S, Loda M. 2003. Fatty acid synthase expression defines distinct molecular signatures in prostate cancer. *Mol Cancer Res* **1:** 707–715.

Seth A, Watson DK. 2005. ETS transcription factors and their emerging roles in human cancer. *Eur J Cancer* **41:** 2462–2478.

Setlur SR, Mertz KD, Hoshida Y, Demichelis F, Lupien M, Perner S, Sboner A, Pawitan Y, Andrén O, Johnson LA, et al. 2008. Estrogen-dependent signaling in a molecularly distinct subclass of aggressive prostate cancer. *J Natl Cancer Inst* **100:** 815–825.

Sharma NL, Massie CE, Ramos-Montoya A, Zecchini V, Scott HE, Lamb AD, Macarthur S, Stark R, Warren AY, Mills IG, et al. 2013. The androgen receptor induces a distinct transcriptional program in castration-resistant prostate cancer in man. *Cancer Cell* **23:** 35–47.

Shin S, Kim T-D, Jin F, Van Deursen JM, Dehm SM, Tindall DJ, Grande JP, Munz J-M, Vasmatzis G, Janknecht R. 2009. Induction of prostatic intraepithelial neoplasia and modulation of androgen receptor by ETS variant 1/ETS-related protein 81. *Cancer Res* **69:** 8102–8110.

Sleeman KE, Kendrick H, Robertson D, Isacke CM, Ashworth A, Smalley MJ. 2007. Dissociation of estrogen receptor expression and in vivo stem cell activity in the mammary gland. *J Cell Biol* **176:** 19–26.

Stanbrough M, Bubley GJ, Ross K, Golub TR, Rubin MA, Penning TM, Febbo PG, Balk SP. 2006. Increased expression of genes converting adrenal androgens to testosterone in androgen-independent prostate cancer. *Cancer Res* **66:** 2815–2825.

Subramanian A, Tamayo P, Mootha VK, Mukherjee S, Ebert BL, Gillette MA, Paulovich A, Pomeroy SL, Golub TR, Lander ES, et al. 2005. Gene set enrichment analysis: A knowledge-based approach for interpreting genome-wide expression profiles. *Proc Natl Acad Sci* **102:** 15545–15550.

Suh JH, Park J-W, Lee C, Moon KC. 2012. ERG immunohistochemistry and clinicopathologic characteristics in Korean prostate adenocarcinoma patients. *Korean J Pathol* **46:** 423–428.

Swinnen JV, Vanderhoydonc F, Elgamal AA, Eelen M, Vercaeren I, Joniau S, Van Poppel H, Baert L, Goossens K, Heyns W, et al. 2000. Selective activation of the fatty acid synthesis pathway in human prostate cancer. *Int J Cancer* **88:** 176–179.

Taylor BS, Schultz N, Hieronymus H, Gopalan A, Xiao Y, Carver BS, Arora VK, Kaushik P, Cerami E, Reva B, et al. 2010. Integrative genomic profiling of human prostate cancer. *Cancer Cell* **18:** 11–22.

Tomlins SA, Rhodes DR, Perner S, Dhanasekaran SM, Mehra R, Sun X-W, Varambally S, Cao X, Tchinda J, Kuefer R, et al. 2005. Recurrent fusion of TMPRSS2 and ETS transcription factor genes in prostate cancer. *Science* **310:** 644–648.

Tomlins SA, Laxman B, Dhanasekaran SM, Helgeson BE, Cao X, Morris DS, Menon A, Jing X, Cao Q, Han B, et al. 2007. Distinct classes of chromosomal rearrangements create oncogenic ETS gene fusions in prostate cancer. *Nature* **448:** 595–599.

Tomlins SA, Laxman B, Varambally S, Cao X, Yu J, Helgeson BE, Cao Q, Prensner JR, Rubin MA, Shah RB, et al. 2008. Role of the TMPRSS2–ERG gene fusion in prostate cancer. *Neoplasia* **10:** 177–188.

Twiddy AL, Leon CG, Wasan KM. 2010. Cholesterol as a potential target for castration-resistant prostate cancer. *Pharm Res* **28:** 423–437.

Vitari AC, Leong KG, Newton K, Yee C, O'Rourke K, Liu J, Phu L, Vij R, Ferrando R, Couto SS, et al. 2011. COP1 is a tumour suppressor that causes degradation of ETS transcription factors. *Nature* **474:** 403–406.

Wang J, Rao S, Chu J, Shen X, Levasseur DN, Theunissen TW, Orkin SH. 2006. A protein interaction network for pluripotency of embryonic stem cells. *Nature* **444:** 364–368.

Wang Q, Li W, Zhang Y, Yuan X, Xu K, Yu J, Chen Z, Beroukhim R, Wang H, Lupien M, et al. 2009. Androgen receptor regulates a distinct transcription program in androgen-independent prostate cancer. *Cell* **138:** 245–256.

Ward PS, Thompson CB. 2012. Metabolic reprogramming: A cancer hallmark even warburg did not anticipate. *Cancer Cell* **21:** 297–308.

Wei G-H, Badis G, Berger MF, Kivioja T, Palin K, Enge M, Bonke M, Jolma A, Varjosalo M, Gehrke AR, et al. 2010. Genome-wide analysis of ETS-family DNA-binding in vitro and in vivo. *EMBO J* **29:** 2147–2160.

Wilt TJ, Brawer MK, Jones KM, Barry MJ, Aronson WJ, Fox S, Gingrich JR, Wei JT, Gilhooly P, Grob BM, et al. 2012. Radical prostatectomy versus observation for localized prostate cancer. *N Engl J Med* **367:** 203–213.

Wu X, Wu J, Huang J, Powell WC, Zhang JF, Matusik RJ, Sangiorgi FO, Maxson RE, Sucov HM, Roy-Burman P. 2001. Generation of a prostate epithelial cell-specific Cre transgenic mouse model for tissue-specific gene ablation. *Mech Dev* **101:** 61–69.

Yu J, Yu J, Mani R-S, Cao Q, Brenner CJ, Cao X, Wang X, Wu L, Li J, Hu M, et al. 2010. An integrated network of androgen receptor, polycomb, and TMPRSS2-ERG gene fusions in prostate cancer progression. *Cancer Cell* **17:** 443–454.

Zadra G, Priolo C, Patnaik A, Loda M. 2010. New strategies in prostate cancer: Targeting lipogenic pathways and the energy sensor AMPK. *Clin Cancer Res* **16:** 3322–3328.

Zong Y, Xin L, Goldstein AS, Lawson DA, Teitell MA, Witte ON. 2009. ETS family transcription factors collaborate with alternative signaling pathways to induce carcinoma from adult murine prostate cells. *Proc Natl Acad Sci* **106:** 12465–12470.